Molecular imaging for the quantitative assessment of tumor proliferation, progression and the early assessment of molecular targeted treatment response

Inaugural Dissertation

zur

Erlangung des Doktorgrades

Dr. nat. med.

der Medizinischen Fakultät

und

der Mathematisch-Naturwissenschafltichen Fakultät

der Universität zu Köln

vorgelegt von

Dr. med. Roland Tillmann Ullrich

Köln, 2010

Berichterstatter: Professor Dr. Wolf

                      Professor Dr. Kloppenburg

Tag der letzten mündlichen Prüfung: 04.11.2010

Table of Contents

1. Abbreviations

[11C]MET   -[11C]Methionine

[18F]FDG   -2-[^{18}F]fluoro-2-deoxy-D-glucose

[18F]FLT   -3'-Deoxy-3'-[18F]-fluoro-L-thymidine

CML   -Chronic Meylogenous Leukemia

EGFR   -Epithelial growth factor receptor

mTor   -mammalian Target of rapamycin

NSCLC   -Non-Small Cell Lung Cancer

PDGFR   -Platelet Derived Growth Factor Receptor

PET   -Positron Emission Tomography

ROC   -Receiver Operating Curve

TK1   -Thymidine Kinase 1

VEGF   -Vascular Endothelial Growth Factor

2. Summary (English)

Molecular imaging allows for in vivo monitoring of important processes for tumor development, tumor growth and, finally, treatment response. The major goal of this study was to investigate different multi-modal imaging techniques for the assessment of different tumor specific molecular processes (Jacobs et al., 2005a; Ullrich et al., 2008a; Ullrich et al., 2008b).

In the first step, I investigated the use of [^{18}F]FLT for the non-invasive *in vivo* assessment of tumor proliferation in different types of tumor models in men and mice. [^{18}F]FLT reacts as a substrate of thymidinkinase 1 (TK1) that is highly expressed during S-phase of the cell cycle. Shields et al could show that the accumulation of [^{18}F]FLT reflects cells entering the s-phase in vitro and in vivo (Shields et al., 1998). Here, we first sought to analyze the accuracy of [^{18}F]FLT to detect tumor cell proliferation in patients with gliomas. We investigated the dynamic [^{18}F]FLT distribution for the asessment of tumor cell proliferation *in vivo* (Ullrich et al., 2008a). In patients with newly diagnosed high grade gliomas we showed by the use of kinetic analyses that the phosphorylation rate of [^{18}F]FLT by thymidine kinase 1 can be detected and, most importantly, is related to tumor cell proliferation as *in vitro* assessed by Ki-67 immunostaining. We concluded that [^{18}F]FLT PET represents an accurate marker for the in vivo assessment of tumor cell proliferation in patients with gliomas.

We next hypothesized that [^{18}F]FLT PET might provide a sensitive marker for monitoring treatment induced G1 arrest in Non small cell lung cancer (NSCLC). Herewith, we analyzed [^{18}F]FLT in comparison to [^{18}F]FDG PET as a marker for monitoring anti-proliferative treatment response. In collaboration with the Cancer Genomic Group by Dr. Roman Thomas we investigated the potential of [^{18}F]FLT to detect treatment response to specific Epithelial growth factor receptor (EGFR) inhibition in an EGFR-dependent NSCLC model. We used two EGFR-inhibition sensitive cell lines harboring the L858R mutation leading to oncogenic dependency on EGFR signaling. To validate the specificity of EGFR-inhibition we applied the EGFR inhibition resistant cell line H1975 harboring both the L858R and the T790M mutation. The T790M mutation prevents Erlotinib from binding to the intracellular domain of the EGFR. Only two days after initiation of treatment we observed a striking decrease in [^{18}F]FLT uptake in the EGFR-mutant tumor xenograft due to

therapy induced G1 arrest. The specificity of this approach is confirmed by a complete lack of [^{18}F]FLT response in the T790M EGFR-resistant xenografts. Moreover, the reduction of [^{18}F]FLT uptake after 2 days translated into dramatic tumor shrinkage 6 days later (Ullrich et al., 2008c). Together, these data strongly suggest [^{18}F]FLT PET as a robust marker to assess tumor proliferation, to detect induction of G1 arrest and, thus, to detect therapy response at a very early time point.

Tumor growth requires new vessel formation as a critical step in tumor progression. In a recent study our group found a significant correlation between the expression of CD31 and [^{11}C]MET uptake in gliomas (Kracht et al., 2003). [^{11}C]MET is transported via the L amino acid transporter that is expressed on endothelial cells suggesting this tracer for imaging angiogenesis. Based on these findings we further investigated the relationship between [^{11}C]MET uptake and angiogenesis during tumor progression by comparing uptake ratios of [^{11}C]MET and the expression of the vascular endothelial growth factor (VEGF) in patients with gliomas. Here, we again found a significant correlation between changes in VEGF expression and [^{11}C]MET uptake (Ullrich et al., 2009). Moreover, increase in [^{11}C]MET uptake of more than 14,6 % was highly sensitive and specific to detect malignant progression in patients with gliomas.

In summary, multi-modal imaging enables to assess tumor relevant processes, to monitor changes in tumor growth and, finally, to assess treatment response to agents targeting those processes.

3. Summary (German)

In dieser Arbeit untersuchten wir das Potential unterschiedlicher Bildgebungsansätze der Positronen-Emissions-Tomographie zur Darstellung relevanter Prozesse für das Tumorwachstum mit dem Ziel diese Bildgebungsansätze zu nutzen, um Therapieansprechen nicht-invasiv bestimmen zu können.

Hierbei untersuchten wir in einem ersten Ansatz die [^{18}F]FLT Positronen-Emissions-Tomographie PET zur nicht-invasiven Bestimmung von Tumorzellproliferation in Menschen und in Mäusen. Der Radiotracer [^{18}F]FLT reagiert als Substrat der Thymidinkinase 1 (TK1). TK1 ist ein Enzym, das vermehrt während der S-Phase des Zellzyklus exprimiert wird. Die Mitarbeiter um Shields konnten in vitro als auch in vivo zeigen, dass [^{18}F]FLT spezifisch in Zellen akkumuliert, die sich in der S-Phase des Zellzyklus befinden. Wir untersuchten das Potential der [^{18}F]FLT PET um Tumorzellproliferation in Patienten mit glialen Gehirntumoren zu bestimmen. Mittels dynamischer [^{18}F]FLT PET Messungen bestimmten wir die Kinetik von [^{18}F]FLT im Tumor. Bei Patienten mit neu-diagnostizierten hochgradigen Gliomen versuchten wir anhand der Kinetik von [^{18}F]FLT im Tumorgewebe die Phosphorylierungsrate von [^{18}F]FLT durch die Thymidinkinase 1 zu detektieren um diese dann mit der Proliferationsrate aus den Tumorgewebeschnitte mittels Ki-67 zu vergleichen. Hierbei zeigten wir, dass wir (a) aus der [^{18}F]FLT Kinetik die TK1 Aktivität bestimmen können und (b) dass die in vivo erhobenen Daten aus der [^{18}F]FLT Kinetik mit der histologisch erhobenen Proliferationsrate korreliert. Wir schließen daraus, dass wir anhand der kinetischen Auswertung der [^{18}F]FLT Verteilung die Proliferationsrate nicht-invasiv in Patienten mit hochgradigen Gliomen bestimmen können.

Aufbauend auf diesen Ergebnissen untersuchten wir das Potential der [^{18}F]FLT PET Bildgebung zur Darstellung von Therapieansprechen. In Zusammenarbeit mit der Gruppe von Dr. Roman Thomas verglichen wir die [^{18}F]FLT PET mit der [^{18}F]FDG PET zur Darstellung von Therapieansprechen von Erlotinib induzierter EGFR-Inhibition in einem EGFR-abhängigen subkutanen NSCLC Modell in der Maus. Als NSCLC Modell verwendeten wir 2 EGFR sensitive Zelllinien, bei denen eine L858R Mutation zu einer onkogenen Abhängigkeit vom EGFR Signalweg führt. Zur Validierung der Spezifität unseres Ansatzes verglichen wir diese beiden Zelllinien mit einer weiteren Zelllinie (H1975), die neben der L858R Mutation die T790M Mutation trägt. Die T790M Mutation führt hierbei zu einer Konformationsänderung in der ATP-

Bindungstasche des EGFR, die eine Bindung von Erlotinib und somit die Erlotinib vermittelte EGFR Rezeptorinhibition verhindert. Bereits nach 2 Tagen Erlotinib-Therapie beobachteten wir eine deutliche Abnahme der [^{18}F]FLT Aufnahme im PET in den L858R mutierten Zellinien. In den Xenotransplanaten mit der zusätzlichen T790M Mutation zeigte sch dagegen keine Veränderung in der [^{18}F]FLT Anreicherung im PET. Die [^{18}F]FLT PET ist somit ein geeignetes Verfahren um Therapieansprechen nach Erlotinib-Therapie frühzeitig zu detektieren.

Die Ausbildung von tumoreigenen Gefäßen ist ein essentieller Schritt zum malignen Wachstum. In einer vorangegangenen Studie fanden wir eine signifikante Korrelation zwischen der Expression des Endothelzellmarkers CD31 und der Anreicherung von [^{11}C]MET in der PET bei Patienten mit Gliomen (Kracht et al., 2003). Die zelluläre Aufnahme von [^{11}C]MET wird über den LAT1 Transporter gesteuert, der insbesondere auf Endothelzellen exprimiert ist. Basierend auf diesen Ergebnissen untersuchten wir den Zusammenhang zwischen der [^{11}C]MET Aufnahme und der Expression des vaskulären Wachstumsfaktors VEGF in Patienten mit Gliomen. Hierbei zeigte sich ein signifikanter Zusammenhang zwischen der [^{11}C]MET Aufnahme und der Expression VEGF. Desweiteren zeigte sich, dass eine Zunahme der [^{11}C]MET Aufnahme über 14,6 % spezifisch und sensitiv für eine Malignisierung des Tumors war. Die [^{11}C]MET PET ist somit ein vielversprechender Marker um nicht invasiv die Malignisierung von Gliomen zu detektieren (Ullrich et al., 2009).

4. List of publications

I.

Ullrich, R., Backes, H., Li, H., Kracht, L., Miletic, H., Kesper, K., Neumaier, B., Heiss, W.D., Wienhard, K., and Jacobs, A.H. (2008a). Glioma proliferation as assessed by 3'-fluoro-3'-deoxy-L-thymidine positron emission tomography in patients with newly diagnosed high-grade glioma. Clin Cancer Res *14*, 2049-2055.

II.

Ullrich, R., Zander, T., Neumaier, B., Shimamura, T., Waerzeggers, Y., Li, H., Koker, M., Sos, ML., Backes, H., Wolf, J., Jacobs, AH., Thomas, RK., Winkeler, A. (2008b). Early detection of erlotinib treatment response in NSCLC by 3'-Deoxy-3'-[18F]-fluoro-L-thymidine ([18F]FLT) positron emission tomography (PET). PLoS One. 2008;3(12):e3908.

III.

Ullrich, R., Kracht, L., Brunn, A., Herholz, K., Frommolt, P., Miletic, H., Deckert, M., Heiss, WD., Jacobs, AH. (2009). [11C]Methionine positron emission tomography as diagnostic marker for the malignant progression and the formation of angiogenesis in patients with gliomas. J Nucl Med. 2009 Nov 12.

Contributions

I.

In this project I designed the concept with Andreas Jacobs, Heiko Backes, Lutz Kracht, Kristina Kesper, Wolf-Dieter Heiss and Klaus Wienhard. Lisa Li and Bernd Neumaier produced the radiotracer FLT. Kristina Kesper gave support for acquiring the patients from the University hospital for Neurology, Cologne. Hrvoje Miletic gave substantial support for the immunohistochemistry of the patient´s samples. I selected the patients and performed the PET measurements together with Kristina Kesper and Lutz Kracht. I analysed the data together with Heiko Backes and Klaus Wienhard, and finally wrote the manuscript. The manuscript was corrected by Andreas Jacobs and approved by all Co-authors.

II.

Within this project I performed the in vivo study including cell preparation, xenografts, oral treatment, excision of the xenografts, immunohistochemical analyses of the frozen tissue section for HE, Ki-67 and TUNEL. Together with Mirjam Koker we performed Annexin V staining by FACS. Thomas Zander, Jürgen Wolf, Andreas Jacobs, Roman Thomas and Alexandra Winkeler contributed to the design of the study. Yannic Waerzeggers supported the in vivo study. Takeshi Shimammura gave support on the results of the cell cycle analysis. Martin Sos gave support on the biochemical analysis. Heiko Backes gave support on PET data reconstruction. Bernd Neumaier produced the radiotacers. I analysed all the data, performed statistical analysis and finally wrote the paper. Roman Thomas and Alexandra Winkeler corrected the manuscript.

III.

I designed the study together with Andreas Jacobs, Lutz Kracht, Karl Herholz and Wolf-Dieter Heiss. Anna Brunn and Martina Deckert provided immunohistochemical staining of the patient´s samples. Peter Frommolt gave support on the statistical analysis. Together with Lutz Kracht I selected the patients that were included in the study, I collected the data, analysed the data, and finally wrote the manuscript. Andreas Jacobs, Karl Herholz, Wolf-Dieter Heiss and Lutz Kracht corrected the manuscript.

5. Introduction

Advances in molecular cell biology have dramatically strengthened our knowledge of molecular signaling pathways being relevant for tumor growth. However, despite improvements in cancer therapies based on these knowledge cancer still remains largely incurable and survival for cancer patients is often measured in months to few years. In the last decades substantial efforts have been made to identify the optimal target for each cancer type. As such, small molecular inhibitors as imatinib for chronic meylogenous leukemia (CML), trastuzumab for breast cancer with ERBB2 amplification and Erlotinib for non small lung cancer (NSCLC) with mutated epithelial growth factor receptor (EGFR) have shown strong treatment efficacy (Baselga et al., 1996; Daley et al., 1990; Lynch et al., 2004; Paez et al., 2004). Moreover, various cancer types present dependency on the PI3K and MAPK signaling pathway as highly promising treatment targets (Sos et al., 2009). However, the non-invasive identification of patients that profit best from the various molecular targeted treatment approaches still remains elusive.
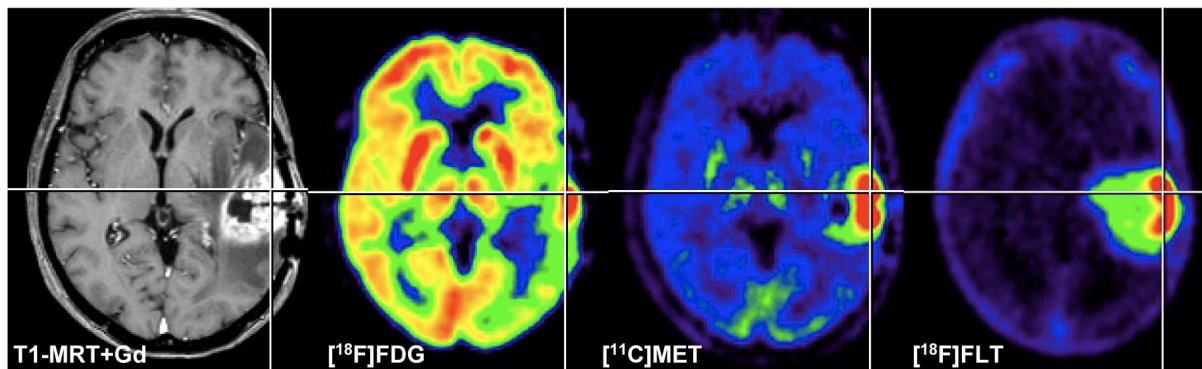
Molecular imaging enables to non-invasively monitor the effect of activation of these relevant signaling pathways and, most importantly, to assess treatment efficacy of these new molecular targeted compounds. To date the evaluation of responses to cancer therapy are mainly based on volumetric and morphological criteria, in particular relative tumour sizes before and after treatment. These criteria were defined more than 25 years ago as the WHO (World Health Organization) and RECIST (Response Evaluation Criteria in Solid Tumors) criteria, respectively (Macdonald et al., 1990; Therasse et al., 2000). Here, Macdonald et al. introduced the 2-dimensional (2D) WHO criteria for the diagnosis of brain tumours. For solid tumours, Therasse et al determined the WHO criteria in 2000 by uni-dimensional measurements of tumor size known as RECIST criteria. RECIST defines response to therapy by a decrease of a 30% in the largest dimension of the tumour (Therasse et al., 2000). However, criteria based on morphological changes are rather limited in their ability to assess early effects of therapy since tumor shrinkage occurs at a rather late time point. Thus, the development of novel targeted cancer therapies would strongly benefit from non-invasive approaches providing target-specific molecular information by functional imaging methods. This would not only allow

patient stratification and selection for molecular-targeted treatment but also provide early assessment of treatment response before any reduction in tumour volume is visible.

Molecular imaging (MI) implies the use of imaging technologies by applying specific molecular probes. MI aims at the non-invasive characterisation of the dynamics of disease-specific molecular changes *in vivo*. To date, Molecular imaging modalities can be divided in two groups: those primarily providing structural information like CT, MRI or ultrasound; and those primarily aiming at functional or molecular information, like PET, SPECT or optical imaging. Molecular imaging usually exploits specific molecular probes as the source of imaging contrast to report on the underlying biochemistry and cell biology associated with disease progression and response to therapy. Functional imaging techniques as PET and SPECT provide a very high sensitivity that allows for the detection of even very low levels of specific tracer accumulation in the picomolar range. Moreover, these methods enable in vivo imaging with unlimited depth penetration, excellent signal-to-background rations and a broad range of clinically applicable probes. Though, the major limitation of radionuclide imaging is its inherently limited spatial resolution (currently 3-7 mm in clinical application, about 1.3 mm in experimental settings). Furthermore, patients are exposed to relevant doses of radiation that limits the number of examinations and the single dose of the tracer. Finally, imaging centers need to have access to a cyclotron and radiochemistry facility. In contrast, MR imaging techniques provide a good depth penetration and a very high spatial resolution. However, temporal resolution is low and the sensitivity to detect molecular imaging probes remains reduced.

Positron-Emission-Tomographie (PET) represents a highly sensitive non-invasive method to detect molecular processes with a very high resolution. PET enables for the *in vivo* assessment of metabolic and molecular processes with a high sensitivity. In patients with tumors, PET provides physiological and biochemical information on the molecular level to characterize the tumor´s extent, its proliferative activity, metabolism and its expression of various tumor specific receptor **(Figure 1)**. The accumulation of each tracer reflects the activity of its transporter via the cell membrane and the activity of specific enzymes by which these tracers are metabolized and trapped.

Figure 1: Parameters of interest in the noninvasive diagnosis of brain tumors. Alteration of the blood-brain barrier and the extent of peritumoral edema are detected by MRI. Signs of increased cell proliferation can be observed by multitracer PET imaging using [^{18}F]FDG, [^{11}C]MET, and [^{18}F]FLT as specific tracers for glucose consumption, amino acid transport, and DNA synthesis, respectively. Secondary phenomena, such as inactivation of ipsilateral cortical cerebral glucose metabolism, may be observed ([^{18}F]FDG), and are of prognostic relevance. (Reproduced with permission from Jacobs A. PET in Gliomas. Stuttgart: Thieme; 2003:72–76.74)

The most commonly used PET tracer in the diagnosis of tumors is 2-[^{18}F]fluoro-2-deoxy-D-glucose ([^{18}F]FDG). [^{18}F]FDG reacts as an analogue of glucose and, thus, its accumulation reflect cellular glucose metabolism. It is well known that tumours mainly rely on anaerobic glycolysis during their energy consumption. Due to the limited efficacy of anaerobic glycolysis and their high demand of energy cancer cells frequently present increased glucose metabolism. This is accompanied by an increased activity of the GLUT1 transporter and high hexokinase activity (Zhao et al., 2005). In contrast to glucose, once [^{18}F]FDG has entered the cell, it is phosphorylated but it is not further metabolised. This results into an intracellular trapping of [^{18}F]FDG in the cell enabling accurate quantification of hexokinase activity in vivo.

[^{18}F]FDG PET has been approved by the Food and Drug Administration (FDA) for the assessment of abnormal glucose metabolism in patients with cancer. Moreover, in 1999 the EORTC-PET Group had established response assessment guidelines for [^{18}F]FDG PET (Young et al., 1999). However, the diagnostic specificity of [^{18}F]FDG PET remains limited due to its usually high background activity in healthy tissue. E.g.
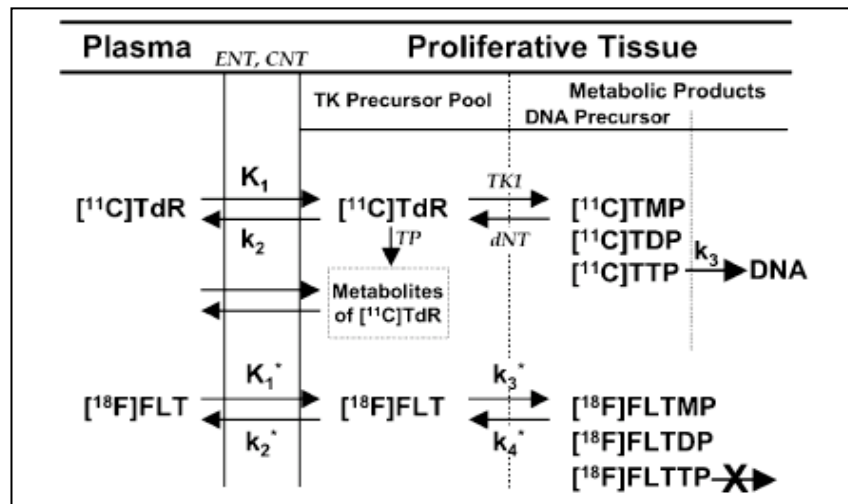
the brain shows high cortical [^{18}F]FDG uptake high glucose metabolism (Phelps and Mazziotta, 1985). Furthermore, high physiological [^{18}F]FDG uptake is also seen in tonsils, salivary glands, reactive lymph nodes, liver, gastrointestinal tract and testis, as well as muscles. In addition, inflammatory cells as macrophages present high [^{18}F]FDG uptake (Buck et al., 2003). Thus, tumoral inflammatory response might mimic high tumor cell [^{18}F]FDG uptake. As anti-cancer treatment might induce inflammatory response within the tumor [^{18}F]FDG PET might present high [^{18}F]FDG uptake due to invasion of macrophages and not due to high tumor cell metabolism (Reinhardt et al., 1997). For these reasons, [^{18}F]FDG PET seems not to be a specific marker for the evaluation of novel therapies in cancer.

Beside glucose metabolism the synthesis of proteins is one of the essential processes for cell proliferation. Due to the proliferation rate of cancer cells, the process of protein synthesis and, thus, amino acid transport is increased in tumor cells (Jager et al., 2005). Thus, amino acid metabolism could provide useful information with regard to tumour metabolism. Nearly all amino acids and slightly modified variants have been radiolabelled, but only a few have clinical use. Among these few are [^{11}C]methionine (MET), [^{18}F]fluorethyl-tyrosine (FET) and [^{11}C]tyrosine (TYR) for PET imaging, and [^{123}I]iodomethyl-tyrosine (IMT) for SPECT imaging (Jager et al., 2001). From these tracers, only [^{11}C]TYR uptake represents both transport and protein synthesis, whereas the remaining tracers represent increased transport into tumour cells. In comparison with [^{18}F]FDG PET imaging is amino acid imaging less influenced by inflammation. In the last years, radiolabelled methionine and thymidine compounds have been shown to be more specific tracers in tumour detection, delineation and staging due to their relatively low uptake in healthy tissue.

Nucleic acids have been radiolabelled as PET tracers for in vivo imaging of cellular proliferation. Today, [^{3}H]thymidine incorporation is widely used for assessing proliferation in vitro (Kelloff et al., 2005). In PET, Thymidine labelled with positron-emitting nuclides enables in vivo imaging of proliferating cells. Thymidine labelled with [^{11}C] in the pyrimidine ring provides the authentic substrate of the thymidine kinase 1 and is incorporated into DNA.

TK1 is a cytosolic enzyme that is expressed during the S phase of the cell cycle. Thus, TK1 expression is specifically increased in dividing cells and decreased in non-dividing cells (Vesselle et al., 2002). Validated kinetic models of [^{11}C]thymidine have been used to image cell proliferation in human tumours and response to

chemotherapy that directed at the de novo DNA synthesis pathway (Wells et al., 2003).
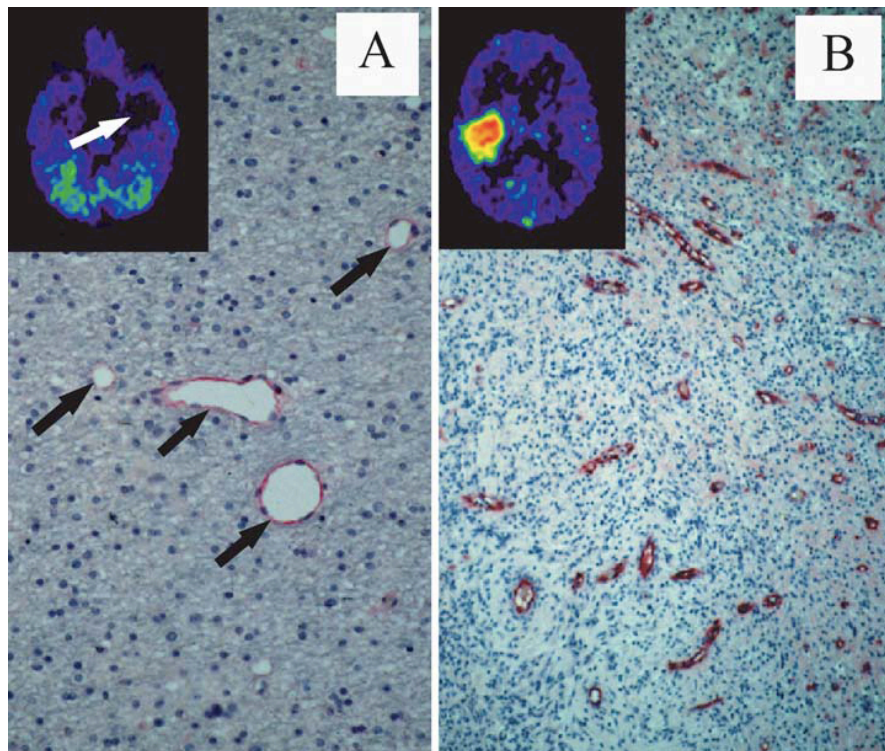
In analogy, the deoxyribose group of thymidine can also be labelled with [^{18}F] at the 3'-deoxy position resulting in 3'-deoxy-3'-fluorothymidine ([^{18}F]FLT) (Shields et al., 1998). [^{18}F]FLT is transported via specific nucleoside transporters from the blood pool into the cells. Within the cells [^{18}F]FLT reacts as an analogue substrate of thymidine which is phosphorylated by the thymidine kinase 1 (TK1) **(see Figure 2)**. Several clinical studies revealed a significant correlation between [^{18}F]FLT uptake and the in vitro proliferation marker Ki-67 in various tumor types (Buck et al., 2003; Wagner et al., 2003). In addition, *in vitro* and animal studies comparing [^{18}F]FDG and [^{18}F]FLT have repeatedly confirmed that [^{18}F]FLT uptake in inflammatory tissue is considerably less than [^{18}F]FDG, which is advantageous. However, [^{18}F]FLT uptake in tumours appears to be lower than [^{18}F]FDG, as demonstrated in many types of cancer (Been et al., 2004). [^{18}F]FLT PET, therefore, seems to be less suitable for staging of cancer and currently most research focuses on response evaluation as [^{18}F]FLT has great potential utility in following response to therapy. A tumour cell that responds to anti-proliferative treatment (as EGFR targeting compounds) may continue to metabolize [^{18}F]FDG to maintain ion gradients or to provide energy for the P-glycoprotein (P-gp) pump function or protein biosynthesis; however, it will not synthesize new DNA, thus will not accumulate [^{18}F]FLT. A decrease in DNA synthesis is likely following either cytostatic or cytotoxic therapy, highlighting the general utility of [^{18}F]FLT PET for detecting response (Kelloff et al., 2005). Clinical studies might benefit from using rigorously quantitative methods to distinguish thymidine delivery and transport from thymidine kinase enzyme activity (Muzi et al., 2005). In a recent study, we demonstrated that [^{18}F]FLT uptake (i) enables to differentiate between low grade and high grade tumours and (ii) is mainly due to increased transport and to a lower extent to phosphorylation by TK1 in gliomas (Jacobs et al., 2005b).

Figure 2: *Dynamic distribution of [^{18}F]FLT from the blood pool into the cell.*
[^{18}F]FLT behaves in a similar manner as [^{11}C]Thymidine. Its uptake is regulated by the nucleoside transporter on the cell membrane reflected by the rate of transport K1 into the cell and k2 from the cell back to the plasma (/min). Within the cell TK1 phosphorylates [^{18}F]FLT to [^{18}F]FLT monophosphate, diphopsphate and triphosphate determined by the rate konstant k3 (/min). The rate constant k4 (/min) reflects the rate of dephosporylation back to [^{18}F]FLT. Of note, in contrast to thymidine only a very small proportion of [^{18}F]FLT is incorporated into the DNA (modified from (Krohn et al., 2005)).

Amino acids tracers such as *[11C]methyl*-[^{11}C]-L-[11C]Methionine ([^{11}C]MET), [^{11}C]-tyrosine, [^{18}F]fluoro-tyrosine and O-(2-[^{18}F]-fluoroethyl)-L-tyrosine have been investigated for the diagnosis of tumors. The increased [^{11}C]MET uptake is due to increased transport mediated by type L-amino acid transporters and this increased transport seems to be directly regulated by tumour growth factors that effects the mTor complex (Miyagawa et al., 1998). [^{11}C]MET PET detects parts of brain tumours as well as infiltrating areas with high sensitivity (87%) and specificity (89%) by an uptake threshold of 1.3 fold (Kracht et al., 2004). Furthermore, [^{11}C]MET uptake correlates with the tumor proliferative activity (Sato et al., 1999) and enables to differentiate between WHO II and WHO grade III/IV gliomas (Sasaki et al., 1998). By using a threshold of 1.5 [^{11}C]MET PET permits the differentiation between non-tumoural lesions and gliomas with a sensitivity of 79 % (Herholz et al., 1998).

[^{11}C]MET also enables to differentiate recurrent tumour from radiation necrosis while the tracer accumulation is nearly independent from disruption of the BBB or macrophage activity (Thiel et al., 2000). Moreover, [^{11}C]MET PET detects parts of brain tumours as well as infiltrating areas with high sensitivity and specificity (Galldiks et al., 2009; Kracht et al., 2004). Interestingly, in one of our recent studies we found that [^{11}C]MET uptake correlates with microvessel density (Kracht et al., 2003). This study indicated that [^{11}C]MET uptake might be regulated by angiogenesis promoting factors **(see Figure 3)**.

Figure 3: *[^{11}C]MET uptake correlates with microvessel density.* In A a patient with a low grade astrocytoma (grade II) presenting low microvessel counts and corresponding low [^{11}C]MET uptake. In contrast in B a glioblastoma with high [^{11}C]MET uptake and high number of red-stained microvessels in the tumor specimen (Kracht et al., 2003).

In summary, PET allows for the in vivo assessment of tumor specific processes enabling monitoring therapy response of therapy approaches targeting these processes. Most importantly, PET is already in a wide clinical use that preclinical findings can directly be translated into clinical trials. In this thesis we aimed to investigate non-invasive multi-modal PET modalities to characterize tumor specific processes and to finally establish non-invasive PET marker for imaging guided treatment response.

6. Present investigation – "Multi-modal imaging of tumor growth driving processes and monitoring molecular targeted treatment by the use of Positron-Emission-Tomography"

6.1 Glioma proliferation as assessed by 3'-fluoro-3'-deoxy-L-thymidine positron emission tomography in patients with newly diagnosed high-grade glioma.

Inhibition of tumor cell proliferation is one of the most relevant targets in the treatment of cancer. Thus, a method that enables to monitor in vivo tumor cell proliferation is highly required for the evaluation of treatment response in patients with cancer. In the present investigation we aimed to investigate the potentials of [^{18}F]FLT PET to assess tumor cell proliferation in patients with brain tumors. We tested the [^{18}F]FLT imaged derived data in comparison to data from the corresponding [^{11}C]MET PET for their potential to assess tumor cell proliferation in vivo. Furthermore, we compared the in vivo assessed data with immunohistochemistry from PET guided stereotactic biopsies.

Material and Methods

Patients

In this study 13 patients with newly diagnosed primary brain tumors (9 male, 4 female, age: median 64.0 years, range: 35 to 71 years) were included. All patients gave their written informed consent on multimodal PET and MR imaging. Patients received T1-weighted MRI before PET measurements. PET and MRI measurements were performed within one week. After MRI/PET scans except for one all gliomas were confirmed by histology and classified according to World Health Organization (WHO) grade (stereotactic biopsy, n=7; resection, n=5). Five patients were classified as astrocytoma grade III, one as oligoastrocytoma grade III and 6 as glioblastoma (grade IV).

PET

PET imaging was performed on an ECAT EXACT (CTI/Siemens; in-plane full width at half maximum, 6 mm; slice thickness, 3.375 mm; axial field of view, 162 mm) and an ECAT EXACT HR (CTI/Siemens; in-plane full width at half maximum, 3.6 mm, slice thickness, 3.125 mm; axial field of view, 150 mm). Ten minute transmission scans with rotating germanium-68/gallium-68 sources were performed for attenuation correction of the PET data.

$[^{11}C]$MET and $[^{18}F]$FLT syntheses were produced in house with a radiolabeling yield of 10 % ± 1.5% and a radiochemical purity of higher than 98%. The mean injected dose of $[^{18}F]$FLT was 321.9 +/- 85.1 MBq (range 111-370 MBq). From all patients arterialized blood samples were taken by a peripheral intravenous catheter. $[^{18}F]$FLT PET images were acquired in the following dynamic sequence: 6 x 10 s, 3 x 20 s, 2 x 30 s, 2 x 60 s, 2 x 150 s and 16 x 300 s.

Tracer accumulation was recorded in a three dimensional mode over 60 min in 47 transaxial slices of the entire brain. For coregistration to the anatomic data, T1, T2 and contrast enhanced MRI scans were performed in all patients on a 1.5 T system (Gyroscan Intera, Philips Medical Systems). MR images were coregistrated to summed PET images by the use of the in-house VINCI software with an accuracy of 2 mm or better.

We used in-house VINCI software for data analysis. Herewith, a region-of-interest (ROI) approach to determine the maximal tracer uptake in $[^{18}F]$FLT and $[^{11}C]$MET PET of the summed images. The circular ROI with a diameter of 8 mm was placed in the tumor region with the highest tracer uptake. To calculate the uptake ratio a reference ROI was placed on the contralateral unaffected tissue. Tracer uptake was calculated as the ratio between tumor and healthy tissue.

The time activity curves were determined in the part of the tumor with the highest uptake. Three consecutive brain slices were included in the calculation. Kinetic analysis was performed by using PMOD biomedical image quantification and kinetic modeling software (PMOD Technologies Ltd.).

Histological assessment of proliferation by immunostaining Ki-67

A representative formalin-fixed, paraffin-embedded section from each specimen was immunohistochemically stained with MIB-1 (Ki-67) antibody by use of the Avidin-Biotin-Peroxidase-Complex (ABC) method and the DCS Detection-Kit with DAB and

H$_2$O$_2$ (DCS, Hamburg, Germany). All cells with nuclear staining of any intensity were regarded as positive. Proliferative activity was defined as the percentage of nuclei stained with MIB-1 per total number of nuclei in the biopsy. The fraction of labelled tumor cells, defined as the Ki-67 labeling index (Ki-67 LI), was assessed over 4 microscopic high power fields (0.16mm^2), that contained the highest average fraction of labelled cells. The Ki-67 LI was determined by scoring the fraction of cells stained with the MIB-1 antibody in 5% intervals.

Statistical Analysis

Parametric statistical tests were used to determine significant correlations between the parameters (Pearson correlation analysis). Correlations were considered significant at a level for $p < 0.05$. Statistical analysis were performed by SPSS software (Release 11.0.1. SPSS Inc., Chicago. IL. USA).

Results

Kinetic analysis of in vivo [^{18}F]FLT distribution: from the blood into the cell

[^{18}F]FLT is a radiolabelled analogue of thymidine. Thymidine is incorporated into DNA during DNA replication. The pathway of thymidine is determined by the transport from the blood into the cell via nucleoside transporter (K1), out of the cells into the blood (k2), its phosphorylation to mono-/di-/tri-phosphate (k3) and its dephosphorylation (k4) **(see Figure 2)**. In contrast to thymidine [^{18}F]FLT is only to a very small proportion incorporated into the DNA. However, the rate of cell proliferation (P) – that is proportional to the rate of incorporation of thymidine into the DNA – can be expressed in terms of the of the thymidine concentration in blood (ThB) by

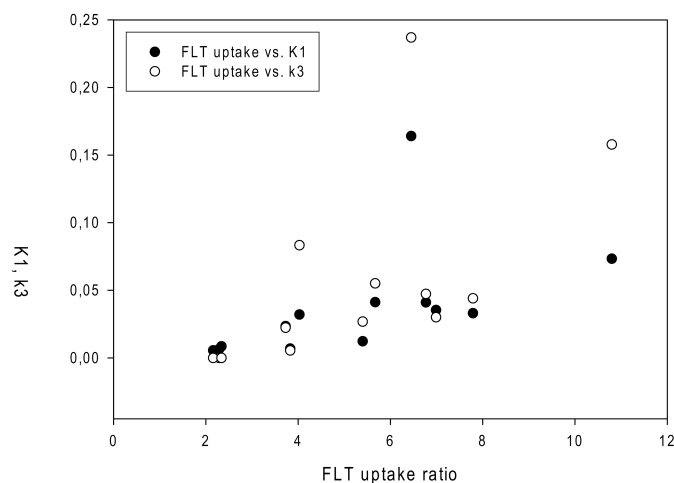$$P \sim \frac{K_{Th1} \cdot k_{Th3}}{(1 + k_{Th4}/k_{DNA}) \cdot k_{Th2} + k_{Th3}} \cdot Th_B$$

Since KTh4 is small compared to KDNA this expression is independent from kDNA. Since the other reactions are the same as in the thymidine pathway we replace the thymidine constants by their fluorothymidine analogue leading to

$$P \sim \frac{K1 \cdot k3}{k2 + k3} \cdot Th_B = Ki \cdot Th_B$$

Thus, the rate of cell proliferation is proportional to the metabolic rate constant KI and the thymidine level in the blood.

Contribution of the rate of transport K1 and the rate of phosphorylation to [18F]FLT uptake in gliomas
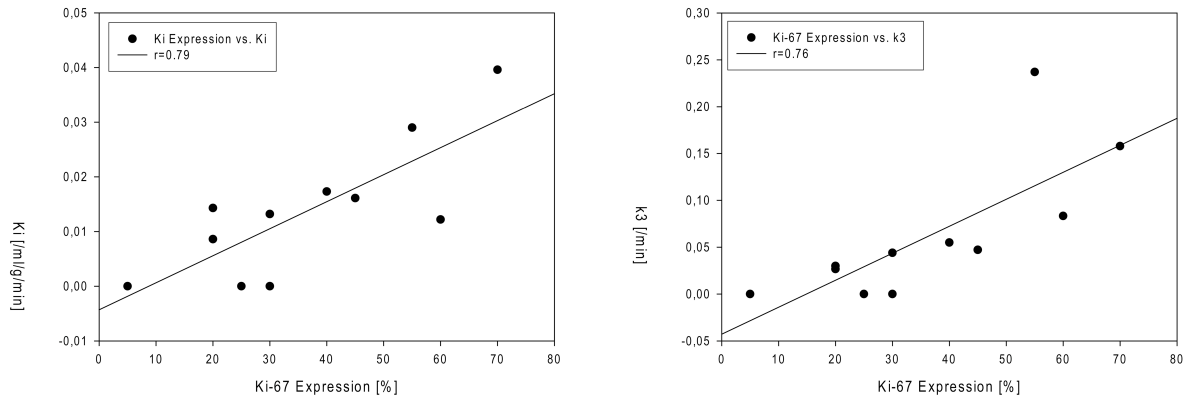
In a first step we investigated the contribution of kinetics of [18F]FLT to its final uptake. We found that the rate constant for transport of [18F]FLT K1 showed a weaker correlation to [18F]FLT uptake than the phosphorylation constant k3 **(see Figure 4)**. This indicates that in high grade gliomas [18F]FLT uptake is rather due to the phosphorylation rate of [18F]FLT by thymidinkinase 1 than to the activity of nucleoside transporter reflecting the high proliferation rate of high grade gliomas. Of note, the calculated rate of proliferation KI (see above) showed the strongest correlation to [18F]FLT uptake.

Figure 4: *Relationship between the ratio of [^{18}F]FLT uptake and its corresponding kinetic constants.* The transport rate K1 showed a weaker correlation to [^{18}F]FLT uptake than the phosphorylation rate k3 (K1: r=0.52, p=0.064; k3: r=0.6, p=0.029).

Comparison of proliferation activity as assessed in vivo by PET with the in vitro proliferation marker Ki-67

In order to proof which kinetic process of [^{18}F]FLT best assesses tumor cell proliferation we compared the image derived data with the in vitro proliferation marker Ki-67. Herewith, we used tumor probes that were obtained from PET imaged guided biopsies or resection. This allowed validating the PET derived findings head-to-head to immunohistochemistry. Here, we found that the phosphorylation rate of [^{18}F]FLT and the rate of tumor cell proliferation as assessed by KI strongly correlate to the expression of Ki-67 **(see Figure 5)**. Of note, neither [^{18}F]FLT nor [^{11}C]MET uptake ratios correlate to Ki-67 expression.

Figure 5: *Correlations between the in vivo derived kinetic constants of [^{18}F]FLT uptake and its corresponding histological Ki-67 staining.* There are significant correlations between the kinetic constant k3 (r=0.88, p<0.001), KI (r=0.79, p=0.004) and the proliferation index of Ki-67.

Concluding remarks

This study demonstrates that [^{18}F]FLT PET enables the non-invasive assessment of tumor cell proliferation in patients with high grade gliomas. Moreover, we show that kinetic analysis of [^{18}F]FLT is required to assess tumor cell proliferation since usual [^{18}F]FLT uptake ratios are not related to tumor cell proliferation as assessed by Ki-67 staining in vitro. These findings strongly encourage to further investigate the potential of [^{18}F]FLT kinetic analysis for the early prediction of clinical outcome and response to therapy in patients with gliomas. Moreover, we showed that blood curves can be non-invasively calculated out of the imaged derived data, thus avoiding invasive collection of arterial blood samples (Backes et al., 2009). Our findings indicate that [^{18}F]FLT PET might represent a highly sensitive method for the non-invasive assessment of therapy response of individual molecular targeted approaches.

6.2 Early detection of erlotinib treatment response in NSCLC by 3'-Deoxy-3'-[18F]-fluoro-L-thymidine ([^{18}F]FLT) positron emission tomography (PET).

The epidermal growth factor receptor (EGFR) signalling pathway represents a promising molecular target in the treatment of patients with advanced NSCLC. Inhibition of EGFR has shown clinical success in patients with advanced non-small cell lung cancer (NSCLC). Somatic mutations of EGFR were found in lung adenocarcinoma that lead to exquisite dependency on EGFR signaling; thus patients with EGFR-mutant tumors are at high chance of response to EGFR inhibitors (Lynch et al., 2004; Paez et al., 2004). However, imaging approaches affording early identification of tumor response in EGFR-dependent carcinomas have so far been lacking. In this study, we investigated head-to-head [^{18}F]FDG to [^{18}F]FLT PET for their potentials to non-invasively assess response to the EGFR tyrosine kinase inhibitor erlotinib in an EGFR dependent lung cancer model.

Material and Methods

Cell cultures

We used the EGFR-tyrosine kinase inhibitor (TKI) sensitive adenocarcinoma cell lines HCC827, PC9 and the resistant cell line H1975. All cell lines were maintained in RPMI 1640 supplemented with 10% heat inactivated fetal bovine serum (FBS, Roche Diagnostics, Mannheim, Germany), 1% penicillin and 1 % streptomycin (P/S, Life Technologies) at 37 ^{0}C in a 5% CO_2/95% air atmosphere.

Western blot analysis

Cells were serum-starved for 24h in the presence or absence of erlotinib. After preparation of cell lysates phosphorylation level of the proteins were determined using antibodies for total EGFR, phospho-EGFR (pEGFR) (both purchased from Biosource), total Akt and phospho-Akt (pAKT) (both obtained from Cell Signaling Technology).

Apoptosis assay

Cells were plated in 6-well plates and incubated for 24h at 5% CO_2 and 37°. Cells were then treated with 0.5 µM erlotinib for 12h, 24h, 36h, 48h, 72h, and 96h and were finally harvested after trypsinization. Then cells were washed with PBS, resuspended in Annexin-V binding buffer and finally stained with Annexin-V-FITC and PI. FACS analysis was performed on a FACS Canto Flow Cytometer (BD Biosciences, Germany) and results were finally calculated using FACS Diva Software.

Cell cycle analysis

Cells were fixed and then treated with RNase A (500 µg/ml). Following resuspension of the cells in propidium iodide and in sodium citrate cells were analysed for DNA content by flow cytometry.

Xenograft model

All animal procedures were in accordance with the German Laws for Animal Protection and were approved by the local animal committee and the Bezirksregierung Köln. Tumors were generated by s. c. injecting 5×10^6 tumor cells into *nu/nu* athymic male mice. When tumors had reached a size of 100 mm^3, animals were randomized into two groups, control (vehicle) and erlotinib-treated mice. Erlotinib (Tarceva) was dosed at 6% Captisol (CyDex, Inc., Lenexa, KS) in water for solution over night. All controls were dosed with the same volume of vehicle. After PET measurement mice were treated daily by oral gavage of 50mg/kg Tarceva. Tumor size was monitored every two days by measuring perpendicular diameters. Tumor volumes were calculated from the determination of the largest diameter and its perpendicular according to the equation [tumor volume = a x (b^2/2)].

PET imaging

Tumor bearing mice were investigated using a R4 microPET scanner (Concord Microsystems, Inc., Knoxville, TN). [^{18}F]FLT and [^{18}F]FDG synthesis were produced in house with a radiolabeling yield of 10 % ± 1.5% and a radiochemical purity of higher than 98%. No-carrier-added [^{18}F]FLT was administered i.v. (tail vein) into experimental animals with a dose of 200 µCi/mouse. No-carrier-added [^{18}F]FDG was injected intraperitoneally (i.p.) with a dose of 200 µCi. Since the biodistribution of

[^{18}F]FDG is comparable for i.v. and i.p. injections after 60min and i.p. injections allow for a more accurate dosage of tracer injection, we decided to use intraperitoneal injections for [^{18}F]FDG. All PET images were performed 60 min after injection. Data evaluation was based on a volume of interest (VOI) analysis of the entire tumor by the use of the in-house VINCI software. For data analysis I assessed the maximal voxel radioactivity within the tumors. I calculated the uptake ratio as described above with the mediastinum as reference. Data were decay corrected and divided by the total injected dose to represent percentage injected dose per gram (%ID/g).

Immunohistochemistry and TUNEL detection

After the last PET measurements animals were sacrificed and s.c. tumors were extracted. After fixation (4% paraformaldehyde, 4^{0}C, 24h; 30% sucrose, 4^{0}C, 24h), tumors were embedded in tissue freezing medium (Jung, Nussloch, Germany) and cut in 10-µm frozen sections. H&E staining on the tissue was done according to standard protocols. Tumor proliferation was assessed using an anti-Ki-67 monoclonal antibody (1:200 dilution, KI6811C06, DCS, Hamburg, Germany), and the percentage of specifically stained cancer cells for Ki-67 was calculated. The number of Ki-67 positive nuclei was determined as percentage of Ki-67 stained nuclei per total number of nuclei in three representative tumor areas ((F1+F2+F3)/3 (%)) that contained the highest average fraction of labelled cells. To quantify the number of apoptotic positive cells TUNEL was performed on cryostat tumor slices with the DeadEnd^{TM} TUNEL system (Promega). Cells were fixed in 4%PFA. Cells were then permeablized with 100ml Proteinase K (20µg/ml). The average numbers of TUNEL positive were counted in three randomly selected fields in two tumor samples from each cell line.
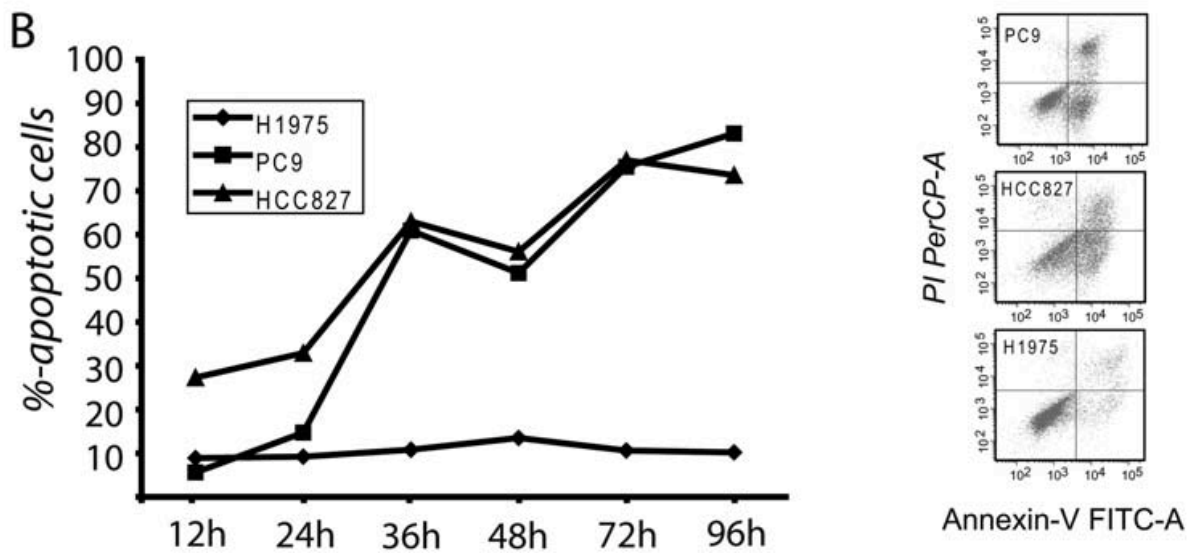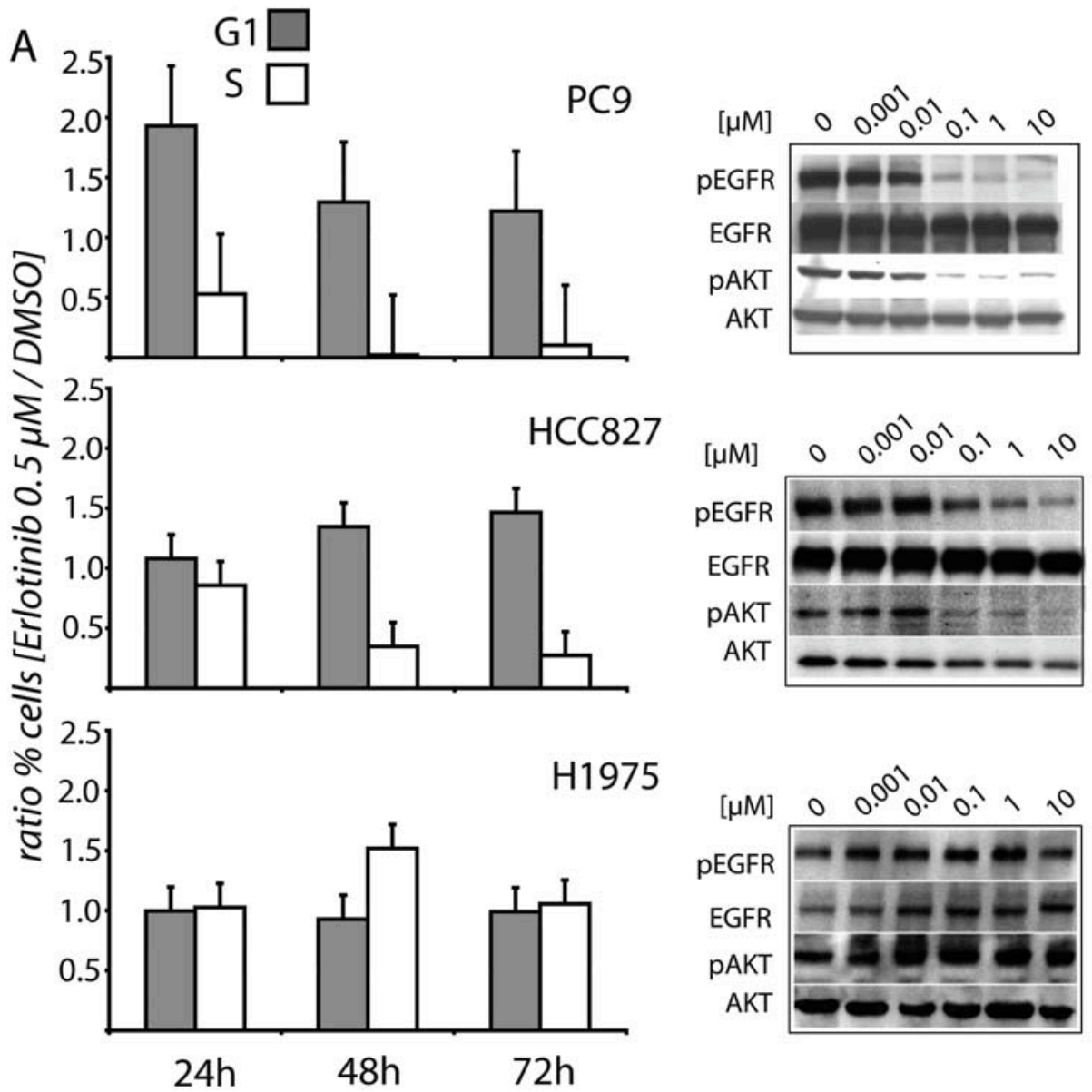
Statistical analysis

Wilcoxon test was performed using SPSS software (release 11.0.1 SPSS, Inc., Chicago. IL.USA), statistical significance was set at $p<0.05$.

Results

In vitro detection of EGFR oncogene dependancy

As a model of EGFR-dependent NSCLC, we employed the cell lines HCC827 and PC9. Both cell lines carry mutated as well as amplified EGFR alleles and are highly sensitive to the EGFR TKI erlotinib in the low nanomolar range (Moyer et al., 1997). As control for the specificity of drug action we used the cell line H1975 expressing both the L858R mutation of EGFR as well as the T790M EGFR resistance mutation. After 24h of treatment with even low doses of erlotinib, we found that the EGFR-sensitive PC9 and the HCC827 cells were arrested in the G1 phase of the cell cycle following erlotinib treatment with a concomitant decrease of cells in the S phase of the cell cycle **(Figure 6A)**. Subsequent to the cell cycle arrest the sensitive cell lines PC9 and HCC827 underwent massive apoptotic cell death 36h after onset of treatment **(Figure 6B)**. This was paralleled by reduction in p-EGFR and p-Akt levels in both cell lines **(Figure 6A)**. In contrast, the T790M-mutant cell line H1975 showed no cell cycle arrest **(Figure 6A)**, no loss of EGFR or Akt phosphorylation **(Figure 6A)** and did not exhibit any signs of apoptotic cell death **(Figure 6B)**, confirming that the observed phenotypes were due to on-target effects of the drug.
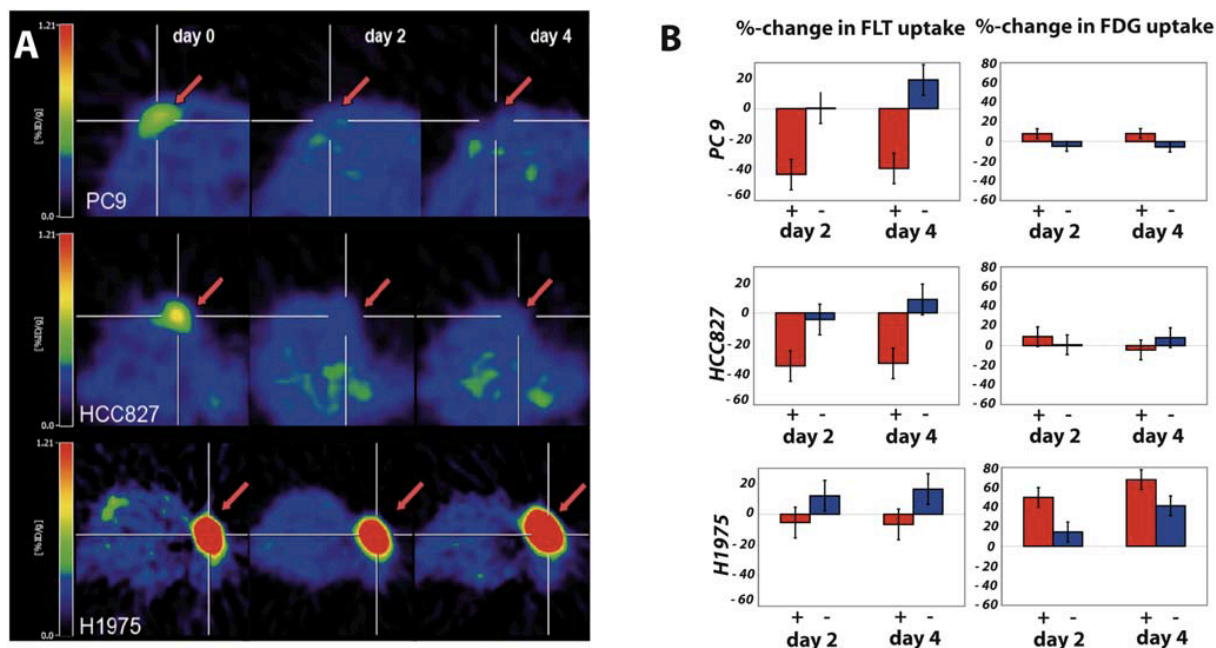
Figure 6: *Erlotinib treatment induces down-regulation of EGFR/EGFR-coupled signaling pathways and cell cycle arrest with subsequent induction of apoptosis in EGFR sensitive tumor cells.* The cell lines HCC827 and PC9 and the T790M cell line H1975 were treated with the indicated doses of erlotinib for 24 hours. Whole-cell lysates were subjected to immunoblotting with the indicated antibodies (A). PC9, HCC827 and H1975 cells were treated with erlotinib (0.5 µM) for 24h, 48h and 72h and analyzed by flow cytometry. Results are shown for the G1 and S phases of the cell cycle (A). Apoptotic effects of erlotinib on EGFR-sensitive cell lines in comparison to the T790M mutant H1975 (B). Annexin V FACS was performed 12h, 24h, 36h, 48h, 72h and 96h after 0.5 µM erlotinib treatment. Images show Annexin V-positive cells after 48h in the different cell lines.
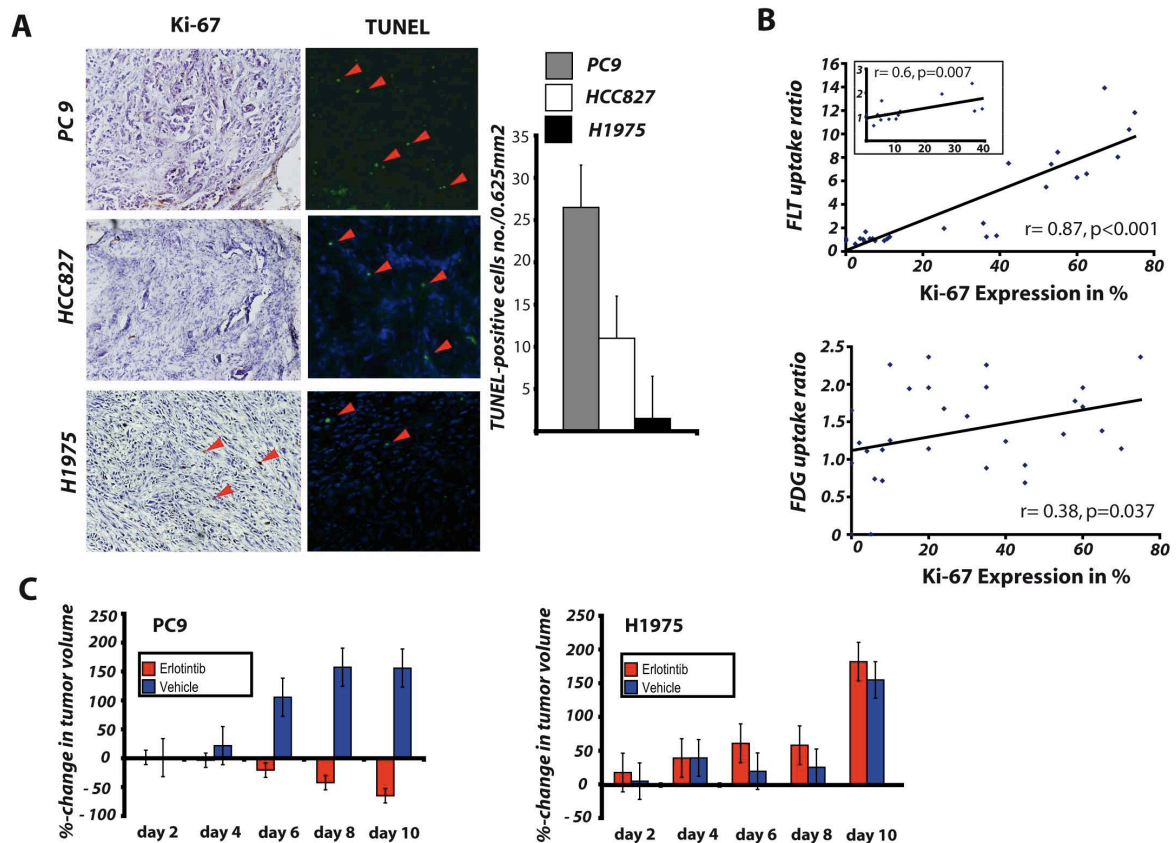
Imaging EGFR inhibition in vivo

In a next step we investigated the feasibility of [^{18}F]FLT and [^{18}F]FDG PET to measure response to erlotinib treatment in a murine tumor xenograft model. HCC827, PC9 and H1975 cell lines were transplanted subcutaneously onto nude mice. After oral treatment with either vehicle or erlotinib (50 mg/kg), mice were imaged by [^{18}F]FLT or [^{18}F]FDG PET. After only 48h of erlotinib treatment we observed a striking reduction of [^{18}F]FLT uptake in the sensitive cell lines HCC827 and PC9. By contrast, no changes in [^{18}F]FLT uptake were observed in mice bearing the resistant cell line H1975 or in the control group treated with the vehicle alone **(Figure 7A)**. After four days of erlotinib treatment [^{18}F]FLT uptake remained decreased in HCC827 and PC9 tumors whereas we observed no decrease in [^{18}F]FLT uptake in the H1975 tumor xenografts. Thus, the reduction in [^{18}F]FLT uptake reflects inhibition of cellular proliferation due to induction of a G1 arrest in EGFR-dependent tumors.

We observed a slight decrease in [^{18}F]FDG uptake after 4 days of erlotinib treatment only in the HCC827 but not in the PC9 xenograft. However, this reduction was far less pronounced in comparison to the results observed with [^{18}F]FLT **(Figure 7B)**. Thus, in our analysis [^{18}F]FLT PET appeared to be superior in detecting response of EGFR-mutant tumors to EGFR inhibition than [^{18}F]FDG PET.

Figure 7: *[^{18}F]FLT PET predicts response to erlotinib therapy as early as 2 days after initiation of treatment*. In **(A)** a representative [^{18}F]FLT PET image of a mouse bearing the sensitive PC9, HCC827 and the resistant H1975 xenografts before beginning of treatment, 48h and 96h after daily erlotinib treatment (Tarceva, 50mg/kg). **(B)** Quantitative analysis of changes in [^{18}F]FLT and [^{18}F]FDG uptake ratios after 48h and 96h daily erlotinib treatment vs. vehicle only as control.

In order to determine whether our in vitro observation of apoptosis following cell cycle arrest was reflected in vivo we analyzed tumor specimens extracted after 4 days of erlotinib treatment for the presence of apoptotic cells by TUNEL staining. This analysis revealed the presence of apoptotic cells in the sensitive cell lines but not in the T790M-carrying tumors **(Figure 8A)**. Most importantly, the appearance of apoptotic cells in the sensitive cells was reflected in dramatic tumor shrinkage starting at day 6 of treatment **(Figure 8C)**. Together, these findings show that that a decrease in [^{18}F]FLT PET is not only reflective of tumor cells arrested in G1 but also predicts induction of apoptotic cell death and tumor response in EGFR-addicted tumors treated with erlotinib.

Figure 8: *Immunostaining of the frozen tissue samples for Ki-67 and TUNEL, relation of [^{18}F]FLT and [^{18}F]FDG uptake to Ki-67 expression, and measurement of tumor volume shrinkage.* (A) Frozen tissue sections were stained for Ki-67 and TUNEL (magnification 10x). Columns, average number of TUNEL positive cells (green cells) were counted in three randomly selected field (area 0.625mm^2) in two tumor samples for each cell line. The Ki-67 labeling index as assessed by the percentage of nuclei stained with MIB-1 per total number of nuclei was compared to uptake ratios of [^{18}F]FLT and [^{18}F]FDG (B). Effects of daily Erlotinib treatment on the tumor size of the xenografts for the assessment of tumor response (C).

32

Concluding remarks

In this study we could demonstrate that [^{18}F]FLT PET is not only an accurate tool to assess tumor cell proliferation in vivo but most importantly a highly sensitive marker to detect treatment response of molecular targeted compounds. Since the selection of patients that benefit from molecular targeted treatment remains crucial [^{18}F]FLT PET might enable to detect treatment response non-invasively and to an early time point. This shall reduce the risk of treatment induced side effects and to enable to offer patients the best individual treatment strategy. Of note, these results built the basis for a clinical study at the University hospital of Cologne that is about to be finished. Here, Zander et al could demonstrate that as seen in the mouse model [^{18}F]FLT enables detecting patients that response to Erlotinib treatment as early as 7 days after initiation of the treatment (Zander et al, in preparation).

6.3 [11C]Methionine positron emission tomography as diagnostic marker for the malignant progression and the formation of angiogenesis in patients with gliomas.

Gliomas are the most frequent brain tumors. The decision for the specific tumor treatment in gliomas is mainly dependent on the grading according to WHO classification. Thus, the early detection of malignant transformation in gliomas from WHO grade II to grade III or from grade III to grade IV is of high clinical importance. However, malignant progression in gliomas is unpredictable and in many cases not clearly detectable on the basis of clinical symptoms and/or MRI findings, alone. In order to decipher the grading, tissue samples have to be obtained by invasive methods as stereotactical biopsy or surgery that are accompanied by high risks for the patients. In previous studies it has been shown that [^{11}C]MET uptake in gliomas is correlated to the histological grading. However, high inter-individual variability of [^{11}C]MET uptake in gliomas does not allow for a non-invasive grading. The purpose of this study was to investigate the potential of intra-individual changes in [^{11}C]MET metabolism in PET to non-invasively detect malignant progression in patients with gliomas.

Patients, Material and Methods

Patients

In this retrospective study, 24 patients with primary supratentorial cerebral gliomas were included. We investigated 14 men and 10 women after having given their written informed consent (mean age 40, SD 11.6 years). All patients that underwent repeat [^{11}C]MET PET imaging and had corresponding neuropathological diagnosis during the time period from 1993 till 2006 were included in the study. The [^{11}C]MET PET investigations were part of the routine preoperative diagnostic procedure and used for guidance of the biopsy from the tumor part with highest [^{11}C]MET uptake. Repeated PET investigations with the corresponding biopsy were performed when there were suspicious findings for tumor progression on MRI/CT and/or suggestive clinical symptoms. The time interval between PET measurements differed from 1 month to 6 years. Information on patients included age, gender, presence of contrast

enhancement on magnetic resonance imaging (MRI) or computerized tomography (CT) scan, and extent of surgical resection (13 stereotactic biopsies, 23 subtotal resections and 21 macroscopic total resections). The tumors were classified according to the World Health Organisation classification of neuroepithelial tumors (WHO). In the initial diagnosis tumor types were distributed as follows: astrocytoma WHO grade II (n=7), anaplastic astrocytoma WHO grade III (n=4), oligoastrocytoma WHO grade II (n=7), anaplastic oligoastrocytoma WHO grade III (n=2), oligodendroglioma WHO grade II (n=1), anaplastic oligodendroglioma WHO grade III (n=2) and glioblastoma WHO grade IV (n=1).

PET

For PET imaging we used an ECAT EXACT (CTI/Siemens; in plane full width at half maximum, 6mm; slice thickness, 3.375; axial field of view, 162 mm) and an ECAT EXACT HR (CTI/Siemens, in plane full width at half maximum, 3.6 mm; slice thickness 3.125 mm; axial field of view, 150 mm). Subsequent images were acquired on the same scanner. All patients fasted for at least 4 hours before PET. Images were acquired in a supine position with eyes closed. Before tracer application a 10-min transmission scan with 3 rotating 68Ga/68Ge sources was performed. [^{11}C]MET was injected intravenously as a bolus injection of 740 MBq (20 mCi). Accumulation of the tracer was recorded over 40 min in 47 transaxial slices of the entire brain. The spatial resolution was 6 mm or better in all dimensions.

Except 4, all PET scans had corresponding contrast enhanced MRI or CT studies. Regions of [^{11}C]MET uptake were compared to areas of contrast enhancement in MRI.

PET data evaluation was performed using a region of interest (ROI) analysis. As [^{11}C]MET uptake at later imaging time points more specifically reflects transport activity rather than early time points we used summed images covering the time frame 20 to 60 minutes after injection for data analysis. As described by Herholz et al. a circular region of interest of 7 mm diameter was placed on the area of the highest [^{11}C]MET uptake to determine the maximal tracer uptake (Herholz et al., 1998). A ROI of the same diameter was placed on the contralateral-mirrored region to measure the corresponding reference. The relative index of [^{11}C]MET uptake was calculated from the ratio of tumor area to the contralateral tissue. The change of

[^{11}C]MET uptake was defined as the relative percentage change between [^{11}C]MET uptakes of two subsequent scans in the same patient.

Histological analysis

Histological analysis and immunohistochemistry of the biopsies of the initial tumors of all patients as well as recurrences obtained by stereotactic biopsy or open surgery were performed on formalin-fixed, paraffin-embedded 4 μm sections. For immunohistochemistry, an automated staining system (Biogenex, San Ramon, CA, USA) using the ABC technique and 3,3'-diaminobenzidine as chromogene and H_2O_2 as co-substrate, was used. In brief, classification of the tumors according to the WHO classification of neuroepithelial tumors was based on H&E staining and immunohistochemistry with monoclonal antibodies against rabbit anti-human MIB-1 (DCS, Hamburg, Germany; clone SP6 (Ki-67 antigen); dilution 1:200) and mouse anti-human p53-protein (Biogenex; clone 1801; dilution 1:200) and polyclonal rabbit anti-human antibodies against GFAP and S100-protein (Dako, Hamburg, Germany; dilution GFAP 1:1000, S100-protein 1:2000). Advanced immunohistochemistry was performed with the following monoclonal mouse anti-human antibodies: EGFR (Merck, Darmstadt, Germany; clone E30; dilution 1:20), PDGFR (BD Biosciences, Heidelberg, Germany; clone 28; dilution 1:200), pRb (Zymed Laboratories, Karlsruhe, Germany; clone Rb1; dilution 1:50), PTEN (Biogenex; clone 28H6; dilution 1:10), and VEGF (DCS; clone VG1; dilution 1:50). Histological evaluation was performed by two independent neuropathologists. The number of immunoreactive nuclei were determined comprising three areas (F1, F2, and F3) of three high power fields each, with maximal frequency, moderate frequency, and minimal frequency, respectively, of immunoreactive nuclei. The number of positive nuclei was determined as F1+F2+F3/3 (%).

Statistical analysis

Statistical analyses were performed by SPSS software (Release 11.0.1, SPSS Inc., Chicago, IL, USA). For correlation analysis, the Pearson method was applied with subsequent parametric tests; two-sample ANOVAs were used for comparisons between the groups with and without malignant progression. Tests were performed two-sided at the significance level 0.05, and the p-values were understood in an explorative sense regarding the multiple hypotheses problem. Sensitivity and
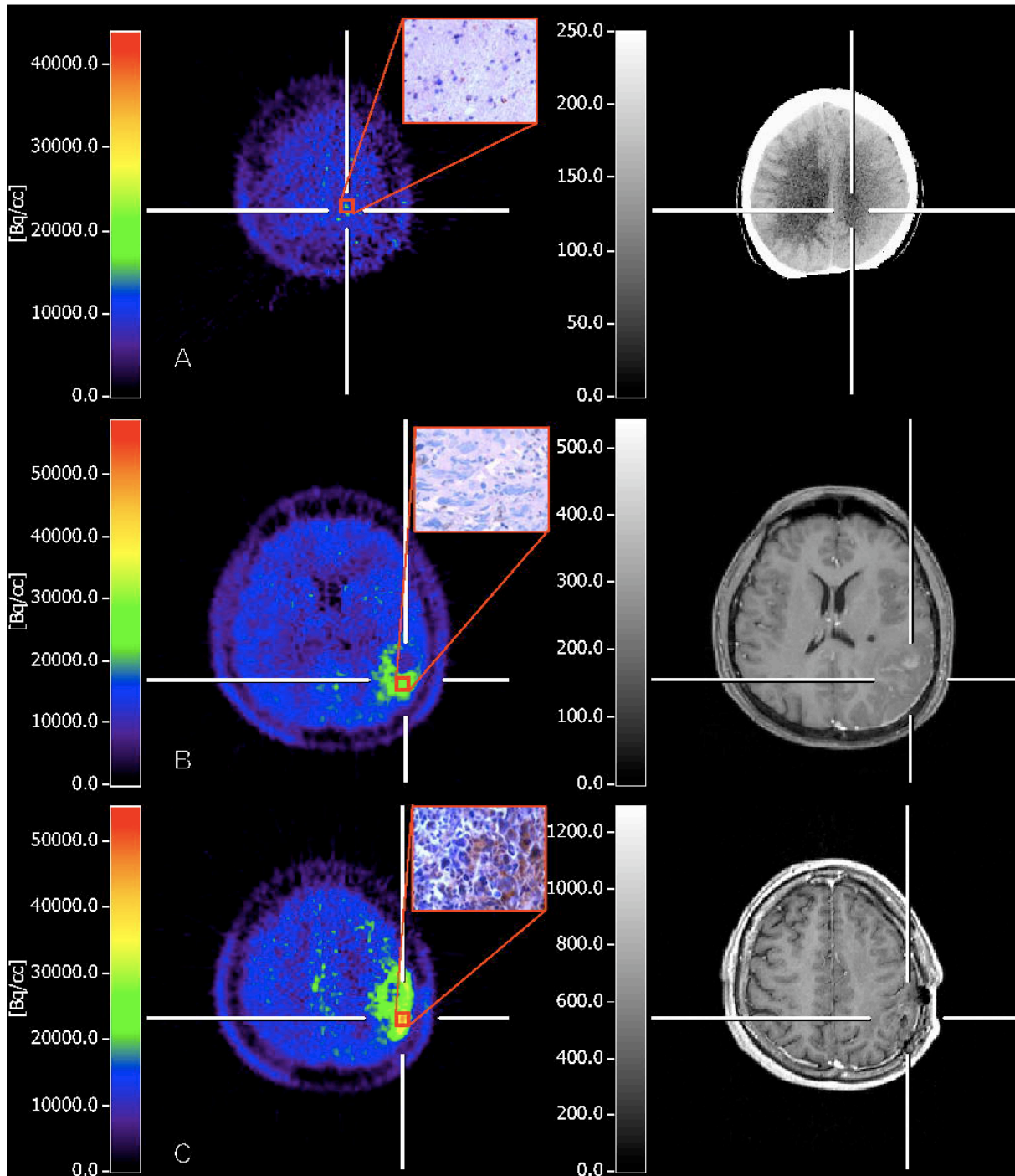
specificity of changes in [^{11}C]MET uptake were calculated for several thresholds and the optimum cut-off was determined by receiver operation characteristics (ROC) analysis. An iterative leave-one-out approach was used to validate the ROC analysis. At each step, one case (i.e. one follow-up) was left out for the analysis, a fit of the model was produced for the remaining follow-ups and a malignant progression prediction was made for the left-out case. This means that each single follow-up value was compared with the cohort of the remaining 32/33 values with regards to its individual percent change of [^{11}C]MET uptake. Moreover, baseline [^{11}C]MET uptake was included as a covariate in a Cox regression model to investigate its relation to the time to histological progression. In order to avoid artificial variance reduction by mixing independent and dependent observations, we used only the data of the first follow-up investigation (n=24) for all methods of statistical inference (Pearson method and two-sample ANOVA).

Results

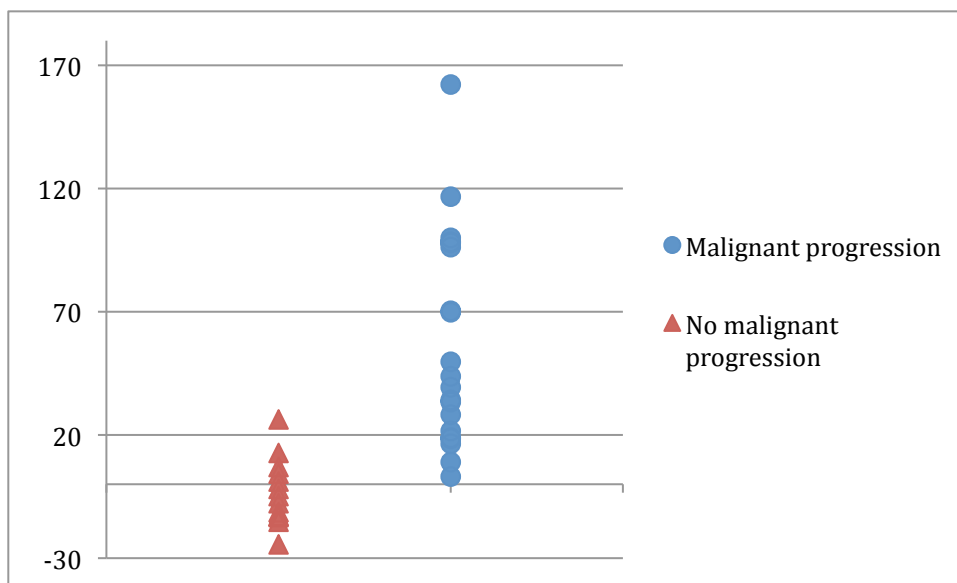### Malignant progression as detected by [^{11}C]MET PET

In 24 patients with repetitive [^{11}C]MET PET investigations and the corresponding histological determined WHO grade we investigated the correlation between changes [^{11}C]MET uptake and histological progression of the tumor. We calculated the percentage change in [^{11}C]MET uptake from the prior [^{11}C]MET PET investigation compared to the subsequent examination. The percent change in [^{11}C]MET uptake was then compared with the progression as assessed by histology and immunohistochemistry **(Figure 9)**.

Figure 9: *[¹¹C]MET PET of a 39 y.o. man with a malignant progression of a recurrent glioma*. In (A) the newly diagnosed astrocytoma grade II with an average [¹¹C]MET uptake of 1.3 to the contralateral gray matter, without any CE on CCT and no immunohistochemical VEGF expression. In (B) one year later the patient presented with a malignant progression to an astrocytoma grade III associated with a significant increase of [¹¹C]MET uptake to the 2.1-fold and only slight contrast enhancement outside of the metabolic active tumor. Histological analysis from the
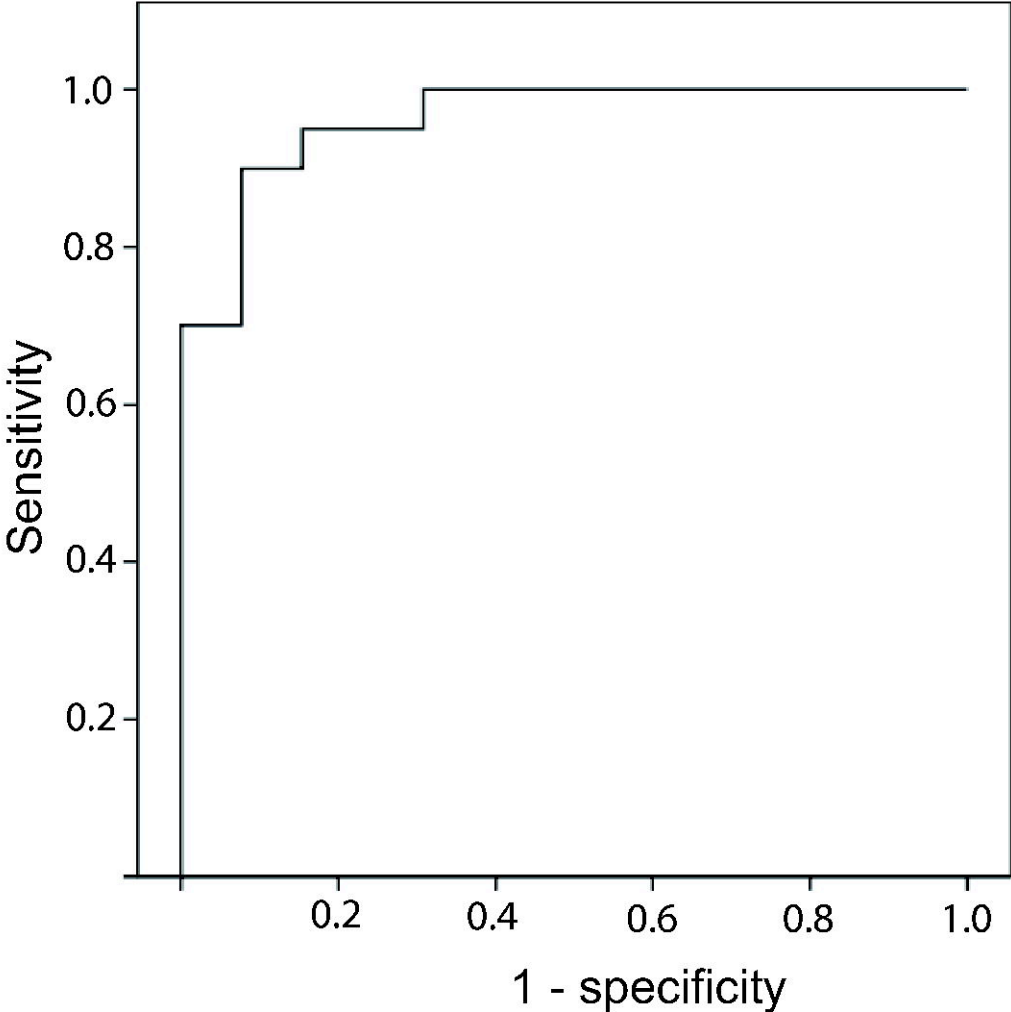
resection showed an increase in cellularity and numerous pleomorphic nuclei and low VEGF expression. (C) In the following year the resection of the tumor confirmed again a malignant progression to a glioblastoma multiforme showing markedly increased uptake of [^{11}C]MET to the 2.8-fold, marginal contrast enhancement in MRI and ~35% of the tumor cells expressing VEGF (original magnification x 400).

Here, we found that the mean percent increase of [^{11}C]MET uptake from the prior [^{11}C]MET PET to the following [^{11}C]MET PET in patients with histologically proven malignant progression was much higher (mean 54.4 %, SD 45.5 %) than in patients without change of the tumor grade (mean 3.9 %, SD 13.7 %) **(Figure 10)**. Statistic analyses revealed a significant difference between changes in [^{11}C]MET uptake in the group with malignant progression in comparison to the group without malignant progression ($p < 0.001$).

Figure 10: *Comparison of changes in [^{11}C]MET uptake between patients with malignant progression and without malignant.* Patients presenting histologically proven progression in WHO grading show a significant increase in [^{11}C]MET uptake according to the prior PET investigation (Values reflect the %-change in [^{11}C]MET uptake from the prior to the following investigation).

We next performed receiver operating characteristics (ROC) analysis to assess the value of change in [^{11}C]MET uptake that best identifies malignant progression **(Figure 11)**. ROC revealed that an increase of 14.6 % determines malignant progression with a sensitivity of 90 % and a specificity of 92.3 %.

Figure 11: *Receiver-operating-characteristic (ROC) analysis to identify the change of [^{11}C]MET uptake for differentiation between malignant progression of the tumor grade from no malignant progression.* The percent increase that best distinguished malignant progression from no malignant progression was at a threshold of 14.6 % with a sensitivity of 90 % and a specificity of 92.3 %.

Correlate of [¹¹C]MET uptake to immunohistochemical tumor marker as determined by histology

We next sought to analyse the relation of changes in [¹¹C]MET uptake to changes of molecular markers as assessed by immunohistochemistry. Here, we found that changes of [¹¹C]MET uptake are related to the expression of the vascular endothelial growth factor (VEGF). However, we did not find a significant correlation between changes in EGFR, PTEN, pRb, p53, Ki-67 and platelet derived growth factor receptor (PDGFR) expression and changes in [¹¹C]MET uptake.

Concluding remarks:

These findings indicate that [¹¹C]MET PET represents an accurate marker to non-invasively detect malignant progression in gliomas. Furthermore, it is well known that the mammalian target of Rapamycin (mTOR) is located downstream of the VEGF / VEGFR2 pathway via PI3K/AKT regulated by VEGF (Kim et al., 2008; Riesterer et al., 2004). mTor again modulates amino-acid transport by regulating the expression of LAT1 (Fuchs and Bode, 2005). Although the correlation between changes in [¹¹C]MET uptake and VEGF expression is relatively weak, we hypothesize that there might be a crosslink between VEGFR2 signalling and amino-acid transport. The activation of VEGF / VEGFR2 signalling induces mTOR kinase activity with mTor being one of the key enzymes regulating amino acid transport. The hypothesis that [¹¹C]MET uptake may serve as surrogate marker for activated VEGFR signalling remains to be investigated.

7. References

Backes, H., **Ullrich, R.**, Neumaier, B., Kracht, L., Wienhard, K., and Jacobs, A.H. (2009). Noninvasive quantification of (18)F-FLT human brain PET for the assessment of tumour proliferation in patients with high-grade glioma. Eur J Nucl Med Mol Imaging.

Baselga, J., Tripathy, D., Mendelsohn, J., Baughman, S., Benz, C.C., Dantis, L., Sklarin, N.T., Seidman, A.D., Hudis, C.A., Moore, J.*, et al.* (1996). Phase II study of weekly intravenous recombinant humanized anti-p185HER2 monoclonal antibody in patients with HER2/neu-overexpressing metastatic breast cancer. J Clin Oncol *14*, 737-744.

Been, L.B., Suurmeijer, A.J., Cobben, D.C., Jager, P.L., Hoekstra, H.J., and Elsinga, P.H. (2004). [18F]FLT-PET in oncology: current status and opportunities. Eur J Nucl Med Mol Imaging *31*, 1659-1672.

Buck, A.K., Halter, G., Schirrmeister, H., Kotzerke, J., Wurziger, I., Glatting, G., Mattfeldt, T., Neumaier, B., Reske, S.N., and Hetzel, M. (2003). Imaging proliferation in lung tumors with PET: 18F-FLT versus 18F-FDG. J Nucl Med *44*, 1426-1431.

Daley, G.Q., Van Etten, R.A., and Baltimore, D. (1990). Induction of chronic myelogenous leukemia in mice by the P210bcr/abl gene of the Philadelphia chromosome. Science (New York, NY *247*, 824-830.

Fuchs, B.C., and Bode, B.P. (2005). Amino acid transporters ASCT2 and LAT1 in cancer: partners in crime? Semin Cancer Biol *15*, 254-266.

Galldiks, N., **Ullrich, R.**, Schroeter, M., Fink, G.R., and Kracht, L.W. (2009). Volumetry of [(11)C]-methionine PET uptake and MRI contrast enhancement in patients with recurrent glioblastoma multiforme. Eur J Nucl Med Mol Imaging.

Herholz, K., Holzer, T., Bauer, B., Schroder, R., Voges, J., Ernestus, R.I., Mendoza, G., Weber-Luxenburger, G., Lottgen, J., Thiel, A.*, et al.* (1998). 11C-methionine PET for differential diagnosis of low-grade gliomas. Neurology *50*, 1316-1322.

Jacobs, A.H., Kracht, L.W., Gossmann, A., Ruger, M.A., Thomas, A.V., Thiel, A., and Herholz, K. (2005a). Imaging in neurooncology. NeuroRx *2*, 333-347.

Jacobs, A.H., Thomas, A., Kracht, L.W., Li, H., Dittmar, C., Garlip, G., Galldiks, N., Klein, J.C., Sobesky, J., Hilker, R.*, et al.* (2005b). 18F-fluoro-L-thymidine and 11C-methylmethionine as markers of increased transport and proliferation in brain tumors. J Nucl Med *46*, 1948-1958.

Jager, P.L., de Korte, M.A., Lub-de Hooge, M.N., van Waarde, A., Koopmans, K.P., Perik, P.J., and de Vries, E.G. (2005). Molecular imaging: what can be used today. Cancer Imaging *5 Spec No A*, S27-32.

Jager, P.L., Vaalburg, W., Pruim, J., de Vries, E.G., Langen, K.J., and Piers, D.A. (2001). Radiolabeled amino acids: basic aspects and clinical applications in oncology. J Nucl Med *42*, 432-445.

Kelloff, G.J., Krohn, K.A., Larson, S.M., Weissleder, R., Mankoff, D.A., Hoffman, J.M., Link, J.M., Guyton, K.Z., Eckelman, W.C., Scher, H.I., *et al.* (2005). The progress and promise of molecular imaging probes in oncologic drug development. Clin Cancer Res *11*, 7967-7985.

Kim, B.W., Choi, M., Kim, Y.S., Park, H., Lee, H.R., Yun, C.O., Kim, E.J., Choi, J.S., Kim, S., Rhim, H., *et al.* (2008). Vascular endothelial growth factor (VEGF) signaling regulates hippocampal neurons by elevation of intracellular calcium and activation of calcium/calmodulin protein kinase II and mammalian target of rapamycin. Cell Signal *20*, 714-725.

Kracht, L.W., Friese, M., Herholz, K., Schroeder, R., Bauer, B., Jacobs, A., and Heiss, W.D. (2003). Methyl-[11C]- l-methionine uptake as measured by positron emission tomography correlates to microvessel density in patients with glioma. Eur J Nucl Med Mol Imaging *30*, 868-873.

Kracht, L.W., Miletic, H., Busch, S., Jacobs, A.H., Voges, J., Hoevels, M., Klein, J.C., Herholz, K., and Heiss, W.D. (2004). Delineation of brain tumor extent with [11C]L-methionine positron emission tomography: local comparison with stereotactic histopathology. Clin Cancer Res *10*, 7163-7170.

Krohn, K.A., Mankoff, D.A., Muzi, M., Link, J.M., and Spence, A.M. (2005). True tracers: comparing FDG with glucose and FLT with thymidine. Nucl Med Biol *32*, 663-671.

Lynch, T.J., Bell, D.W., Sordella, R., Gurubhagavatula, S., Okimoto, R.A., Brannigan, B.W., Harris, P.L., Haserlat, S.M., Supko, J.G., Haluska, F.G., *et al.* (2004). Activating mutations in the epidermal growth factor receptor underlying responsiveness of non-small-cell lung cancer to gefitinib. N Engl J Med *350*, 2129-2139.

Macdonald, D.R., Cascino, T.L., Schold, S.C., Jr., and Cairncross, J.G. (1990). Response criteria for phase II studies of supratentorial malignant glioma. J Clin Oncol *8*, 1277-1280.

Miyagawa, T., Oku, T., Uehara, H., Desai, R., Beattie, B., Tjuvajev, J., and Blasberg, R. (1998). "Facilitated" amino acid transport is upregulated in brain tumors. J Cereb Blood Flow Metab *18*, 500-509.

Moyer, J.D., Barbacci, E.G., Iwata, K.K., Arnold, L., Boman, B., Cunningham, A., DiOrio, C., Doty, J., Morin, M.J., Moyer, M.P., *et al.* (1997). Induction of apoptosis and cell cycle arrest by CP-358,774, an inhibitor of epidermal growth factor receptor tyrosine kinase. Cancer research *57*, 4838-4848.

Muzi, M., Vesselle, H., Grierson, J.R., Mankoff, D.A., Schmidt, R.A., Peterson, L., Wells, J.M., and Krohn, K.A. (2005). Kinetic analysis of 3'-deoxy-3'-fluorothymidine PET studies: validation studies in patients with lung cancer. J Nucl Med *46*, 274-282.

Paez, J.G., Janne, P.A., Lee, J.C., Tracy, S., Greulich, H., Gabriel, S., Herman, P., Kaye, F.J., Lindeman, N., Boggon, T.J., *et al.* (2004). EGFR mutations in lung cancer: correlation with clinical response to gefitinib therapy. Science (New York, NY *304*, 1497-1500.

Phelps, M.E., and Mazziotta, J.C. (1985). Positron emission tomography: human brain function and biochemistry. Science *228*, 799-809.

Reinhardt, M.J., Kubota, K., Yamada, S., Iwata, R., and Yaegashi, H. (1997). Assessment of cancer recurrence in residual tumors after fractionated radiotherapy: a comparison of fluorodeoxyglucose, L-methionine and thymidine. J Nucl Med *38*, 280-287.

Riesterer, O., Zingg, D., Hummerjohann, J., Bodis, S., and Pruschy, M. (2004). Degradation of PKB/Akt protein by inhibition of the VEGF receptor/mTOR pathway in endothelial cells. Oncogene *23*, 4624-4635.

Sasaki, M., Kuwabara, Y., Yoshida, T., Nakagawa, M., Fukumura, T., Mihara, F., Morioka, T., Fukui, M., and Masuda, K. (1998). A comparative study of thallium-201 SPET, carbon-11 methionine PET and fluorine-18 fluorodeoxyglucose PET for the differentiation of astrocytic tumours. European journal of nuclear medicine *25*, 1261-1269.

Sato, N., Suzuki, M., Kuwata, N., Kuroda, K., Wada, T., Beppu, T., Sera, K., Sasaki, T., and Ogawa, A. (1999). Evaluation of the malignancy of glioma using 11C-methionine positron emission tomography and proliferating cell nuclear antigen staining. Neurosurgical review *22*, 210-214.

Shields, A.F., Grierson, J.R., Dohmen, B.M., Machulla, H.J., Stayanoff, J.C., Lawhorn-Crews, J.M., Obradovich, J.E., Muzik, O., and Mangner, T.J. (1998). Imaging proliferation in vivo with [F-18]FLT and positron emission tomography. Nat Med *4*, 1334-1336.

Sos, M.L.*, Fischer, S.*, **Ullrich, R.*,** Peifer, M.*, Heuckmann, J.M., Koker, M., Heynck, S., Stuckrath, I., Weiss, J., Fischer, F*., et al.* (2009). Identifying genotype-dependent efficacy of single and combined PI3K- and MAPK-pathway inhibition in cancer. Proceedings of the National Academy of Sciences of the United States of America. ***equally contributed**

Therasse, P., Arbuck, S.G., Eisenhauer, E.A., Wanders, J., Kaplan, R.S., Rubinstein, L., Verweij, J., Van Glabbeke, M., van Oosterom, A.T., Christian, M.C., *et al.* (2000). New guidelines to evaluate the response to treatment in solid tumors. European Organization for Research and Treatment of Cancer, National Cancer Institute of the United States, National Cancer Institute of Canada. J Natl Cancer Inst *92*, 205-216.

Thiel, A., Pietrzyk, U., Sturm, V., Herholz, K., Hovels, M., and Schroder, R. (2000). Enhanced accuracy in differential diagnosis of radiation necrosis by positron emission tomography-magnetic resonance imaging coregistration: technical case report. Neurosurgery *46*, 232-234.

Ullrich, R., Backes, H., Li, H., Kracht, L., Miletic, H., Kesper, K., Neumaier, B., Heiss, W.D., Wienhard, K., and Jacobs, A.H. (2008a). Glioma proliferation as assessed by 3'-fluoro-3'-deoxy-L-thymidine positron emission tomography in patients with newly diagnosed high-grade glioma. Clin Cancer Res *14*, 2049-2055.

Ullrich, R.T., Kracht, L., Brunn, A., Herholz, K., Frommolt, P., Miletic, H., Deckert, M., Heiss, W.D., and Jacobs, A.H. (2009). Methyl-L-11C-Methionine PET as a Diagnostic Marker for Malignant Progression in Patients with Glioma. J Nucl Med.

Ullrich, R.T., Kracht, L.W., and Jacobs, A.H. (2008b). Neuroimaging in patients with gliomas. Seminars in neurology *28*, 484-494.

Ullrich, R.T., Zander, T., Neumaier, B., Koker, M., Shimamura, T., Waerzeggers, Y., Borgman, C.L., Tawadros, S., Li, H., Sos, M.L*., et al.* (2008c). Early detection of erlotinib treatment response in NSCLC by 3'-deoxy-3'-[F]-fluoro-L-thymidine ([F]FLT) positron emission tomography (PET). PLoS One *3*, e3908.

Vesselle, H., Grierson, J., Muzi, M., Pugsley, J.M., Schmidt, R.A., Rabinowitz, P., Peterson, L.M., Vallieres, E., and Wood, D.E. (2002). In vivo validation of 3'deoxy-3'-[(18)F]fluorothymidine ([(18)F]FLT) as a proliferation imaging tracer in humans: correlation of [(18)F]FLT uptake by positron emission tomography with Ki-67 immunohistochemistry and flow cytometry in human lung tumors. Clin Cancer Res *8*, 3315-3323.

Wagner, M., Seitz, U., Buck, A., Neumaier, B., Schultheiss, S., Bangerter, M., Bommer, M., Leithauser, F., Wawra, E., Munzert, G*., et al.* (2003). 3'-[18F]fluoro-3'-deoxythymidine ([18F]-FLT) as positron emission tomography tracer for imaging proliferation in a murine B-Cell lymphoma model and in the human disease. Cancer Res *63*, 2681-2687.

Wells, P., Aboagye, E., Gunn, R.N., Osman, S., Boddy, A.V., Taylor, G.A., Rafi, I., Hughes, A.N., Calvert, A.H., Price, P.M*., et al.* (2003). 2-[11C]thymidine positron emission tomography as an indicator of thymidylate synthase inhibition in patients treated with AG337. J Natl Cancer Inst *95*, 675-682.

Young, H., Baum, R., Cremerius, U., Herholz, K., Hoekstra, O., Lammertsma, A.A., Pruim, J., and Price, P. (1999). Measurement of clinical and subclinical tumour response using [18F]-fluorodeoxyglucose and positron emission tomography: review and 1999 EORTC recommendations. European Organization for Research and Treatment of Cancer (EORTC) PET Study Group. Eur J Cancer *35*, 1773-1782.

Zhao, S., Kuge, Y., Mochizuki, T., Takahashi, T., Nakada, K., Sato, M., Takei, T., and Tamaki, N. (2005). Biologic correlates of intratumoral heterogeneity in 18F-FDG distribution with regional expression of glucose transporters and hexokinase-II in experimental tumor. J Nucl Med *46*, 675-682.

8. Acknowledgments

9. Appendix: Publications I-III

Glioma Proliferation as Assessed by 3'-Fluoro-3'-Deoxy-L-Thymidine Positron Emission Tomography in Patients with Newly Diagnosed High-Grade Glioma

Roland Ullrich,[1,2] Heiko Backes,[3] Hongfeng Li,[1] Lutz Kracht,[1] Hrvoje Miletic,[4] Kristina Kesper,[1] Bernd Neumaier,[1] Wolf-Dieter Heiss,[1] Klaus Wienhard,[1] and Andreas H. Jacobs[1,2,5]

Abstract

Purpose: The aim of this study was to investigate the relationship between the *in vivo* derived kinetic parameters of 3'-deoxy-3'-^{18}F-fluorothymidine (^{18}F-FLT) and the proliferation rate measured *in vitro* by Ki-67 staining in patients with newly diagnosed high-grade gliomas.

Experimental Design: Thirteen patients with newly diagnosed high-grade gliomas were investigated with ^{18}F-FLT and *methyl*-[11]C- L-methionine (^{11}C-MET) positron emission tomography (PET) and T1-, Gd-T1 −, and T2-weighted magnetic resonance imaging on consecutive days. Tracer kinetic parameters of ^{18}F-FLT as well as the standardized uptake value and the tumor-to-background (T/B) ratio of ^{18}F-FLT and ^{11}C-MET were determined. Data of kinetic modeling, standardized uptake value, and T/B values derived from ^{18}F-FLT-PET were compared with T/B values derived from ^{11}C-MET-PET and to the *in vitro* proliferation marker Ki-67.

Results: A significant correlation was observed between the metabolic rate constant Ki and the proliferation index as measured by Ki-67 immunostaining [Ki, r = 0.79 (*P* = 0.004)]. Also, the phosphorylation rate constant k3 correlated with Ki-67 [k3, r = 0.76 (*P* = 0.006)], whereas the rate constant for transport through the blood brain barrier K1 showed a weaker correlation with Ki-67 [K1, r = 0.62 (*P* = 0.044)]. No significant correlation between ^{11}C-MET and ^{18}F-FLT uptake ratios and Ki-67 was observed.

Conclusions: This study shows that kinetic analysis of ^{18}F-FLT tracer uptake is essential for the *in vivo* assessment of tumor proliferation in high-grade gliomas, whereas uptake ratios of ^{11}C-MET and ^{18}F-FLT failed to correlate with the *in vitro* determined proliferation marker. Thus, kinetic analysis of ^{18}F-FLT might provide an accurate method for the assessment of early response to glioma treatment in the future.

Positron emission tomography (PET) with radiolabeled amino and nucleic acids allows metabolic imaging of tumor activity *in vivo*. *Methyl*-[11]C- L-methionine (^{11}C-MET) and 2-^{18}F-fluoro-deoxy-D-glucose have been established as markers in the diagnosis of gliomas. 2-^{18}F-fluoro-deoxy-D-glucose enables to detect brain tumors because of their increased glucose consumption. However, the high cortical background level of glucose limits the capacity of 2-^{18}F-fluoro-deoxy-D-glucose to distinguish tumoral tissue from normal brain tissue. ^{11}C-MET enables to determine with high sensitivity the delineation of the extent of the tumor, the effect of treatment, and the differentiation of recurrent tumor from radiation necrosis (1). Methionine uptake correlates to microvessel density (2), to the proliferative cell nuclear antigen index indicating the malignancy of brain tumors (3), and to the expression of the LAT1 amino acid transporter (4). However, kinetic analysis remains limited because of the short half-life of ^{11}C and the fast metabolism of ^{11}C-MET.

Shields et al. (5) have developed 3'-deoxy-3'-^{18}F-fluoro-L-thymidine (^{18}F-FLT) as a tracer to image proliferation *in vivo*. They established ^{18}F-FLT as an analogue substrate of thymidine, which is intracellulary phosphorylated by the thymidine kinase 1 (TK1). TK1 is a cytosolic enzyme that is expressed with the onset of the S phase during DNA synthesis and that is decreased in nondividing cells. Activity of TK1 increases up to 10-fold during the S phase, after which it is directly degraded (6). Compared with normal proliferating tissue, the increase of TK1 activity is even higher in proliferating tumor cells (7) and can be imaged by ^{18}F-FLT as selective substrate for TK1 that converts ^{18}F-FLT to its nucleotide monophosphate. This ^{18}F-FLT monophosphate is not further metabolized and accumulates in the cell.

In several clinical studies, ^{18}F-FLT has been validated to assess proliferation of different types of tumors *in vivo* (8–11). Correlations between the standard uptake value (SUV) of

^{18}F-FLT and the Ki-67 expression *in vitro* have been shown in lung cancer, malignant lymphoma, colorectal cancer, and recently, in brain tumors (12–15). In a mixed population of patients with newly diagnosed and recurrent gliomas, our group recently showed that ^{18}F-FLT uptake (*a*) enables to differentiate between low-grade and high-grade tumors; (*b*) is mainly due to increased transport and to a lower extent to phosphorylation by TK1; and, finally, (*c*) that ^{18}F-FLT-, ^{11}C-MET-PET, as well as Gd-enhanced magnetic resonance imaging (MRI) yield complementary information on the activity and the extent of gliomas (16).

The long half-life of ^{18}F allows for kinetic analysis, providing the differentiation between metabolized and nonmetabolized ^{18}F-FLT in the tissue. Especially in brain tumors, kinetic modeling enables to distinguish between increased ^{18}F-FLT uptake due to increased transport through the blood brain barrier (BBB) and increased uptake due to an increased TK1 activity (16, 17).

The aim of this study was to measure tumor proliferation noninvasively *in vivo* in patients with nontreated newly diagnosed high-grade gliomas using kinetic modeling and to investigate the correlation between the kinetic parameters of ^{18}F-FLT and the immunohistochemical proliferation marker Ki-67.

Materials and Methods

Patients

Thirteen patients suffering from newly diagnosed primary central nervous system tumors (9 male and 4 female; median age, 64.0 y; range, 35-71 y) were included in this prospective study after giving their written informed consent on multimodal PET and MRI. The study protocol differed from our previous study (16) only with respect to patients with newly diagnosed tumors. After the PET scan, except for one, all gliomas were confirmed by histology and classified according to WHO grade (stereotactic biopsy, *n* = 7; resection, *n* = 5). Five patients were classified as astrocytoma grade III, one as oligoastrocytoma grade III, and six as glioblastoma (grade IV; Table 1). All patients underwent Gd-diethylenetriaminepentaacetic acid–enhanced MRI within 6 d before the PET investigation. PET investigation was done when there were suspicious findings for tumor proliferation in the MRI.

PET

Data acquisition. PET imaging was done on an ECAT EXACT (CTI/Siemens; in-plane full-width at half maximum, 6 mm; slice thickness, 3.375 mm; axial field of view, 162 mm) and an ECAT EXACT HR (CTI/Siemens; in-plane full-width at half maximum, 3.6 mm; slice thickness, 3.125 mm; axial field of view, 150 mm). Ten-minute transmission scans with rotating germanium-68/gallium-68 sources were done for attenuation correction of the PET data.

[11]C-MET and ^{18}F-FLT syntheses were done as described previously (16). The radiolabeling yield of ^{18}F-FLT was 10% ± 1.5%, and the radiochemical purity of ^{18}F-FLT was >98%.

The mean injected dose of ^{18}F-FLT was 321.9 ± 85.1 MBq (range, 111-370 MBq). From all patients, arterialized blood samples were taken by a peripheral i.v. catheter. ^{18}F-FLT-PET images were acquired in the following dynamic sequence: 6×10, 3×20, 2×30, 2×60, 2×150, and 16×300 s.

Tracer accumulation was recorded in a three dimensional mode >60 min in 47 transaxial slices of the entire brain as described previously (2, 16).

For coregistration to the anatomic data, T_1, T_2, and contrast enhanced MRI scans were done in all patients on a 1.5 T system (Gyroscan Intera; Philips Medical Systems). Magnetic resonance images were coregistrated to summed PET images with an accuracy of 2 mm or better (18).

Data analysis. We used a region-of-interest approach to determine the maximal tracer uptake in ^{18}F-FLT- and ^{11}C-MET-PET of the summed images. The circular region-of-interest with a diameter of 8 mm was placed in the tumor region with the highest tracer uptake. To calculate the uptake ratio, a reference region-of-interest was placed on the contralateral unaffected tissue. Uptake and SUV were then calculated as previously described (2, 16). Coregistration and region-of-interest calculation was done by using the VINCI software (19).

Mankoff et al. (20, 21) established a kinetic model to quantify the incorporation of thymidine into DNA. In analogy to this kinetic model for thymidine, Muzi et al. (22) validated a compartment model for ^{18}F-FLT in patients with lung cancer to quantify TK1 activity. They used a four-parameter two-compartment model with strong constant estimates that correlate to the *in vitro* proliferation marker Ki-67. In this model, the rate constant K1 determines the transport across the BBB into the tissue and k2 determines the return from the tissue to the blood. The rate constant k3 represents the intracellular phosphorylation of ^{18}F-FLT, and the small proportion that is dephosphorylated back to ^{18}F-FLT is

Table 1. Clinical data, PET uptake values, kinetic rate constants k3 and Ki, and percentage expression of the *in vitro* proliferation marker Ki-67

Pat. no.	Age (y)	Sex	Location	Histology	^{11}C-MET uptake ratio	^{18}F-FLT uptake ratio	^{18}F-FLT SUV	k3 (tumor; 1/min)	Ki (tumor; 1/mL/g/min)	Ki-67 (%)
1	57	M	R/BG	—	1.6	3.83	0.8	0.0055	0.0016	—
2	58	F	L/T	Astrocytroma grade III	3.73	10.8	2.42	0.1578	0.0396	70
3	70	F	R/PT	Glioblastoma	3.2	5.67	1.87	0.055	0.0173	40
4	71	M	R/O	Astrocytoma grade III	1.8	5.4	1.61	0.0267	0.0086	20
5	56	F	R/T	Astrocytoma grade III	2.46	2.29	0.44	0	0	25
6	66	M	L/P	Glioblastoma	3.6	7.79	1.88	0.044	0.0132	30
7	35	M	L/PO	Glioblastoma	3	3.73	1.32	0.0223	0.012	—
8	69	M	R/BG	Astrocytoma grade III	2.4	2.16	0.41	0	0	5
9	54	M	BS	Astrocytoma grade III	1.9	2.34	0.63	0	0	30
10	63	F	L/P	Glioblastoma	4.6	6.99	1.7	0.03	0.0143	20
11	67	M	L/P	Glioblastoma	2.8	6.45	1.75	0.237	0.029	55
12	64	M	R/F	Glioblastoma	3.2	6.77	1.3	0.0472	0.0161	45
13	66	M	R/F	Oligoastrocytoma III	4.5	4.03	1.24	0.0833	0.0122	60

Abbreviations: Pat. no., patent number; M, male; F, female; R, right; L, left; BG, basal ganglia; BS, brain stem; T, temporal; PT, parietotemporal; PO, parietooccipital; O, occipital; P, parietal; F, frontal.

represented by k4 (23). Also, blood volume was included as a parameter in the model.

We also used a four-parameter (+blood volume) two-compartment model including k4. Although Akaike's Information Criterion values between the four-parameter model and the three-parameter model were not significantly different, we decided to use the four-parameter two-compartment model because ignoring k4 as kinetic constant rate in the kinetic model leads to an overestimation of the influx of ^{18}F-FLT as reported previously (24, 25).

^{18}F-FLT is the radiolabeled analogue of the endogenous thymidine. Thymidine is incorporated into DNA during production and is therefore strongly related to proliferation. The main purpose of ^{18}F-FLT analysis consists in obtaining information about the endogenous processes of thymidine and thereby measuring cellular proliferation. The pathway of thymidine is determined by transport from blood into tissue (K_{Th1}), out of the tissue into blood (k_{Th2}), its phosphorylation (k_{Th3}), and its dephosphorylation (k_{Th4}). In contrast to fluorothymidine, thymidine is incorporated into DNA, i.e., the thymidine pathway has an additional rate constant describing the incorporation of thymidine into DNA (k_{DNA}). This constant cannot be determined from the fluorothymidine analysis. However, the rate of cell proliferation (P), which is proportional to the rate of thymidine incorporation into DNA, can be expressed in terms of the thymidine rate constants and the thymidine concentration in blood (Th_B) by

$$P \sim \frac{K_{Th1} \cdot k_{Th3}}{(1 + k_{Th4}/k_{DNA}) \cdot k_{Th2} + k_{Th3}} \cdot Th_B$$

If k_{Th4} is small compared with k_{DNA}, which is a reasonable assumption, because the dephosphorylation rate is low, this expression is independent of k_{DNA}. Because the other reactions are also present in the fluorothymidine pathway, we replace the thymidine rate constants by their fluorothymidine analogues leading to

$$P \sim \frac{K1 \cdot k3}{k2 + k3} \cdot Th_B = Ki \cdot Th_B$$

Thus, the rate of cell proliferation is proportional to the influx constant rate constant Ki and the thymidine level in the blood plasma.

The time activity curves were determined in the part of the tumor with the highest uptake. Three consecutive brain slices were included in the calculation. Kinetic analysis was done by using PMOD biomedical image quantification and kinetic modeling software (PMOD Technologies Ltd.).

Histologic assessment of proliferation by immunostaining Ki-67

A representative formalin-fixed, paraffin-embedded section from each specimen was immunohistochemically stained with MIB-1 (Ki-67) antibody by use of the Avidin-Biotin-Peroxidase-Complex method and the DCS Detection kit with 3,3′-diaminobenzidine and H_2O_2 (DCS). All cells with nuclear staining of any intensity were regarded as positive. Proliferative activity was defined as the percentage of nuclei stained with MIB-1 per total number of nuclei in the biopsy. The fraction of labeled tumor cells, defined as the Ki-67 labeling index, was assessed over four microscopic high power fields (0.16 mm^2) that contained the highest average fraction of labeled cells. The Ki-67 labeling index was determined by scoring the fraction of cells stained with the MIB-1 antibody in 5% intervals.

Statistical analysis

Parametric statistical tests were used to determine significant correlations between the parameters (Pearson correlation analysis).

Correlations were considered significant at a level of P value <0.05. Statistical analysis were done by SPSS software (Release 11.0.1.; SPSS, Inc.).
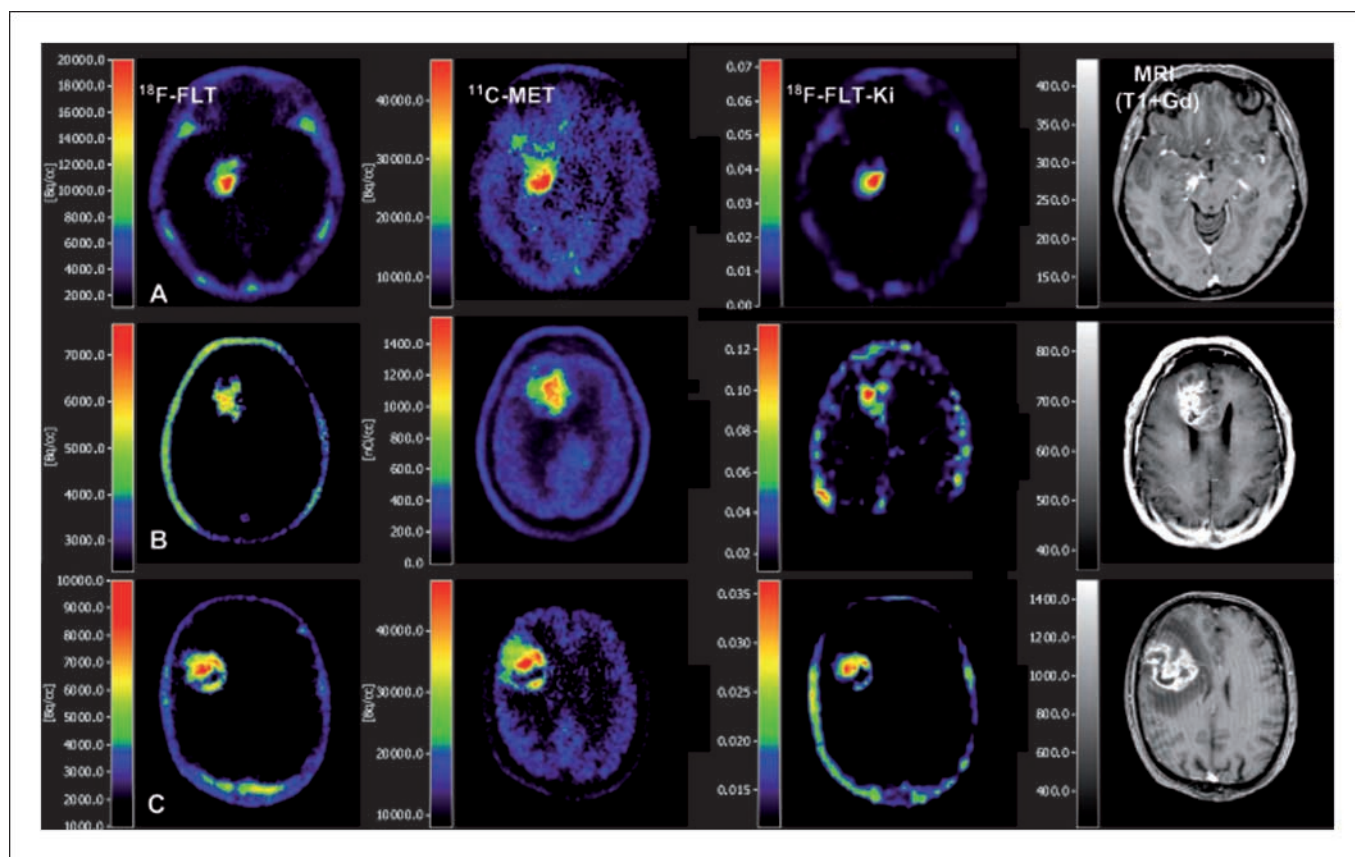
Results

Distribution of ^{18}F-FLT and 11C-MET uptake. The uptake ratios and SUV were calculated by placing a circular region-of-interest in the area of the tumor with highest tracer uptake (Table 1). ^{18}F-FLT uptake ratios varied from 2.2 to 10.8 (mean, 5.3; SD, 2.5), SUV from 0.4 to 2.4 (mean, 1.3; SD 0.6), and ^{11}C-MET uptake ratios ranged from 1.6 to 4.6 (mean, 3.0; SD, 0.9). Restricted to the histologic grading mean values of SUV, ^{18}F-FLT and ^{11}C-MET uptake were higher in patients with WHO grade IV gliomas (n = 6) than in patients with WHO grade III gliomas [n = 6; fluorothymidine-SUV, 1.6 ± 0.3 (WHO IV) versus 1.1 ± 0.8 (WHO III); fluorothymidine uptake ratio, 6.2 ± 1.4 (WHO IV) versus 4.5 ± 3.3 (WHO III); methionine uptake ratio, 3.4 ± 0.6 (WHO IV) versus 2.8 ± 1.1 (WHO III); Fig. 1]. ^{18}F-FLT uptake ratio correlated weakly to ^{11}C-MET uptake ratio (r = 0.65; P = 0.016), indicating the relation between uptake of amino acids and nucleosides in tumor regions with a disrupted BBB.

Contribution of the kinetic parameter K1 and k3 to ^{18}F-FLT uptake. Data of kinetic analysis are summarized in Table 2. Kinetic model analysis provides the rate constants for transport (K1), reflux (k2), intracellular phosphorylation (k3), and dephosphorylation (k4) of fluorothymidine and the fraction of blood volume. The metabolic rate Ki of ^{18}F-FLT is calculated from the rate constants as described above. To analyze the contribution of the kinetic constants to ^{18}F-FLT uptake measured in PET, we calculated their correlation to ^{18}F-FLT uptake. The kinetic constant K1 showed a weaker relation to ^{18}F-FLT uptake (r = 0.52; P = 0.064) than the phosphorylation rate constant k3 (r = 0.60; P = 0.029; Fig. 2). These results may indicate that in high-grade newly diagnosed gliomas, tracer uptake is more related to the phosphorylation rate than to the transport through the BBB. The metabolic rate of ^{18}F-FLT Ki showed the strongest correlation to ^{18}F-FLT uptake (r = 0.87; P < 0.001).

Kinetic parameters for transport and proliferation were ~2-fold higher in grade IV tumors than in grade III tumors, which did not reach statistical significance [K1, 0.056 ± 0.021 (WHO IV) versus 0.023 ± 0.01 (WHO III); k3, 0.072 ± 0.033 (WHO IV) versus 0.045 ± 0.02 (WHO III); Ki, 0.017 ± 0.002 (WHO IV) versus 0.010 ± 0.006 (WHO III)]. Interestingly, K1 and k3 values of the one oligoastrocytoma were higher than K1 and k3 of all but one astrocytoma (K1, 0.032 versus 0.021 ± 0.029; k3, 0.083 versus 0.037 ± 0.069).

Sensitivity analysis of the parameter estimates. The sensitivity analysis calculates the effect of the variation of a parameter on the model output at a certain time, i.e., on the time activity curve. Figure 3 gives a representative example of the sensitivity analysis for this kinetic model. At the beginning, the time activity curve is completely determined by the blood volume. After the bolus has passed the tissue, the transport process starts. The sensitivity of the model to K1 increases during the first 15 minutes until having reached a steady state. The sensitivity to the phosphorylation rate k3 increases rapidly in the first 15 minutes and then with a lower slope over the entire investigation. The negative sensitivity of the time activity curve

Fig. 1. Coregistered ^{18}F-FLT, ^{11}C-MET, parametric map of metabolism Ki, and MRI T_1 + Gd. *A,* a 58-y-old patient with an astrocytoma grade III. The ^{18}F-FLT-PET shows an uptake of 10.8-fold to the contralateral tissue with a high metabolic constant Ki (Ki = 0.039 mL/g/min) and a 3.73-fold ^{11}C-MET uptake corresponding to a high Ki-67 expression of 70%. *B,* an oligoastrocytoma grade III of a 66-y-old patient with relatively high ^{11}C-MET uptake (4.5-fold) and a relatively low ^{18}F-FLT uptake (4.03-fold) but high values of Ki (Ki = 0.0122 mL/g/min) and of Ki-67 expression (60%). A 63-y-old patient with a first diagnosed glioblastoma: the ^{18}F-FLT-PET and ^{11}C-MET image in *C* show high tracer uptake ratios in ^{18}F-FLT (6.77-fold) and in ^{11}C-MET uptake (3.22-fold) to the contralateral tissue, an increased kinetic metabolic constant Ki (0.0161 mL/g/min) according to a high %−Ki-67 expression of 45%.

to the rate constants k2 and k4 reflects that an increase of these constants decreases the model output. At the end of scan time, sensitivity curves for k2, k3, and k4 have not reached their plateau, i.e., steady state has not been reached.

In all cases, the correlation matrix of the model parameters shows covariances between K1 and k2 and between k3 and k4, which arises from the fact that they describe the same reactions (forward and reverse). All other covariances are negligible.

Table 2. Kinetic analysis including k4 in the tumor

Pat. no.	Tumor											
	Ki	SD	K1	SD	k2	SD	k3	SD	k4	SD	vB	SD
1	0.0016	0.0667	0.0069	0.0064	0.0185	0.1217	0.0055	0.326	0	—*	0.0492	0.0105
2	0.0396	0.0114	0.0733	0.0331	0.1344	0.2895	0.1578	0.2911	0.0241	0.0176	0.1343	0.0225
3	0.0173	0.0182	0.0411	0.0237	0.0753	0.1816	0.055	0.181	0.0149	0.0408	0.1016	0.0231
4	0.0086	0.0025	0.0123	0.074	0.0117	208.121	0.0267	6308	3.54460	6151	0.112	0.732
5	0.0000	0.0000	0.0066	0.006	0.0099	0.204	0	—*	—†	—†	0.07	0.0169
6	0.0132	0.0123	0.033	0.0081	0.066	0.0813	0.044	0.1057	0.022	0.0394	0.0452	0.0087
7	0.0120	0.0489	0.0234	0.0087	0.0212	0.0737	0.0223	0.2448	0.0163	0.2049	0.072	0.0129
8	0.0000	0.0000	0.0056	0.6064	0.0135	838	0	—*	—†	—†	0.0435	0.07
9	0.0000	0.0000	0.0086	0.0136	0.0195	7,454	0	—*	—†	—†	0.0533	0.0291
10	0.0143	0.0213	0.0353	0.0112	0.0442	0.0728	0.03	0.109	0.012	0.0617	0.11	0.016
11	0.0290	0.0101	0.164	0.058	1.107	0.6781	0.237	0.1851	0.03	0.186	0.125	0.0227
12	0.0161	0.0102	0.041	0.0068	0.0732	0.0645	0.0472	0.0789	0.0191	0.0268	0.0644	0.0081
13	0.0122	0.0067	0.032	0.008	0.135	0.1513	0.0833	0.1338	0.024	0.0255	0.044	0.0069

*The SD cannot be calculated when the parameter is equal to 0.
† k4 is not defined when k3 = 0.

Thus, our choice of the model with two compartments and one blood pool is also justified on a statistical basis.

Ki-67 expression. MIB-1 immunohistochemistry was done in 11 of 13 patient biopsy samples. The tumor probe of one patient was too small to evaluate a representative region for Ki-67 expression; the other patient did not undergo surgery after the PET scan. Mean Ki-67 expression in high grade gliomas ranged between 5% and 70% (mean, 31.4%; SD 19.5%). Differences in Ki-67 expression between the WHO grade III and IV were not found (WHO III: mean, 32.5%; SD, 26.2%; WHO IV: mean, 30%; SD, 9.4%) indicating that *in vitro* measurement of proliferative activity is not necessarily related to WHO grading.

Analyzing Ki-67 according to the histologic type of astrocytoma, the proliferative fraction of the one oligoastrocytoma was with 60% relatively high compared with the astrocytomas (mean, 27%; SD, 11.2).

Comparison of proliferation activity in vitro *by Ki-67 expression and* in vivo *by PET.* Linear regression analysis revealed a strong correlation between the metabolic rate constant of ^{18}F-FLT Ki and the *in vitro* expression of Ki-67 ($r = 0.79$; $P = 0.004$; Fig. 4). Also, the phosphorylation rate constant of ^{18}F-FLT k3 correlates with Ki-67 ($r = 0.76$; $P = 0.006$; Fig. 4). The transport rate K1 shows a weaker correlation with the proliferation marker Ki-67 ($r = 0.62$; $P = 0.044$).

The correlation of the ^{18}F-FLT uptake ratio and the proliferation index was not statistically significant ($r = 0.57$; $P = 0.70$). Likewise the ratio of ^{11}C-MET uptake did not show any significant correlation with Ki-67 expression ($r = 0.43$; $P = 0.19$).

Discussion

In a patient population with newly diagnosed high grade gliomas WHO III and IV, we show that kinetic modeling of ^{18}F-FLT enables to determine tumor proliferation *in vivo* via the metabolic constant Ki. Furthermore, this *in vivo* obtained proliferation marker correlates strongly with the *in vitro* proliferation rate as determined by Ki-67 immunostaining. These data indicate that kinetic modeling of ^{18}F-FLT uptake in tumor tissue facilitates (*a*) to assess the proliferation rate *in vivo*
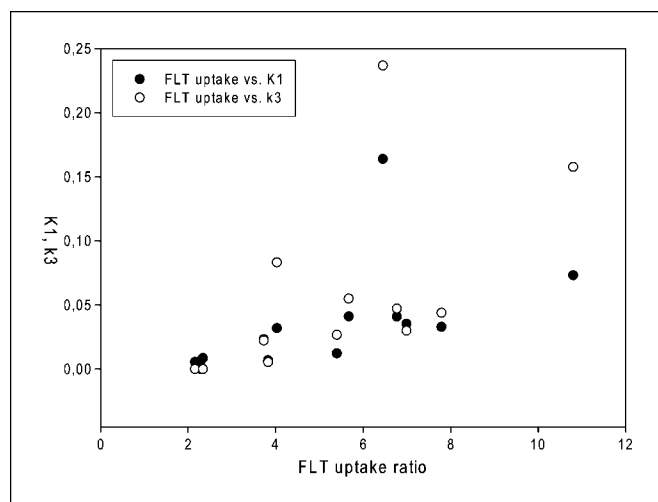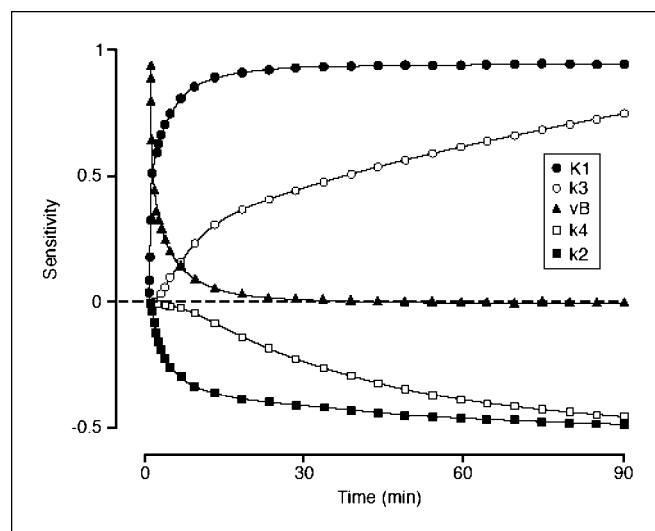
Fig. 3. Sensitivity curve of the kinetic parameters in the ^{18}F-FLT model. Sensitivity of each parameter conforms to the extent that the parameter changes the model. vB, blood vessel.

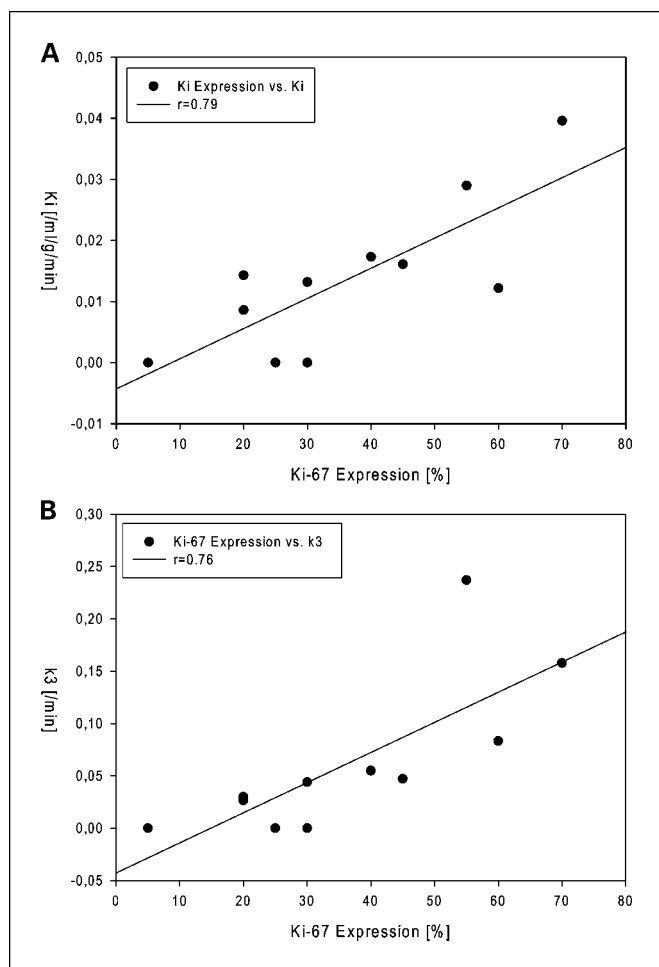and (*b*) to distinguish the proportion of ^{18}F-FLT uptake that is due to transport through the BBB from the proportion, which is due to intracellular proliferation. This distinction between tracer transport and phosphorylation enables to further analyze ^{18}F-FLT uptake to obtain a highly sensitive tool for the quantification of tumor proliferation and, thereby, the potential for monitoring antiproliferative treatment.

T2-weighted images and contrast-enhanced MRI is commonly used for the primary diagnosis of brain tumors. In MRI, T2-weighted hyperintense signal and contrast enhancement provide rather indirect signs for tumor growth. Therapeutic procedures as chemotherapy, radiotherapy, and surgery even induce disturbance of the BBB and, hence, contrast enhancement. Therefore, MRI is not suitable neither for monitoring response to therapy nor for the prediction of clinical outcome.

In our recent PET imaging studies, we showed in a heterogeneous patient population with newly diagnosed and recurrent gliomas of various WHO grades that tracers such as ^{11}C-MET and ^{18}F-FLT provide complementary information on the activity and extent of a glioma (16). We showed that ^{11}C-MET detects the extent of gliomas with a high sensitivity and specificity, and that uptake of ^{11}C-MET is correlated to microvessel density (2, 26). ^{11}C-MET might therefore be an accurate tool to reflect tumor angiogenesis. However, for the determination of tumor proliferation as well as for monitoring response to antiproliferative therapy strategies ^{18}F-FLT is the more favorable marker.

In vitro studies have shown that ^{18}F-FLT uptake reflects TK1 activity (27, 28). Cytosolic TK1 is a cell cycle–regulated enzyme that is activated during the salvage DNA synthesis pathway. ^{18}F-FLT serves as a selective substrate for TK1 and reacts only to a very small part with the mitochondrial TK2. TK1 converts ^{18}F-FLT to its monophosphate as a first step to incorporate the nucleoside into the DNA. As soon as the cells have passed the S phase, TK1 will be degraded (6). Unlike thymidine, only <1% of ^{18}F-FLT is incorporated into the DNA (29). The rate-limiting factor for ^{18}F-FLT—in contrast to

Fig. 2. Relationship between ^{18}F-FLT uptake ratio and the kinetic constants.

Fig. 4. Correlation of kinetic constants k3 (*A*) and Ki (*B*) to proliferation index Ki-67 (MIB). Pearson rank correlation coefficient is $r = 0.88$ ($P < 0.001$) for k3 and $r = 0.79$ ($P = 0.004$) for Ki, respectively.

thymidine—is therefore phosphorylation and not the incorporation into the DNA.

We have shown in this study that the proliferation rate can be obtained from the kinetics of ^{18}F-FLT if the rate constant for dephosphorylation of thymidine (k_{Th4}) is small compared with its rate constant for incorporation into DNA. Because k_{Th4} is small, this condition is always satisfied if k_{DNA} and, therefore, the proliferation rate is sufficiently high—which is always the case in highly proliferating tissues such as tumors.

The metabolic constant Ki determined *in vivo* strongly correlates with Ki-67 expression. This relation confirms the assumption mentioned above that the proliferation rate is proportional to the product of Ki and the thymidine level in the blood plasma, which has not been determined in this study. We also observed a strong correlation between k3 and Ki-67 indicating that a high proliferation rate is related to a high phosphorylation rate rather than to an increased transport through the BBB in high-grade gliomas. These findings support the notion that a detailed kinetic analysis enables determination of tumor proliferation *in vivo*.

It is further interesting to examine the relation of ^{18}F-FLT SUV or uptake ratios—which do not require kinetic modeling and can therefore be much easier obtained from the PET data—to proliferation in high-grade gliomas. Uptake ratios did not correlate with the *in vitro* proliferation marker Ki-67. The failure of uptake values to detect tumor proliferation is due to the fact that uptake values do not allow to distinguish whether the accumulation of ^{18}F-FLT is mainly caused by transport respectively breakdown of the BBB or to proliferation. This assumption conforms to the patient study recently reported by Wells et al. (30) with ^{11}C-Thymidine PET that behaves in analogy to ^{18}F-FLT. In a patient with a brain tumor, they found a strong divergence between the increasing transport parameter and a declining flux constant (Ki) after several treatment strategies. The declining parameter Ki was finally correlated with the patient's clinical outcome. Thus, uptake ratios and SUV might cause misleading estimates of tumor proliferation.

In contrast to our results, Chen et al. (15) recently described a significant correlation between ^{18}F-FLT SUV and the expression of the *in vitro* marker Ki-67 in brain tumors. However, low-grade gliomas were also included in this study. This might suggest that tracer uptake values, determined as SUV, correlate to *in vitro* proliferation in a WHO grade–dependent manner but not within a single WHO grade. We suggest that the metabolic rate constant Ki is the more sensitive parameter for imaging proliferation of high-grade gliomas than tracer uptake ratios of ^{18}F-FLT and ^{11}C-MET.

The correlation between k3 and the ^{18}F-FLT uptake ratio indicates that in untreated gliomas with a high *in vitro* proliferation index, ^{18}F-FLT uptake is more related to phosphorylation than to transport of ^{18}F-FLT through the BBB. Also, the strong correlation between k3, and the metabolic rate constant Ki confirms the effect of the phosphorylation rate k3 on the amount of ^{18}F-FLT uptake in the tumor. These results correspond with our previous findings where we found a strong correlation between the kinetic constants K1 and k3 and ^{18}F-FLT uptake ratio (16). Although in the previously studied heterogeneous patient group with newly diagnosed and recurrent gliomas of various WHO grades, we observed a stronger correlation of K1 than of k3 to ^{18}F-FLT uptake. In treated brain tumors, the major proportion of ^{18}F-FLT uptake is due to transport because of the treatment-induced disturbance of the BBB. In contrast, in the present study in nontreated patients with high-grade gliomas, the contribution of the phosphorylation rate—expressed by k3—to ^{18}F-FLT uptake was higher than of the transport rate constant K1. This underlines the capability and the necessity of kinetic analysis to distinguish between tracer uptake caused by an increased transport through the disturbed BBB and cellular tumor proliferation.

It should be pointed out that a limitation of stereotactic biopsy is its limited size, which sometimes is not representative for the entire tumor. However, in our study, PET data were used for guidance of stereotactic biopsy from the most active tumor part.

A detailed analysis of the heterogeneous tumor compartments of ^{18}F-FLT permits to distinguish high-proliferating from low-proliferating tumor areas. Thus, ^{18}F-FLT analysis allows for the detection of the strongest proliferating part of the tumor. Because the most proliferating part of the tumor is mainly responsible for tumor progression, ^{18}F-FLT analysis enables a more precise estimation of the malignancy and may also serve as an accurate measure of the antiproliferative treatment strategies.

In summary, kinetic analysis of ^{18}F-FLT in patients with newly diagnosed high-grade gliomas provides a useful method for the determination of proliferation rate *in vivo*. However, with regard to the limited number of patients included in this study, the potential of ^{18}F-FLT kinetic analysis for the early prediction of clinical outcome and response to therapy remains to be further investigated. This study indicates that evaluation of therapy efficiency of individual molecular-targeted approaches may benefit from ^{18}F-FLT kinetic analysis.

References

1. Jacobs AH, Dittmar C, Winkeler A, Garlip G, Heiss WD. Molecular imaging of gliomas. Mol Imaging 2002;1:309–35.
2. Kracht LW, Friese M, Herholz K, et al. Methyl-[11C]-l-methionine uptake as measured by positron emission tomography correlates to microvessel density in patients with glioma. Eur J Nucl Med Mol Imaging 2003;30:868–73.
3. Sato N, Suzuki M, Kuwata N, et al. Evaluation of the malignancy of glioma using 11C-methionine positron emission tomography and proliferating cell nuclear antigen staining. Neurosurg Rev 1999;22:210–4.
4. Miyagawa T, Oku T, Uehara H, et al. "Facilitated" amino acid transport is upregulated in brain tumors. J Cereb Blood Flow Metab 1998;18:500–9.
5. Shields AF, Grierson JR, Dohmen BM, et al. Imaging proliferation *in vivo* with [F-18] FLT and positron emission tomography. Nat Med 1998;4:1334–6.
6. Sherley JL, Kelly TJ. Regulation of human thymidine kinase during the cell cycle. J Biol Chem 1988;263:8350–8.
7. Toyohara J, Waki A, Takamatsu S, Yonekura Y, Magata Y, Fujibayashi Y. Basis of FLT as a cell proliferation marker: comparative uptake studies with [3H]thymidine and [3H]arabinothymidine, and cell-analysis in 22 asynchronously growing tumor cell lines. Nucl Med Biol 2002;29:281–7.
8. Wells P, Gunn RN, Alison M, et al. Assessment of proliferation *in vivo* using 2-[(11)C]thymidine positron emission tomography in advanced intra-abdominal malignancies. Cancer Res 2002;62:5698–702.
9. Vesselle H, Grierson J, Muzi M, et al. *In vivo* validation of 3′deoxy-3′-[(18)F]fluorothymidine ([(18)F]FLT) as a proliferation imaging tracer in humans: correlation of [(18)F]FLT uptake by positron emission tomography with Ki-67 immunohistochemistry and flow cytometry in human lung tumors. Clin Cancer Res 2002;8:3315–23.
10. Buck AK, Bommer M, Stilgenbauer S, et al. Molecular imaging of proliferation in malignant lymphoma. Cancer Res 2006;66:11055–61.
11. Buck AK, Halter G, Schirrmeister H, et al. Imaging proliferation in lung tumors with PET:18F-FLT versus 18F-FDG. J Nucl Med 2003;44:1426–31.
12. Francis DL, Visvikis D, Costa DC, et al. Potential impact of [18F]3′-deoxy-3′-fluorothymidine versus [18F]fluoro-2-deoxy-D-glucose in positron emission tomography for colorectal cancer. Eur J Nucl Med Mol Imaging 2003;30:988–94.
13. Buck AK, Schirrmeister H, Hetzel M, et al. 3-deoxy-3-[(18)F]fluorothymidine-positron emission tomography for noninvasive assessment of proliferation in pulmonary nodules. Cancer Res 2002;62:3331–4.
14. Wagner M, Seitz U, Buck A, et al. 3′-[18F]fluoro-3′-deoxythymidine ([18F]-FLT) as positron emission tomography tracer for imaging proliferation in a murine B-Cell lymphoma model and in the human disease. Cancer Res 2003;63:2681–7.
15. Chen W, Cloughesy T, Kamdar N, et al. Imaging proliferation in brain tumors with 18F-FLT PET: comparison with 18F-FDG. J Nucl Med 2005;46:945–52.
16. Jacobs AH, Thomas A, Kracht LW, et al. 18F-fluoro-L-thymidine and 11C-methylmethionine as markers of increased transport and proliferation in brain tumors. J Nucl Med 2005;46:1948–58.
17. Muzi M, Spence AM, O'Sullivan F, et al. Kinetic analysis of 3′-deoxy-3′-18F-fluorothymidine in patients with gliomas. J Nucl Med 2006;47:1612–21.
18. Cizek J, Herholz K, Vollmar S, Schrader R, Klein J, Heiss WD. Fast and robust registration of PET and MR images of human brain. Neuroimage 2004;22:434–42.
19. Vollmar S CJ, Sue M, Klein J, Jacobs AH, Herholz K. VINCI - Volume Imaging in Neurological Research, Co-Registration and ROIs Forschung und wissenschaftliches Rechnen 2003. In: Kremer K, Macho V, editors. Göttingen: Gesellschaft für wissenschaftliche Datenverarbeitung; 2004. p. 115–31.
20. Mankoff DA, Shields AF, Graham MM, Link JM, Eary JF, Krohn KA. Kinetic analysis of 2-[carbon-11]thymidine PET imaging studies: compartmental model and mathematical analysis. J Nucl Med 1998;39:1043–55.
21. Mankoff DA, Shields AF, Link JM, et al. Kinetic analysis of 2-[11C]thymidine PET imaging studies: validation studies. J Nucl Med 1999;40:614–24.
22. Muzi M, Vesselle H, Grierson JR, et al. Kinetic analysis of 3′-deoxy-3′-fluorothymidine PET studies: validation studies in patients with lung cancer. J Nucl Med 2005;46:274–82.
23. Krohn KA, Mankoff DA, Muzi M, Link JM, Spence AM. True tracers: comparing FDG with glucose and FLT with thymidine. Nucl Med Biol 2005;32:663–71.
24. Patlak CS, Blasberg RG. Graphical evaluation of blood-to-brain transfer constants from multiple-time uptake data. Generalizations. J Cereb Blood Flow Metab 1985;5:584–90.
25. Spence AM, Muzi M, Graham MM, et al. Glucose metabolism in human malignant gliomas measured quantitatively with PET, 1-[C-11]glucose and FDG: analysis of the FDG lumped constant. J Nucl Med 1998;39:440–8.
26. Kracht LW, Miletic H, Busch S, et al. Delineation of brain tumor extent with [11C] L-methionine positron emission tomography: local comparison with stereotactic histopathology. Clin Cancer Res 2004;10:7163–70.
27. Rasey JS, Grierson JR, Wiens LW, Kolb PD, Schwartz JL. Validation of FLT uptake as a measure of thymidine kinase-1 activity in A549 carcinoma cells. J Nucl Med 2002;43:1210–7.
28. Barthel H, Perumal M, Latigo J, et al. The uptake of 3′-deoxy-3′-[18F]fluorothymidine into L5178Y tumours *in vivo* is dependent on thymidine kinase 1 protein levels. Eur J Nucl Med Mol Imaging 2005;32:257–63.
29. Grierson JR, Schwartz JL, Muzi M, Jordan R, Krohn KA. Metabolism of 3′-deoxy-3′-[F-18]fluorothymidine in proliferating A549 cells: validations for positron emission tomography. Nucl Med Biol 2004;31:829–37.
30. Wells JM, Mankoff DA, Eary JF, et al. Kinetic analysis of 2-[11C]thymidine PET imaging studies of malignant brain tumors: preliminary patient results. Mol Imaging 2002;1:145–50.

PLoS ONE

Early Detection of Erlotinib Treatment Response in NSCLC by 3′-Deoxy-3′-[18F]-Fluoro-L-Thymidine ([18F]FLT) Positron Emission Tomography (PET)

Roland T. Ullrich[1,2], Thomas Zander[6], Bernd Neumaier[1], Mirjam Koker[1], Takeshi Shimamura[4,5], Yannic Waerzeggers[1], Christa L. Borgman[4,5], Samir Tawadros[6], Hongfeng Li[1], Martin L. Sos[1], Heiko Backes[1], Geoffrey I. Shapiro[4,5], Jürgen Wolf[6], Andreas H. Jacobs[1,2,3], Roman K. Thomas[1,6,7,9]*, Alexandra Winkeler[1,2,9]

1 Max Planck Institute for Neurological Research with Klaus-Joachim-Zülch-Laboratories of the Max Planck Society, Medical Faculty of the University of Cologne, Cologne, Germany, 2 Center for Molecular Medicine Cologne (CMMC), Cologne, Germany, 3 Klinikum Fulda, Fulda, Germany, 4 Department of Medical Oncology, Dana-Farber Cancer Institute, Brigham and Women's Hospital and Harvard Medical School, Boston, Massachusetts, United States of America, 5 Department of Medicine, Brigham and Women's Hospital and Harvard Medical School, Boston, Massachusetts, United States of America, 6 Department I of Internal Medicine and Center of Integrated Oncology Köln – Bonn, University of Cologne, Cologne, Germany, 7 Chemical Genomics Center of the Max Planck Society, Dortmund, Germany

Abstract

Background: Inhibition of the epidermal growth factor receptor (EGFR) has shown clinical success in patients with advanced non-small cell lung cancer (NSCLC). Somatic mutations of EGFR were found in lung adenocarcinoma that lead to exquisite dependency on EGFR signaling; thus patients with EGFR-mutant tumors are at high chance of response to EGFR inhibitors. However, imaging approaches affording early identification of tumor response in EGFR-dependent carcinomas have so far been lacking.

Methodology/Principal Findings: We performed a systematic comparison of 3′-Deoxy-3′-[18F]-fluoro-L-thymidine ([18F]FLT) and 2-[18F]-fluoro-2-deoxy-D-glucose ([18F]FDG) positron emission tomography (PET) for their potential to identify response to EGFR inhibitors in a model of EGFR-dependent lung cancer early after treatment initiation. While erlotinib-sensitive tumors exhibited a striking and reproducible decrease in [18F]FLT uptake after only two days of treatment, [18F]FDG PET based imaging revealed no consistent reduction in tumor glucose uptake. In sensitive tumors, a decrease in [18F]FLT PET but not [18F]FDG PET uptake correlated with cell cycle arrest and induction of apoptosis. The reduction in [18F]FLT PET signal at day 2 translated into dramatic tumor shrinkage four days later. Furthermore, the specificity of our results is confirmed by the complete lack of [18F]FLT PET response of tumors expressing the T790M erlotinib resistance mutation of EGFR.

Conclusions: [18F]FLT PET enables robust identification of erlotinib response in EGFR-dependent tumors at a very early stage. [18F]FLT PET imaging may represent an appropriate method for early prediction of response to EGFR TKI treatment in patients with NSCLC.

Introduction

Inhibition of the epidermal growth factor receptor (EGFR) tyrosine kinase by small molecule kinase inhibitors has evolved as a critical therapeutic strategy in non-small cell lung cancer (NSCLC). However, only a subset of patients responds to the treatment; most of these were found to carry activating mutations in EGFR [1,2,3]. Sensitive methods for mutation detection in clinical specimens have been developed that enable patient selection for genetically informed cancer therapy [4,5]. However, additional patients whose tumors lack EGFR mutations might also benefit from EGFR inhibitors.

Positron emission tomography using [18F]FDG PET is an effective means to staging of NSCLC patients and is now part of routine staging protocols [6,7]. Furthermore, [18F]FDG PET has been found to enable identification of NSCLC patients responding to chemotherapy [8] and in mice bearing EGFR-mutant tumors responding to gefitinib [9]. Given that EGFR inhibitor-induced

apoptosis in EGFR-mutant tumors is preceded by a pronounced cell cycle arrest [10], we hypothesized that imaging modalities reflecting tumor cell proliferation rather than glucose metabolism might afford even earlier measurements of tumor growth inhibition.

[^{18}F]-fluoro-L-thymidine ([^{18}F]FLT) PET has been developed as a specific marker to measure cellular proliferation *in vivo* [11]. As an analog substrate of thymidine, [^{18}F]FLT is phosphorylated by thymidine kinase 1 (TK1). TK1 is a cytosolic enzyme that is synthesized when proliferating cells enter the S-phase for DNA synthesis [12]. Moreover, [^{18}F]FLT uptake values have been shown to correlate to tumor cell proliferation as assessed by Ki-67 immunostaining [13,14]. Thus, [^{18}F]FLT PET might serve as an effective means to measure drug-induced cell cycle inhibition in vivo. Supporting this notion is the recent observation of an advantage of [^{18}F]FLT over [^{18}F]FDG PET in measuring response of BRAF V600E-mutant melanomas to Mek inhibition after five days of treatment [15]. Here, we directly compared [^{18}F]FDG to [^{18}F]FLT PET in their ability to measure the immediate changes in cellular proliferation following inhibition of a dominant oncogenic signal.

Results and Discussion

As a model of EGFR-dependent NSCLC, we employed the cell lines HCC827 and PC9. Both cell lines carry mutated as well as amplified EGFR alleles and are highly sensitive to the EGFR TKI erlotinib in the low nanomolar range [10]. We used the cell line H1975 expressing both the L858R mutation of EGFR as well as the T790M EGFR resistance mutation as a control for specificity of drug action. After 24h of treatment with even low doses of erlotinib, sensitive cells were arrested in the G1 phase of the cell cycle following erlotinib treatment with a concomitant decrease of cells in the S phase of the cell cycle (**Fig. 1A**). Subsequent to the cell cycle arrest the sensitive cell lines PC9 and HCC827 underwent massive apoptotic cell death 36h after onset of treatment (**Fig. 1B**). This was paralleled by reduction in p-EGFR and p-Akt levels in both cell lines (**Fig. 1A**). By comparison, the T790M-mutant cell line H1975 showed no cell cycle arrest (**Fig. 1A**), no loss of EGFR or Akt phosphorylation (**Fig. 1A**) and did not exhibit any signs of apoptotic cell death (**Fig. 1B**), confirming that the observed phenotypes were due to on-target effects of the drug.

We next sought to determine the feasibility of [^{18}F]FLT and [^{18}F]FDG to measure response to erlotinib treatment using a murine tumor xenograft model. HCC827, PC9 or H1975 cell lines were individually transplanted subcutaneously onto nude mice. After oral treatment with either vehicle or erlotinib, mice were imaged by [^{18}F]FLT or [^{18}F]FDG PET. After only 48h of erlotinib treatment we observed a striking reduction of [^{18}F]FLT uptake in the sensitive cell lines HCC827 and PC9. By contrast, no changes in [^{18}F]FLT uptake were observed in mice bearing the resistant cell line H1975 or in the control group treated with the vehicle alone (**Fig. 2A**). Quantitative analysis revealed a mean reduction of [^{18}F]FLT uptake of 34.6% in the HCC827 xenografts and of 43% in the PC9 xenografts after two days of treatment (p = 0.04) (**Fig. 2B**). In the resistant H1975 xenografts [^{18}F]FLT uptake only slightly decreased by 5.4% (p = 0.12) (**Fig. 2B**). After four days of erlotinib treatment [^{18}F]FLT uptake remained decreased in HCC827 and PC9 tumors whereas we observed no decrease in [^{18}F]FLT uptake in the H1975 tumor xenografts. Thus, the reduction in [^{18}F]FLT uptake reflects inhibition of cellular proliferation due to induction of a G1 arrest in EGFR-dependent tumors.
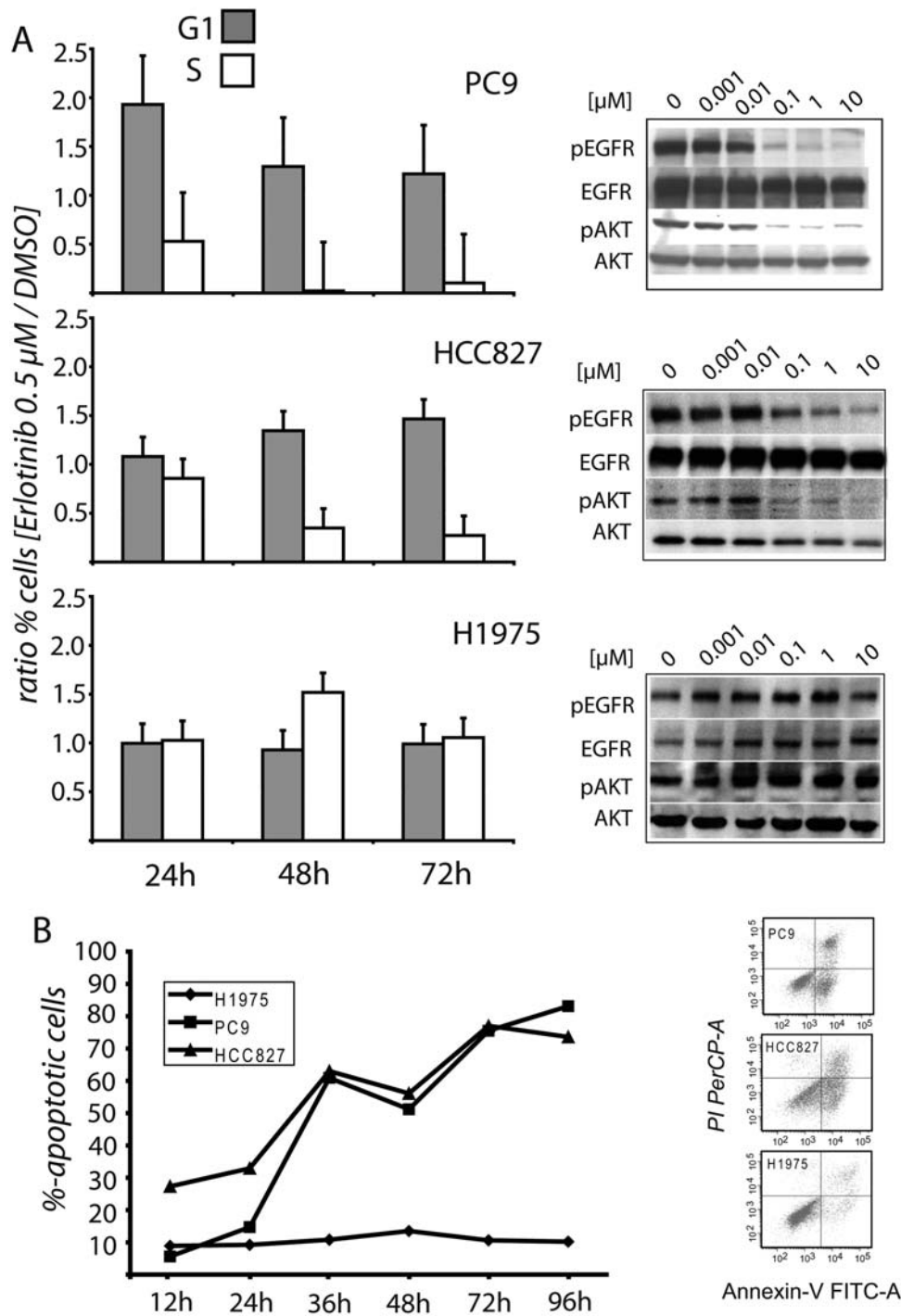
By comparison, we observed a slight decrease in [^{18}F]FDG uptake after 4 days of erlotinib treatment only in the HCC827 but not in the PC9 xenograft. However, this reduction was far less pronounced in comparison to the results observed with [^{18}F]FLT (**Fig. 2B**). In a quantitative analysis of these results, the [^{18}F]FDG uptake ratios in the PC9 and the HCC827 xenografts were not significantly decreased after either 2 days or 4 days of treatment (p = 0.13). As expected, H1975 xenografts did not show significant changes in glucose uptake after either 48 or 96 hours of erlotinib treatment (**Fig. 2B**). Thus, in our analysis [^{18}F]FLT PET appeared to be superior in detecting response of EGFR-mutant tumors to EGFR inhibition than [^{18}F]FDG PET.

We next analyzed cellular proliferation in tumors extracted from the mice that had undergone PET imaging by Ki-67 staining. On visual microscopic inspection of these tissue specimens, erlotinib-treated PC9 and HCC827 xenografts but not H1975 tumors exhibited a substantial reduction in Ki-67 positive cells as compared to the vehicle-treated controls (**Fig. 3A** and data not shown). Quantitative analysis revealed that [^{18}F]FLT uptake ratios correlated significantly with expression of Ki-67 (r = 0.87, p<0.001, **Fig. 3B**). By contrast, the correlation with [^{18}F]FDG PET was far lower (r = 0.38, p = 0.037, **Fig. 3B**). Thus, [^{18}F]FLT-based in-vivo measurements of inhibition of proliferation are correlated with in vitro assessed cellular proliferation.
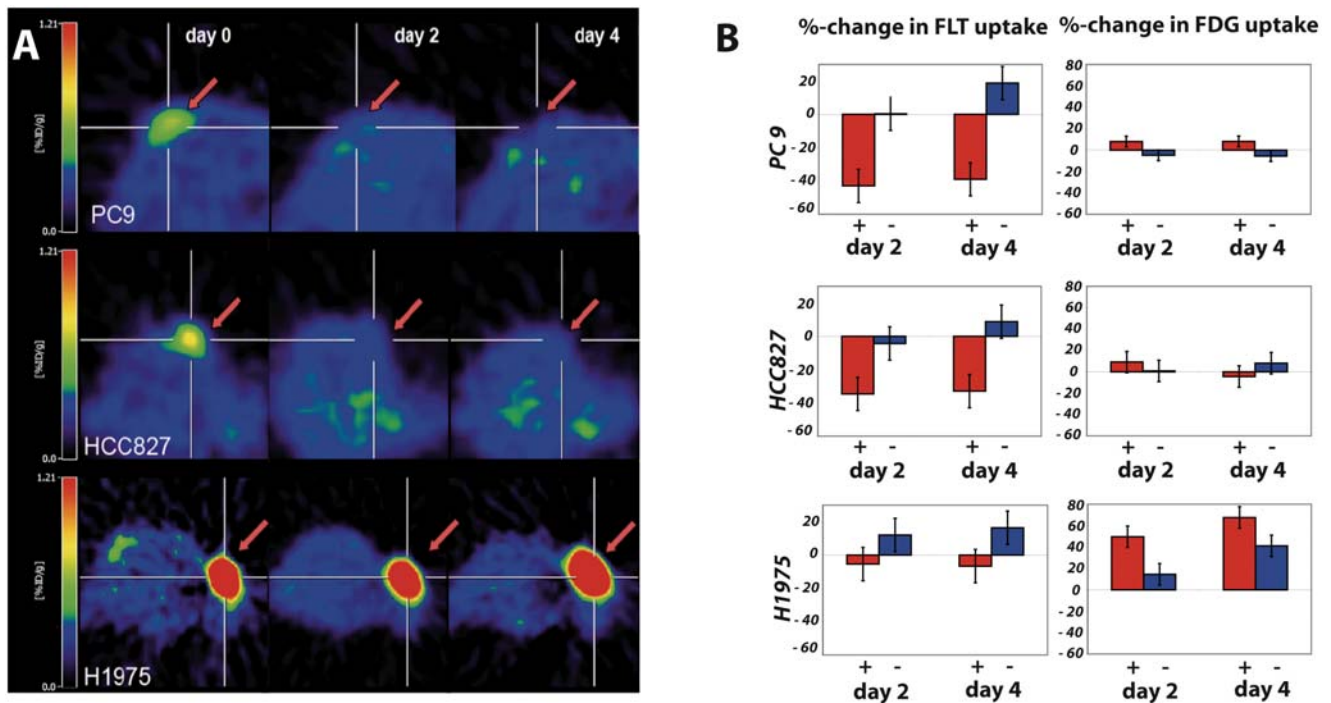
In order to determine whether our in vitro observation of apoptosis following cell cycle arrest was reflected in vivo we analyzed tumor specimens extracted after 4 days of erlotinib treatment for the presence of apoptotic cells by TUNEL staining. This analysis revealed the presence of apoptotic cells in the sensitive cell lines but not in the T790M-carrying tumors (**Fig. 3A**). Furthermore, the appearance of apoptotic cells in the sensitive cells was reflected in dramatic tumor shrinkage starting at day 6 of treatment (**Fig. 3C**). Together, these findings show that that a decrease in [^{18}F]FLT PET is not only reflective of tumor cells arrested in G1 but predicts induction of apoptotic cell death and tumor response in EGFR-addicted tumors treated with erlotinib.

The assessment of therapy response poses a great challenge in oncology. In particular, the advent of molecularly targeted cancer therapeutics questions the relevance of conventional morphology-based response methods such as those defined in the RECIST criteria [16]. Here, we show that [^{18}F]FLT PET enables detection of a therapeutic response in mice receiving erlotinib treatment for EGFR-mutant lung cancer as early as 48 hours after onset of treatment. Strikingly, we reliably saw [^{18}F]FLT PET responses when morphological changes were still absent and 4 days before actual tumor shrinkage was observed. The observed responses were specifically due to inhibition of EGFR kinase activity as mice with tumors expressing the T790M resistance allele of EGFR did not exhibit any signs of apoptosis or therapeutic response. Furthermore, early detection of treatment response was limited to [^{18}F]FLT PET. [^{18}F]FDG PET measurements that had previously been suggested for this purpose [9] failed in our study to robustly identify the responding tumors after only two days of treatment. We suggest that glucose metabolism as assessed by [^{18}F]FDG PET rather indirectly reflects tumor cell proliferation and is therefore not a suitable marker for EGFR inhibition at that early stage of treatment. Thus, a therapy-induced reduction in [^{18}F]FDG PET signal is likely to be a later event, occurring during actual tumor shrinkage.

In summary, [^{18}F]FLT PET enables detecting tumor cells arrested in G1 before morphological changes thereby providing a surrogate marker for erlotinib-induced apoptosis and tumor shrinkage at a very early time point. Thus, [^{18}F]FLT PET might

Figure 1. Erlotinib treatment induces down-regulation of EGFR/EGFR-coupled signaling pathways and cell cycle arrest with subsequent induction of apoptosis in EGFR sensitive tumor cells. The erlotinib sensitive cell lines HCC827 and PC9 and the erlotinib-resistant cell line H1975 were treated with the indicated doses of erlotinib for 24 hours. Whole-cell lysates were subjected to immunoblotting with the indicated antibodies **(A)**. PC9, HCC827 and H1975 cells were treated with erlotinib (0.5 µM) for 24h, 48h and 72h; nuclei were prepared, stained with propidium iodide and analyzed by flow cytometry. Results are shown for the G1 and S phases of the cell cycle **(A)**. Apoptotic effects of erlotinib on EGFR-sensitive cell lines in comparison to the T790M mutant H1975 **(B)**. Annexin V FACS was performed 12h, 24h, 36h, 48h, 72h and 96h after 0.5 µM erlotinib treatment. Images show Annexin V-positive cells after 48h in the different cell lines.
doi:10.1371/journal.pone.0003908.g001

Figure 2. [18F]FLT PET indicates response to therapy after 2 days of erlotinib treatment. In (A) a representative [18F]FLT PET image of a mouse bearing the sensitive PC9, HCC827 and the resistant H1975 xenografts before beginning of treatment, 48h and 96h after daily erlotinib treatment (Tarceva, 50mg/kg). (B) Quantitative analysis of changes in [18F]FLT and [18F]FDG uptake ratios after 48h and 96h daily erlotinib treatment vs. vehicle only as control (PC9: n = 8; vehicle, n = 2; HCC827: n = 7; vehicle, n = 2; H1975: n = 8; vehicle, n = 2).
doi:10.1371/journal.pone.0003908.g002

be an appropriate method for the early identification of patients benefiting from EGFR TKI treatment.

Materials and Methods

Cell cultures

We used the EGFR-tyrosine kinase inhibitor (TKI) sensitive adenocarcinoma cell lines HCC827, PC9 and the resistant cell line H1975. All cell lines were maintained in RPMI 1640 supplemented with 10% heat inactivated fetal bovine serum (FBS, Roche Diagnostics, Mannheim, Germany), 1% penicillin and 1% streptomycin (P/S, Life Technologies) at 37°C in a 5% CO_2/95% air atmosphere.

Western blot analysis

Cells were serum-starved for 24h in the presence or absence of erlotinib. After preparation of cell lysates phosphorylation level of the proteins were determined using antibodies for total EGFR, phospho-EGFR (pEGFR) (both purchased from Biosource), total Akt and phospho-Akt (pAKT) (both obtained from Cell Signaling Technology).

Apoptosis assay

Cells were plated in 6-well plates, after 24h of incubation treated with erlotinib for 12h, 24h, 36h, 48h, 72h, and 96h and finally harvested after trypsinization. Then cells were washed with PBS, resuspended in Annexin-V binding buffer and finally stained with Annexin-V-FITC and PI. FACS analysis was performed on a FACS Canto Flow Cytometer (BD Biosciences, Germany) and results were calculated using FACS Diva Software.

Cell cycle analysis

Cells were fixed and then treated with RNase A (500 μg/ml). Following resuspension of the cells in propidium iodide and in sodium citrate cells were analysed for DNA content by flow cytometry.
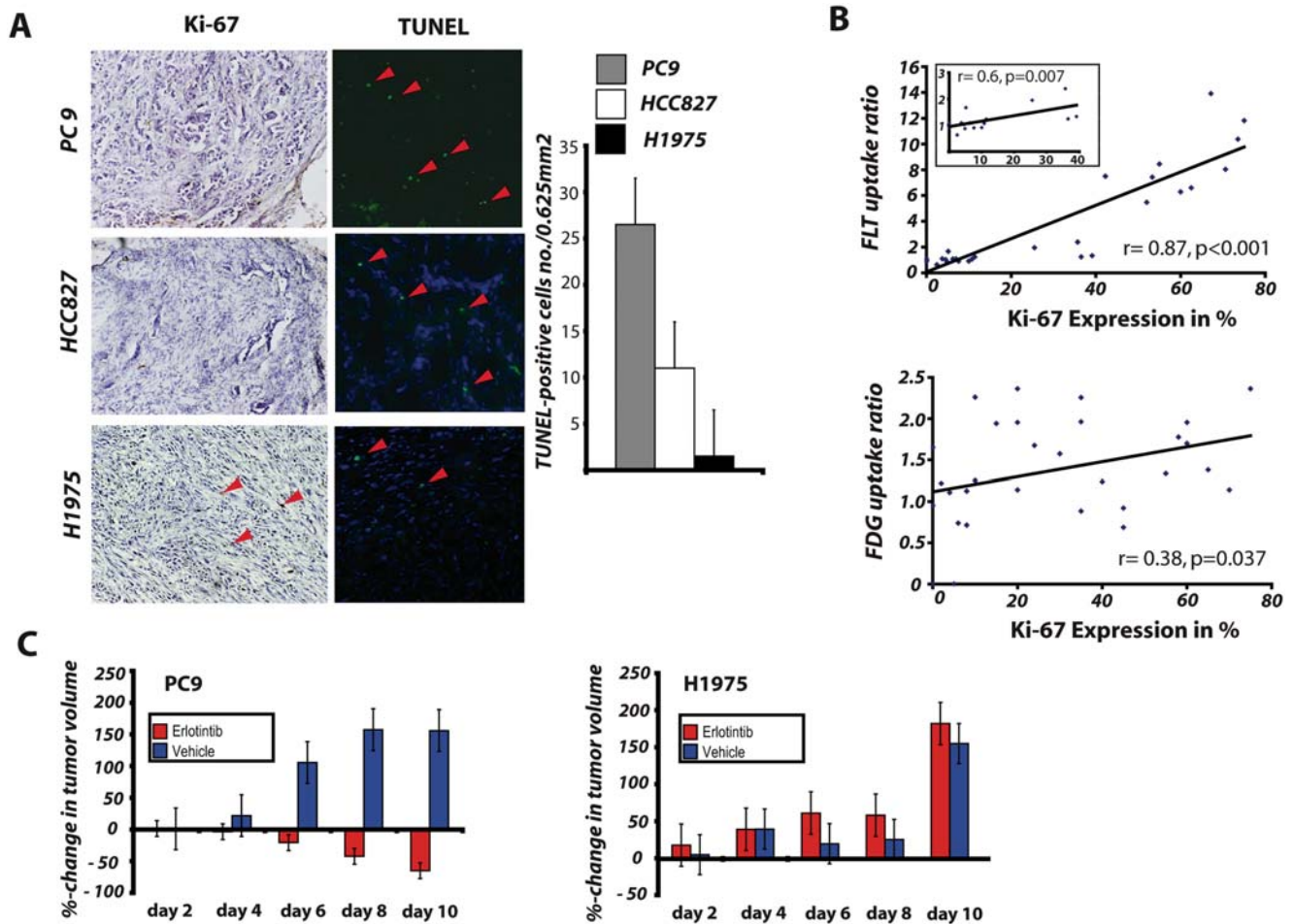
Xenograft model

All animal procedures were in accordance with the German Laws for Animal Protection and were approved by the local animal committee and the Bezirksregierung Köln. Tumors were generated by s. c. injecting 5×10^6 tumor cells into nu/nu athymic male mice. When tumors had reached a size of 100 mm³, animals were randomized into two groups, control (vehicle) and erlotinib-treated mice. Erlotinib (Tarceva) was dosed at 6% Captisol (CyDex, Inc., Lenexa, KS) in water for solution over night. All controls were dosed with the same volume of vehicle. After PET measurement mice were treated daily by oral gavage of 50mg/kg Tarceva. Tumor size was monitored every two days by measuring perpendicular diameters. Tumor volumes were calculated from the determination of the largest diameter and its perpendicular according to the equation [tumor volume = a×(b²/2)].

PET imaging

Tumor bearing mice were investigated using a R4 microPET scanner (Concord Microsystems, Inc., Knoxville, TN). [18F]FLT and [18F]FDG synthesis were performed as described previously [17,18]. No-carrier-added [18F]FLT was administered i.v. (tail vein) into experimental animals with a dose of 200 μCi/mouse. No-carrier-added [18F]FDG was injected intraperitoneally (i.p.) with a dose of 300 μCi. Since the biodistribution of [18F]FDG is

Figure 3. Immunohistochemistry of tumor tissue for Ki-67 expression and TUNEL, relation of [18F]FLT and [18F]FDG uptake to Ki-67 expression, and measurement of tumor volume for the assessment of treatment response. (A) Frozen tissue was stained for Ki-67 and TUNEL (magnification 10×). Columns, average number of TUNEL positive cells (green cells) were counted in three randomly selected field (area 0.625mm^2) in two tumor samples for each cell line. The Ki-67 labeling index as assessed by the percentage of nuclei stained with MIB-1 per total number of nuclei was compared to uptake ratios of [18F]FLT and [18F]FDG (B). Effects of daily Erlotinib treatment on the tumor size of the xenografts for the assessment of tumor response (C).
doi:10.1371/journal.pone.0003908.g003

comparable for i.v. and i.p. injections after 60min and i.p. injections allow for a more accurate dosage of tracer injection, we decided to use intraperitoneal injections for [18F]FDG as recently described [19,20]. All PET images were performed 60 min after injection. Data evaluation was based on a volume of interest (VOI) analysis of the entire tumor. For data analysis we used the maximal voxel radioactivity within the tumors. To determine the uptake ratio we chose the mediastinum as reference since we observed constant uptake for [18F]FLT and [18F]FDG in this region. Data were decay corrected and divided by the total injected dose to represent percentage injected dose per gram (%ID/g).

Immunohistochemistry and TUNEL detection

After the last PET measurements animals were sacrificed and s.c. tumors were extracted. After fixation (4% paraformaldehyde, 4°C, 24h; 30% sucrose, 4°C, 24h), tumors were embedded in tissue freezing medium (Jung, Nussloch, Germany) and cut in 10-μm frozen sections. H&E staining on the tissue was done according to standard protocols. Tumor proliferation was assessed using an anti-Ki-67 monoclonal antibody (1:200 dilution, KI6811C06, DCS,

Hamburg, Germany), and the percentage of specifically stained cancer cells for Ki-67 was calculated. The number of Ki-67 positive nuclei was determined as percentage of Ki-67 stained nuclei per total number of nuclei in three representative tumor areas ((F1+F2+F3)/3 (%)) that contained the highest average fraction of labelled cells as described recently [14]. To quantify the number of apoptotic positive cells TUNEL was performed on cryostat tumor slices with the DeadEnd^{TM} TUNEL system (Promega) following the manufacturer's directions. The average numbers of TUNEL positive were counted in three randomly selected fields in two tumor samples from each cell line.

Statistical analysis

Wilcoxon test was performed using SPSS software (release 11.0.1 SPSS, Inc., Chicago. IL.USA), statistical significance was set at $p < 0.05$.

Author Contributions

References

1. Lynch TJ, Bell DW, Sordella R, Gurubhagavatula S, Okimoto RA, et al. (2004) Activating mutations in the epidermal growth factor receptor underlying responsiveness of non-small-cell lung cancer to gefitinib. N Engl J Med 350: 2129–2139.

2. Paez JG, Janne PA, Lee JC, Tracy S, Greulich H, et al. (2004) EGFR mutations in lung cancer: correlation with clinical response to gefitinib therapy. Science 304: 1497–1500.

3. Pao W, Miller V, Zakowski M, Doherty J, Politi K, et al. (2004) EGF receptor gene mutations are common in lung cancers from "never smokers" and are associated with sensitivity of tumors to gefitinib and erlotinib. Proc Natl Acad Sci U S A 101: 13306–13311.

4. Thomas RK, Nickerson E, Simons JF, Janne PA, Tengs T, et al. (2006) Sensitive mutation detection in heterogeneous cancer specimens by massively parallel picoliter reactor sequencing. Nat Med 12: 852–855.

5. Thomas RK, Baker AC, Debiasi RM, Winckler W, Laframboise T, et al. (2007) High-throughput oncogene mutation profiling in human cancer. Nat Genet.

6. Pieterman RM, van Putten JW, Meuzelaar JJ, Mooyaart EL, Vaalburg W, et al. (2000) Preoperative staging of non-small-cell lung cancer with positron-emission tomography. N Engl J Med 343: 254–261.

7. Weber WA, Dietlein M, Hellwig D, Kirsch CM, Schicha H, et al. (2003) [PET with (18)F-fluorodeoxyglucose for staging of non-small cell lung cancer]. Nuklearmedizin 42: 135–144.

8. Weber WA, Petersen V, Schmidt B, Tyndale-Hines L, Link T, et al. (2003) Positron emission tomography in non-small-cell lung cancer: prediction of response to chemotherapy by quantitative assessment of glucose use. J Clin Oncol 21: 2651–2657.

9. Su H, Bodenstein C, Dumont RA, Seimbille Y, Dubinett S, et al. (2006) Monitoring tumor glucose utilization by positron emission tomography for the prediction of treatment response to epidermal growth factor receptor kinase inhibitors. Clin Cancer Res 12: 5659–5667.

10. Moyer JD, Barbacci EG, Iwata KK, Arnold L, Boman B, et al. (1997) Induction of apoptosis and cell cycle arrest by CP-358,774, an inhibitor of epidermal growth factor receptor tyrosine kinase. Cancer Res 57: 4838–4848.

11. Shields AF, Grierson JR, Dohmen BM, Machulla HJ, Stayanoff JC, et al. (1998) Imaging proliferation in vivo with [F-18]FLT and positron emission tomography. Nat Med 4: 1334–1336.

12. Toyohara J, Waki A, Takamatsu S, Yonekura Y, Magata Y, et al. (2002) Basis of FLT as a cell proliferation marker: comparative uptake studies with [3H]thymidine and [3H]arabinothymidine, and cell-analysis in 22 asynchronously growing tumor cell lines. Nucl Med Biol 29: 281–287.

13. Buck AK, Schirrmeister H, Hetzel M, Von Der Heide M, Halter G, et al. (2002) 3-deoxy-3-[(18)F]fluorothymidine-positron emission tomography for noninvasive assessment of proliferation in pulmonary nodules. Cancer Res 62: 3331–3334.

14. Ullrich R, Backes H, Li H, Kracht L, Miletic H, et al. (2008) Glioma proliferation as assessed by 3′-fluoro-3′-deoxy-L-thymidine positron emission tomography in patients with newly diagnosed high-grade glioma. Clin Cancer Res 14: 2049–2055.

15. Solit DB, Santos E, Pratilas CA, Lobo J, Moroz M, et al. (2007) 3′-deoxy-3′-[18F]fluorothymidine positron emission tomography is a sensitive method for imaging the response of BRAF-dependent tumors to MEK inhibition. Cancer Res 67: 11463–11469.

16. Therasse P, Arbuck SG, Eisenhauer EA, Wanders J, Kaplan RS, et al. (2000) New guidelines to evaluate the response to treatment in solid tumors. European Organization for Research and Treatment of Cancer, National Cancer Institute of the United States, National Cancer Institute of Canada. J Natl Cancer Inst 92: 205–216.

17. Hamacher K, Coenen HH, Stocklin G (1986) Efficient stereospecific synthesis of no-carrier-added 2-[18F]-fluoro-2-deoxy-D-glucose using aminopolyether supported nucleophilic substitution. J Nucl Med 27: 235–238.

18. Machulla H, Blocther A, Kuntzsch M, Piert M, Wei R, et al. (2000) Simplified labeling approach for synthesizing 3-deoxy-3-[F-18]fluorothymidine ([F-18]FLT). J Radiochem Nucl Chem 243: 843–846.

19. Fueger BJ, Czernin J, Hildebrandt I, Tran C, Halpern BS, et al. (2006) Impact of animal handling on the results of 18F-FDG PET studies in mice. J Nucl Med 47: 999–1006.

20. Schiffer WK, Mirrione MM, Dewey SL (2007) Optimizing experimental protocols for quantitative behavioral imaging with 18F-FDG in rodents. J Nucl Med 48: 277–287.

Methyl-L-11C-Methionine PET as a Diagnostic Marker for Malignant Progression in Patients with Glioma

Roland T. Ullrich*[1,2], Lutz Kracht*[1], Anna Brunn[3], Karl Herholz[4], Peter Frommolt[5], Hrvoje Miletic[6,7], Martina Deckert[3], Wolf-Dieter Heiss[1], and Andreas H. Jacobs[1,2,8,9]

[1]Max Planck Institute for Neurological Research with Klaus Joachim Zülch Laboratories, Cologne, Germany; [2]Center for Molecular Medicine, University of Cologne, Cologne, Germany; [3]Department of Neuropathology, University of Cologne, Cologne, Germany; [4]University of Manchester, Manchester, United Kingdom; [5]Institute of Medical Statistics, Informatics and Epidemiology, University of Cologne, Cologne, Germany; [6]Department of Biomedicine, University of Bergen, Bergen, Norway; [7]Department of Pathology, Haukeland University Hospital, Bergen, Norway; [8]Klinikum Fulda, Fulda, Germany; and [9]European Institute of Molecular Imaging–EIMI, University of Muenster, Muenster, Germany

Methyl-L-11C-methionine (11C-MET) PET has been shown to detect brain tumors with a high sensitivity and specificity. In this study, we investigated the potential of 11C-MET PET to noninvasively detect tumor progression in patients with gliomas. Moreover, we analyzed the relationship between changes in 11C-MET uptake on PET and changes in various molecular immunohistochemical markers during progression of gliomas. **Methods:** Twenty-four patients with histologically proven glioma were investigated repeatedly with 11C-MET PET. 11C-MET uptake was determined for a circular region of interest. Histologic and molecular analyses for tumor progression were performed after open surgery and stereotactic biopsy, respectively. **Results:** In patients with malignant progression, the mean increase in 11C-MET uptake was 54.4% (SD, 45.5%; range, 3.1%−162.2%), whereas in patients without a change in tumor grade, mean 11C-MET uptake did not significantly change (3.9%; SD, 13.7%; range, −24.4% to 26.3%). The difference in the change in 11C-MET uptake between the group with malignant progression and the group without malignant progression was highly significant ($P < 0.001$). Receiver-operating-curve analysis revealed a sensitivity of 90% and a specificity of 92.3% for the detection of malignant transformation by an increase in 11C-MET uptake of more than 14.6%. Increased 11C-MET uptake of more than 14.6% was indicative of malignant progression in all but 3 leave-one-out iterations. A detailed immunohistochemical analysis demonstrated a significant correlation between changes in 11C-MET uptake and the expression of vascular endothelial growth factor. **Conclusion:** These data suggest that 11C-MET-PET represents a noninvasive method to detect malignant progression in patients with gliomas. Moreover, the increase in 11C-MET uptake during malignant progression is reflected by an increase in angiogenesis-promoting markers as vascular endothelial growth factor.

Gliomas are the most common primary brain tumors. More than 50% of gliomas belong to the malignant subtype glioblastoma (*1*). The most important criterion for therapeutic management and prognosis is histologic grading. WHO grade II gliomas have a median overall survival of more than 5 y, whereas anaplastic gliomas show a median survival of only 2–5 y (*2*). Most patients with glioblastoma succumb to the disease within 2 y (*2*). Thus, noninvasive imaging–based technology for the detection of malignant progression is required to select the best possible treatment regimen.

Several studies evaluated methyl-L-11C-methionine (11C-MET) PET for monitoring the effect of treatment and for differentiating recurrent tumor from radiation necrosis (*3–7*). Uptake of 11C-MET is facilitated by amino acid transporter, which is upregulated in glioma capillaries (*8*). 11C-MET PET detects the most malignant parts of brain tumors, as well as infiltrating areas, with high sensitivity and specificity (*9,10*). 11C-MET uptake correlates with microvessel density (*9*) and with the proliferative cell nuclear antigen index (*11*), demonstrating its relevance for evaluation of tumor malignancy. Although 11C-MET uptake correlates with tumor grade (*12,13*), high interindividual variability in 11C-MET uptake does not allow for accurate noninvasive grading (*14*).

The purpose of this study was to investigate the accuracy of intraindividual changes in 11C-MET uptake as a noninvasive indicator of malignant progression in gliomas and to compare changes in 11C-MET uptake with changes in the

molecular profile as determined by immunohistochemistry from tissue samples.

MATERIALS AND METHODS

Patients

This retrospective study included 24 patients with primary supratentorial cerebral gliomas (Table 1). We investigated 14 male patients and 10 female patients (mean age, 40 y; SD, 11.6 y). Each patient gave written informed consent for additional PET imaging, which is not a standard diagnostic tool for patients with gliomas in Germany. All patients who underwent repeated ^{11}C-MET PET and had a corresponding neuropathologic diagnosis during the period from 1993 to 2006 were included in the study (Fig. 1). The ^{11}C-MET PET investigations were part of the routine preoperative diagnostic procedure and were used to guide the biopsy so that the tumor portion with the highest ^{11}C-MET uptake would be obtained. Repeated PET investigations with corresponding biopsy were performed when there were findings suggestive of tumor progression on MRI or CT or suggestive clinical symptoms. The interval between PET measurements varied from 1 mo to 6 y. In total, data from 57 PET scans that had a corresponding histologic diagnosis within the following 3 weeks were available for 24 patients. ^{11}C-MET PET was performed after combined radio- and chemotherapy in 9 of 57 cases, after radiotherapy alone in 8 of 57 cases, and without preceding radio- or chemotherapy in 40 of 57 cases.

All 24 patients underwent baseline ^{11}C-MET PET, 16 of 24 underwent follow-up ^{11}C-MET once, 7 of 24 underwent follow-up ^{11}C-MET twice, and 1 of 24 underwent follow-up ^{11}C-MET 3 times. Information on the patients included age, sex, presence of contrast enhancement on MRI or CT, and extent of surgical resection (13 stereotactic biopsies, 23 subtotal resections, and 21 macroscopic total resections). The tumors were graded according to the World Health Organization (WHO) classification for neuroepithelial tumors (2).

In the initial histologic diagnosis, tumor types were distributed as follows: WHO grade II astrocytoma ($n = 10$), WHO grade III anaplastic astrocytoma ($n = 3$), WHO grade II oligoastrocytoma ($n = 7$), WHO grade III anaplastic oligoastrocytoma ($n = 2$), WHO grade II oligodendroglioma ($n = 1$), and WHO grade III anaplastic oligodendroglioma ($n = 1$) (Table 1).
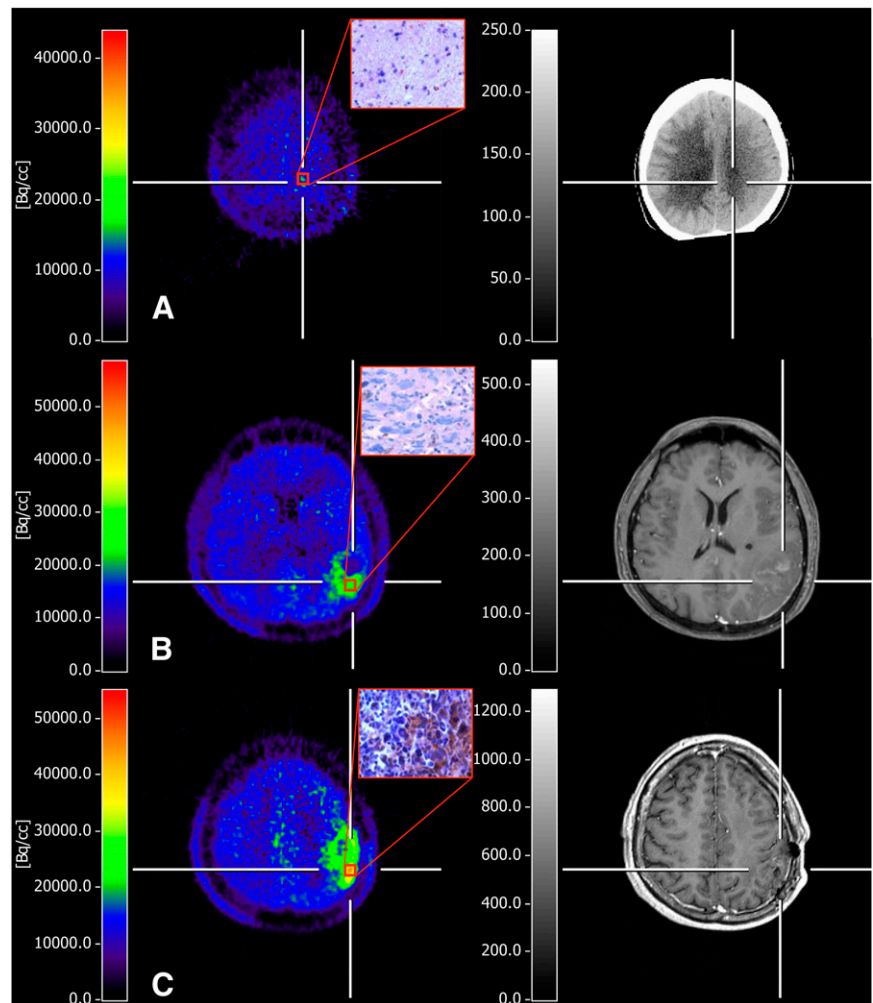
PET Studies

For PET imaging, we used an ECAT EXACT scanner (CTI/Siemens; in-plane full width at half maximum, 6 mm; slice thickness, 3.375 mm; axial field of view, 162 mm) and an ECAT EXACT HR scanner (CTI/Siemens; in-plane full width at half maximum, 3.6 mm; slice thickness, 3.125 mm; axial field of view, 150 mm) (15,16). Subsequent imaging was performed on the same scanner. All patients fasted for at least 4 h before undergoing PET. Images were acquired with the patient supine with eyes closed. Before tracer application, a 10-min transmission scan with 3 rotating ^{68}Ga/[68]Ge sources was obtained. ^{11}C-MET was synthesized according the method of Berger et al. (17) and injected intravenously as a bolus injection of 740 MBq (20 mCi). Accumulation of the tracer was recorded 0–60 min after tracer injection. For assessment of ^{11}C-MET PET images, frames recorded 20–60 min after tracer application in 47 transaxial slices of the entire brain were used. The spatial resolution was 6 mm or better in all dimensions.

TABLE 1. Patient Data at Study Entry

Patient no.	Age (y)	Sex	Initial histology and WHO grade	Resection	Radiotherapy before PET	Chemotherapy before PET
1	32	F	Astrocytoma II	T/P	Yes (9)/yes (3)	Yes (9)/no
2	46	F	Oligoastrocytoma II	S/P	No/no	No/no
3	10	M	Astrocytoma II	T/T	No/yes (6)	No/yes (6)
4	40	F	Astrocytoma II	P/P/P	No/no/yes (36)	No/no/yes (36)
5	28	M	Astrocytoma II	S/S	No/yes (150)	No/no
6	49	F	Oligoastrocytoma II	T/T	No/no	No/no
7	26	M	Oligoastrocytoma II	T/P/P	No/no/yes (159)	No/no/no
8	35	M	Astrocytoma III	S/S	No/yes (24)	No/yes (24)
9	32	F	Oligoastrocytoma II	T/T/T/T	No/yes (376)/yes (53)/no	No/no/no/no
10	35	F	Oligoastrocytoma II	P/P	Yes (156)/no	No/no
11	53	M	Oligodendroglioma II	T/P/P	No/yes (126)/no	No/no/no
12	29	M	Astrocytoma II	T/S	No/no	No/no
13	40	M	Oligoastrocytoma II	T/T/P	No/no/yes (12)	No/no/yes (12)
14	30	M	Oligoastrocytoma III	P/P	No/no	No/no
15	23	M	Astrocytoma III	P/T	No/yes (50)	No/yes (50)
16	27	F	Oligodendroglioma III	S/P	No/yes (9)	No/yes (9)
17	39	M	Oligoastrocytoma II	T/T	No/no	No/no
18	38	F	Astrocytoma II	T/T/S	No/no/yes (102)	No/no/no
19	57	F	Astrocytoma II	S/T	No/no	No/no
20	37	M	Astrocytoma II	S/T/T	No/no/yes (25)	No/no/yes (25)
21	34	M	Astrocytoma II	P/S	No/no	No/no
22	59	F	Astrocytoma II	P/P/P	No/no/no	No/no/no
23	47	M	Oligoastrocytoma III	O/P	No/yes (25)	No/yes (25)
24	58	M	Astrocytoma III	S/P	No/no	No/no

T = total resection; P = partial resection; S = stereotactic biopsy; O = open biopsy.
Data in parentheses are interval (in weeks) between PET scan and chemo- or radiotherapy.

FIGURE 1. ^{11}C-MET PET of 39-y-old man with malignant progression of recurrent glioma. (A) Newly diagnosed grade II astrocytoma with average ^{11}C-MET uptake of 1.3 to contralateral gray matter, with no enhancement on contrast-enhanced CT and no immunohistochemical VEGF expression. (B) One year later, patient presented with malignant progression to grade III astrocytoma associated with significant increase in ^{11}C-MET uptake (to 2.1-fold) and only slight contrast enhancement outside metabolically active tumor. Histologic analysis from resection showed increase in cellularity, numerous pleomorphic nuclei, and low VEGF expression. (C) In following year, resection of tumor again confirmed malignant progression to glioblastoma multiforme, showing markedly increased uptake of ^{11}C-MET (to 2.8-fold), marginal contrast enhancement on MRI, and ~35% of tumor cells expressing VEGF (original magnification, ×400). PET-guided biopsies were taken from region with highest ^{11}C-MET uptake, which was in different locations within same tumor over time.

RGB

In 20 of 24 patients, 48 of 57 PET scans had corresponding contrast-enhanced MRI ($n = 36$) or CT ($n = 12$) scans. In 12 of 24 patients, MRI and PET were performed, in 6 of 24 patients MRI and CT and PET were performed, in 2 of 24 patients CT and PET were performed, and in 4 of 24 patients only PET was performed. Regions of ^{11}C-MET uptake were compared with areas of contrast enhancement on MRI or CT.

PET data were evaluated using a region-of-interest analysis. Because ^{11}C-MET uptake at later imaging times more specifically reflects transport activity, we used summed images covering the time frame 20–60 min after injection for data analysis. As described by Herholz et al., a circular region of interest 7 mm in diameter was placed on the area of highest ^{11}C-MET uptake to determine the maximal tracer uptake (18). A mirrored, contralateral region of interest of the same diameter was placed as a reference. The relative index of ^{11}C-MET uptake was calculated as the ratio of tumor area to reference area. The change in ^{11}C-MET uptake was defined as the relative percentage change in ^{11}C-MET uptake between 2 subsequent scans of the same patient.

MRI/CT Studies

MRI was performed on a 1.5-T system (Gyroscan ACS-NT; Philips Medical Systems) using a head coil. T1-weighted spin-echo enhanced images were acquired with a slice thickness of 2 mm and a matrix of 512×512 pixels. To monitor gadopentetate dimeglumine enhancement of the tumors, we used a T1-weighted 3-dimensional gradient-echo sequence. CT was performed after administration of contrast medium (Solutrast 300R; Bracco). We acquired 22–40 CT images 2 mm thick.

Histologic Analysis

Histologic analysis and immunohistochemistry of the biopsy samples of the initial tumors of all patients, as well as recurrences obtained by stereotactic biopsy or open surgery, were performed on formalin-fixed, paraffin-embedded 4-μm sections. For immunohistochemistry, we applied an automated staining system (BioGenex) using the avidin-biotin-peroxidase complex technique, with 3,3′-diaminobenzidine as chromogene and H_2O_2 as cosubstrate. In brief, classification of the tumors according to the WHO classification of neuroepithelial tumors was based on hematoxylin and eosin staining and immunohistochemistry with monoclonal antibodies against rabbit antihuman MIB-1 (DCS, Innovative Diagnostik-Systeme; clone SP6; dilution, 1:200) and mouse antihuman p53 protein (BioGenex; clone 1801; dilution, 1:200) and polyclonal rabbit antihuman antibodies against glial fibrillary acidic protein and S100 protein (Dako; dilution, glial fibrillary acidic protein, 1:1,000; S100-protein, 1:2,000). Advanced immunohistochemistry was performed with the following monoclonal mouse antihuman antibodies: epidermal growth factor receptor (Merck; clone E30; dilution, 1:20), platelet-derived growth factor

jnm065904-sn ■ 11/6/09

receptor (BD Biosciences; clone 28; dilution, 1:200), retinoblastoma protein (pRb) (Zymed Laboratories; clone Rb1; dilution, 1:50), pentaerythritol tetranitrate (PTEN) (Biogenex; clone 28H6; dilution, 1:10), and vascular endothelial growth factor (VEGF) (DCS; clone VG1; dilution, 1:50). Histologic evaluation was performed by 2 independent neuropathologists. The number of immunoreactive nuclei was determined, comprising 3 areas (F1, F2, and F3) of 3 high-power fields each, with maximal frequency, moderate frequency, and minimal frequency, respectively, of immunoreactive nuclei. The number of positive nuclei was determined as F1 plus F2 plus F3, divided by 3 (%).

Statistical Analysis

Statistical analyses were performed using SPSS software (release 11.0.1, SPSS Inc.). For correlation analysis, the Pearson method was applied, with subsequent parametric tests; 2-sample ANOVA was used for comparisons between the groups with and without malignant progression. Tests were performed 2-sided at a significance level of 0.05, and the P values were understood in an explorative sense regarding the multiple-hypothesis problem. The sensitivity and specificity of changes in ^{11}C-MET uptake were calculated for several thresholds, and the optimum cut-off was determined by receiver-operating-characteristic analysis. An iterative leave-one-out approach was used to validate the receiver-operating-characteristic analysis. At each step, 1 case (i.e. 1 follow-up) was left out of the analysis; a fit of the model was produced for the remaining follow-ups, and a malignant progression prediction was made for the left-out case. Thus, each follow-up value was compared with the cohort of the remaining 32 of 33 values with regard to its individual percentage change in ^{11}C-MET uptake. Moreover, baseline ^{11}C-MET uptake was included as a covariate in a Cox regression model to investigate its relation to the time to histologic progression. To avoid an artificial reduction of variance caused by the mixing of independent and dependent observations, we used the data of only the first follow-up investigation ($n = 24$) for all methods of statistical inference (Pearson method and 2-sample ANOVA).

RESULTS

Malignant Progression as Detected by ^{11}C-MET PET

For evaluation of the correlation between ^{11}C-MET uptake and histologic progression of the tumor, we calculated the percentage change in ^{11}C-MET uptake between the prior ^{11}C-MET PET examination and the subsequent examination. The percentage change in ^{11}C-MET uptake was then compared with the progression as assessed by histology and immunohistochemistry.

For the 24 patients, 57 PET scans with corresponding histologic investigations were available. Among the 24 patients, 16 patients underwent 1 follow-up investigation, 7 patients underwent 2, and 1 patient underwent 3, leading to a total of 33 follow-up investigations. Among these 33, 20 showed histologically proven malignant progression of the tumor. Eleven tumors progressed from grade II to grade III, 6 from grade III to grade IV, and 3 from grade II to grade IV. In 13 cases, the biopsy did not indicate malignant progression.
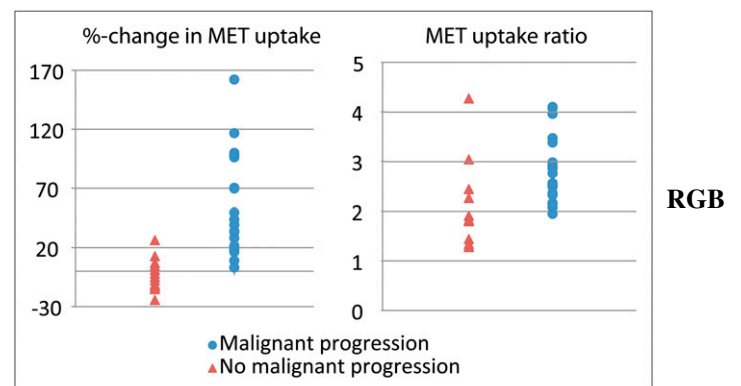
The mean percentage increase in ^{11}C-MET uptake between PET studies in the group with histologically proven malignant progression was 54.4% (SD, 45.5%;

range, 3.1%−162.2%). In contrast, the mean percentage change in ^{11}C-MET uptake in the group without a change in tumor grade was 3.9% (SD, 13.7%; range, −24.4% to 26.3%) (Fig. 2). The mean difference in change in ^{11}C-MET uptake between the group with malignant progression and the group without was highly significant ($P < 0.001$). [**Fig. 2**]

To identify the percentage increase in ^{11}C-MET uptake that best distinguished malignant from nonmalignant progression, we performed a receiver-operating-characteristic analysis (Fig. 3) and calculated the sensitivity and specificity for each value. The percentage change in ^{11}C-MET uptake that best determined malignant progression was 14.6% (sensitivity, 90%; specificity, 92.3%). The area under the curve was 0.96. At a threshold of 14.6%, we identified in only 2 of 20 cases (10%) false-negative ^{11}C-MET uptake findings of malignant progression. In both these tumors, the percentage increase in ^{11}C-MET uptake was less than 14.6% (3.1% and 9.0%, respectively). Malignant progression in both these cases was from grade III to grade IV. We had only 1 false-positive ^{11}C-MET uptake finding; uptake increased by 26.3% whereas the tumor remained histologically stable at grade II. For the 14.6% threshold, positive predictive value was 94.7% and negative predictive value was 85.7%. In the 33-fold cross-validation using the leave-one-out strategy, we correctly classified 30 of 33 follow-up investigations; 1 observation was false-positive and 2 were false-negative, using the 14.6% threshold for change in ^{11}C-MET uptake. [**Fig. 3**]
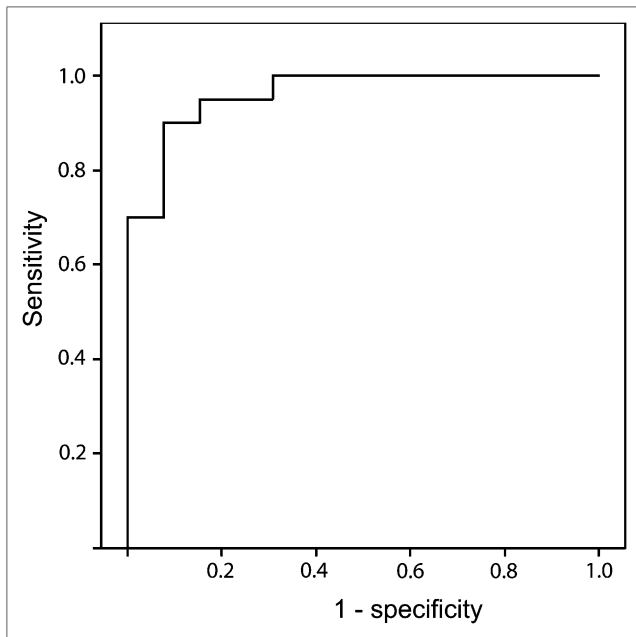
The increase in ^{11}C-MET uptake clearly differed between progression from grade II to grade III and progression from grade III to grade IV, being 72.9% (SD, 46.2%) and 33.5% (SD, 35.4%), respectively (Table 2). The change in uptake for progression from grade II to IV was heterogeneous: 77% in 1 case but only 18.5% and 18.9% in the other 2 cases. [**Table 2**]

We further analyzed the influence of baseline ^{11}C-MET uptake on the time to tumor progression but found no interrelationship between these parameters ($P = 0.96$).

FIGURE 2. Comparison of value of ^{11}C-MET uptake ratio at time of biopsy vs. percentage change in ^{11}C-MET uptake in distinguishing malignant from nonmalignant progression.

FIGURE 3. Receiver operating characteristic analysis to identify change in ^{11}C-MET uptake for differentiation between malignant progression of tumor grade and no malignant progression. Percentage increase that best distinguished malignant progression from no malignant progression was at threshold of 14.6%, with sensitivity of 90% and specificity of 92.3%.

Moreover, we compared absolute ^{11}C-MET uptake ratios at follow-up with changes in ^{11}C-MET uptake for their potential in distinguishing between malignant and non-malignant progression: for changes in ^{11}C-MET uptake in patients with malignant progression (38.2%−83.3%) and without malignant progression (−13.2% to 6.6%), the 95% confidence intervals were separated, whereas for absolute ^{11}C-MET uptake ratios at follow-up, the 95% confidence intervals overlapped (1.5–2.7 uptake ratio for malignant progression and 2.4–3.1 uptake ratio for stable disease), suggesting that relative changes between uptake ratios more sensitively distinguish malignant progression from stable disease (Fig. 2).

Changes in Contrast Enhancement on MRI or CT During Malignant Progression

For 48 of 57 PET investigations, corresponding MRI ($n = 36$) or CT ($n = 12$) had been performed within 6 d beforehand. Using a yes/no categorization, we analyzed for the presence or absence of changes in tumor accumulation

of contrast agent in 28 PET-corresponding follow-up investigations. We compared regions of contrast enhancement on the MRI or CT with regions of increased ^{11}C-MET uptake (Table 3).

The MRI or CT measurements were obtained in 17 cases of histologically proven malignant progression and in 11 cases of no progression. We did not observe coherence between newly appearing contrast enhancement on MRI and an increase in ^{11}C-MET uptake and histologic malignant progression. In 8 of 17 cases with histologically proven malignant progression, tumor progression could be detected by newly appearing contrast enhancement on MRI or CT. In 6 of 17 cases, we observed contrast enhancement at baseline as well as at follow-up. In 3 of 17 cases, we observed contrast enhancement neither at baseline nor at follow-up.

In 7 of 11 cases without histologically proven malignant progression, we observed contrast enhancement on baseline MRI or CT as well as at follow-up. In 1 of 11 cases, MRI and CT showed contrast enhancement neither in the prior investigation nor in the subsequent investigation. Three of 11 patients showed newly appearing contrast enhancement on MRI without histologic signs of malignant progression.

Correlation of Molecular Changes on Immunostaining with Metabolic Changes on ^{11}C-MET PET

Histologic analysis was performed on the 52 biopsy samples that corresponded to the PET investigation. All 52 samples were immunostained for Ki-67, VEGF, epidermal growth factor receptor, p53, PTEN, platelet-derived growth factor receptor, and pRb. To avoid an artificial reduction of variance caused by mixing independent and dependent observations, we used only the data of the first follow-up investigations in determining correlations between changes in ^{11}C-MET uptake and changes in the expression of molecular markers. Changes in the expression level of VEGF correlated to changes in ^{11}C-MET uptake ($r = 0.62$, $P = 0.005$), indicating that an increase in ^{11}C-MET uptake was related to tumor angiogenesis (Fig. 4). No significant correlation was observed between changes in ^{11}C-MET uptake and changes in the expression pattern of Ki-67, epidermal growth factor receptor, p53, PTEN, platelet-derived growth factor receptor, or pRb.

DISCUSSION

This study indicated that ^{11}C-MET PET enables the noninvasive detection of malignant progression in patients who have gliomas with clinical or radiologic findings of

TABLE 2. Changes in ^{11}C-MET Uptake in Patients Without Tumor Progression or with Various Degrees of Progression

Parameter	None ($n = 13$)	From grade II to III ($n = 11$)	From grade III to IV ($n = 6$)	From grade II to IV ($n = 3$)
		Malignant progression		
Mean	3.9%	72.9%	33.5%	38.1%
SD	13.7%	46.2%	35.4%	33.6%

TABLE 3. Changes in Contrast Enhancement in Relation to Histologically Proven Malignant Progression

Malignant progression	Newly appearing contrast enhancement on MRI/CT	
	Present	Absent
Present	8	9
Absent	3	8

tumor progression. Moreover, a correlation was found between changes in ^{11}C-MET uptake and changes in VEGF expression, suggesting a potential link between amino acid transport and tumor angiogenesis.

In gliomas, the early detection of malignant transformation from WHO grade II to grade III or from WHO grade III to grade IV is of high clinical importance because the decision to apply a specific treatment depends mainly on the WHO grade. The mean interval for progression from low-grade glioma to high-grade glioma ranges from 4 to 5 y (19,20). Moreover, malignant progression in gliomas is unpredictable and in many cases not clearly detectable on the basis of clinical symptoms or MRI findings alone. Thus, ^{11}C-MET PET might provide sensitive and specific information on tumor activity and malignant progression in patients with gliomas when a clear answer cannot be obtained on the basis of clinical or MRI findings alone. Repeated ^{11}C-MET PET gives a clear indication of malignant glioma progression and should be used in conjunction with MRI to decrease the need for diagnostic stereotactic interventions.
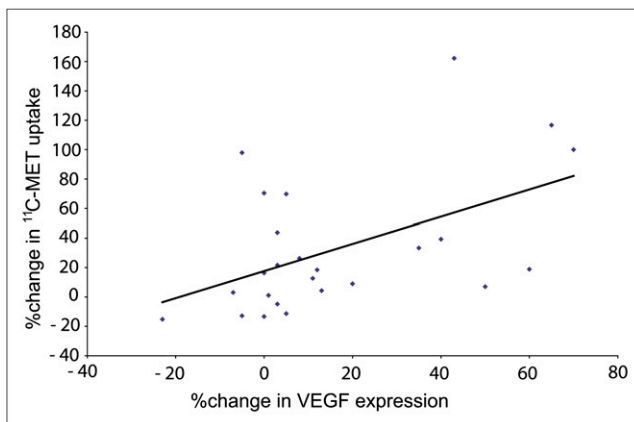
One major limitation of the study was the lack of an independent sample of patients without clinical or radiologic signs of malignant progression to validate the accuracy of the calculated threshold for the change in ^{11}C-MET uptake. However, because of the radiation exposure and the risks related to invasive stereotactic biopsies, the inclusion of patients without signs suggestive of malignant pro-

RGB

FIGURE 4. Correlation between changes in expression of VEGF and changes in ^{11}C-MET uptake during first follow-up investigation.

gression is not ethically feasible. Thus, we performed a cross-validation in a leave-one-out strategy for all receiver-operating-characteristic analyses to confirm whether the assessed threshold for changes in ^{11}C-MET uptake was accurate in indicating malignant progression. However, 1 patient in the study showed an increase in ^{11}C-MET uptake without histologic signs of malignant progression. Thus, future prospective studies with constant time points between ^{11}C-MET PET investigations are required to confirm the accuracy of the determined threshold and to validate the specificity of ^{11}C-MET PET in detecting malignant progression.

Although it has been shown that the high interindividual variability of ^{11}C-MET PET does not allow for glioma grading at first diagnosis (14)—most likely because of the differential effects of oligodendroglial tumor components on tumor vessels and the related amino acid uptake—we here demonstrated that ^{11}C-MET PET may be valuable for the intraindividual follow-up of biologically active glioma tissue after treatment to determine the time of tumor progression. The important parameter is not the absolute ^{11}C-MET uptake ratio but the change between two ^{11}C-MET measurements within the same individual.

We further sought to analyze the relationship between changes in ^{11}C-MET uptake and molecular markers as assessed by immunohistochemistry. We found that changes in ^{11}C-MET uptake are related to VEGF expression. It is well known that the mammalian target of rapamycin is downstream from the VEGF/VEGF receptor 2 pathway via phosphatidylinositol-3′-kinase/AKT regulated by VEGF (21,22). Mammalian target of rapamycin again modulates amino acid transport by regulating the expression of L-type amino acid transporter 1 (23). Although the correlation between changes in ^{11}C-MET uptake and VEGF expression is relatively weak, we hypothesize that there might be a crosslink between VEGF receptor 2 signaling and amino acid transport. The activation of VEGF/VEGF receptor 2 signaling induces mammalian target of rapamycin kinase activity, with mammalian target of rapamycin being a key enzyme regulating amino acid transport. The hypothesis that ^{11}C-MET uptake may serve as a surrogate marker for activated VEGF receptor signaling remains to be investigated. We did not find a significant correlation between changes in epidermal growth factor receptor, PTEN, pRb, p53, Ki-67, or platelet-derived growth factor receptor expression and changes in ^{11}C-MET uptake. Although epidermal growth factor, PTEN, pRb, p53, and Ki-67 are major factors in the genetic pathway to malignant transformation in gliomas, they contribute mainly to changes in the cell cycle and therefore cell proliferation (24–27).

One major effect of VEGF is the induction of vascular permeability, with consequent disruption of the vascular barrier (28,29). To evaluate the relationship between ^{11}C-MET uptake and leakage of the blood–brain barrier, we further analyzed whether ^{11}C-MET uptake is accompanied by contrast enhancement on MRI as a marker of high

vascular permeability. Interestingly, we observed in 21% of the patients ^{11}C-MET accumulation without contrast enhancement on MRI. This observation underlines—as reported in previous studies—the fact that ^{11}C-MET uptake is not related mainly to an elevated diffusion through leakage of endothelial cell–cell junctions but to specific amino acid transporter systems (8,18,30). Consequently, ^{11}C-MET can be considered a radiolabeled tracer for determining the activity of the amino acid transport system independently of the state of the blood–brain barrier.

We further examined the value of newly appearing contrast enhancement in detecting malignant progression. In this study, contrast enhancement on MRI or CT was not indicative of malignant progression in WHO grade. Although not all our patients underwent MRI, these findings are in line with a previous study by Scott at al. describing the inaccuracy of contrast enhancement as a marker for assessing glioma malignancy in 314 patients (31). Over the study period, new MRI parameters such as diffusion or perfusion-weighted imaging were implemented in the diagnosis of brain tumors. It remains to be investigated whether changes in diffusion or perfusion-weighted imaging might allow for the detection of malignant progression in patients with gliomas, as well.

CONCLUSION

These data suggest that ^{11}C-MET PET is a marker for the noninvasive detection of malignant progression in patients with gliomas. Because of the relatively few patients in this retrospective study, prospective studies are required to further validate these results.

ACKNOWLEDGMENTS

REFERENCES

1. *Statistical Report: Primary Brain Tumors in the United States, 1997–2001.* Hinsdale, IL: Central Brain Tumor Registry of the United States; 2004.
2. Louis DN, Ohgaki H, Wiestler OD, et al. The 2007 WHO classification of tumours of the central nervous system. *Acta Neuropathol.* 2007;114:97–109.
3. Tsuyuguchi N, Takami T, Sunada I, et al. Methionine positron emission tomography for differentiation of recurrent brain tumor and radiation necrosis after stereotactic radiosurgery: in malignant glioma. *Ann Nucl Med.* 2004;18:291–296.
4. Jacobs AH, Kracht LW, Gossmann A, et al. Imaging in neurooncology. *NeuroRx.* 2005;2:333–347.
5. Jacobs AH, Li H, Winkeler A, et al. PET-based molecular imaging in neuroscience. *Eur J Nucl Med Mol Imaging.* 2003;30:1051–1065.
6. Thiel A, Pietrzyk U, Sturm V, Herholz K, Hovels M, Schroder R. Enhanced accuracy in differential diagnosis of radiation necrosis by positron emission tomography–magnetic resonance imaging coregistration: technical case report. *Neurosurgery.* 2000;46:232–234.
7. Van Laere K, Ceyssens S, Van Calenbergh F, et al. Direct comparison of ^{18}F-FDG and ^{11}C-methionine PET in suspected recurrence of glioma: sensitivity, inter-observer variability and prognostic value. *Eur J Nucl Med Mol Imaging.* 2005;32:39–51.
8. Miyagawa T, Oku T, Uehara H, et al. "Facilitated" amino acid transport is upregulated in brain tumors. *J Cereb Blood Flow Metab.* 1998;18:500–509.
9. Kracht LW, Friese M, Herholz K, et al. Methyl-[^{11}C]-l-methionine uptake as measured by positron emission tomography correlates to microvessel density in patients with glioma. *Eur J Nucl Med Mol Imaging.* 2003;30:868–873.
10. Kracht LW, Miletic H, Busch S, et al. Delineation of brain tumor extent with [^{11}C]L-methionine positron emission tomography: local comparison with stereotactic histopathology. *Clin Cancer Res.* 2004;10:7163–7170.
11. Sato N, Suzuki M, Kuwata N, et al. Evaluation of the malignancy of glioma using ^{11}C-methionine positron emission tomography and proliferating cell nuclear antigen staining. *Neurosurg Rev.* 1999;22:210–214.
12. Derlon JM, Bourdet C, Bustany P, et al. [^{11}C]L-methionine uptake in gliomas. *Neurosurgery.* 1989;25:720–728.
13. Ogawa T, Shishido F, Kanno I, et al. Cerebral glioma: evaluation with methionine PET. *Radiology.* 1993;186:45–53.
14. Ceyssens S, Van Laere K, de Groot T, Goffin J, Bormans G, Mortelmans L. [^{11}C]methionine PET, histopathology, and survival in primary brain tumors and recurrence. *Am J Neuroradiol.* 2006;27:1432–1437.
15. Wienhard K, Eriksson L, Grootoonk S, Casey M, Pietrzyk U, Heiss WD. Performance evaluation of the positron scanner ECAT EXACT. *J Comput Assist Tomogr.* 1992;16:804–813.
16. Wienhard K, Dahlbom M, Eriksson L, et al. The ECAT EXACT HR: performance of a new high resolution positron scanner. *J Comput Assist Tomogr.* 1994;18:110–118.
17. Berger G, Maziere M, Knipper R, Prenant C, Comar D. Automated synthesis of ^{11}C-labelled radiopharmaceuticals: imipramine, chlorpromazine, nicotine and methionine. *Int J Appl Radiat Isot.* 1979;30:393–399.
18. Herholz K, Holzer T, Bauer B, et al. ^{11}C-methionine PET for differential diagnosis of low-grade gliomas. *Neurology.* 1998;50:1316–1322.
19. Watanabe K, Sato K, Biernat W, et al. Incidence and timing of p53 mutations during astrocytoma progression in patients with multiple biopsies. *Clin Cancer Res.* 1997;3:523–530.
20. McCormack BM, Miller DC, Budzilovich GN, Voorhees GJ, Ransohoff J. Treatment and survival of low-grade astrocytoma in adults: 1977–1988. *Neurosurgery.* 1992;31:636–642.
21. Riesterer O, Zingg D, Hummerjohann J, Bodis S, Pruschy M. Degradation of PKB/Akt protein by inhibition of the VEGF receptor/mTOR pathway in endothelial cells. *Oncogene.* 2004;23:4624–4635.
22. Kim BW, Choi M, Kim YS, et al. Vascular endothelial growth factor (VEGF) signaling regulates hippocampal neurons by elevation of intracellular calcium and activation of calcium/calmodulin protein kinase II and mammalian target of rapamycin. *Cell Signal.* 2008;20:714–725.
23. Fuchs BC, Bode BP. Amino acid transporters ASCT2 and LAT1 in cancer: partners in crime? *Semin Cancer Biol.* 2005;15:254–266.
24. Narita Y, Nagane M, Mishima K, Huang HJ, Furnari FB, Cavenee WK. Mutant epidermal growth factor receptor signaling down-regulates p27 through activation of the phosphatidylinositol 3-kinase/Akt pathway in glioblastomas. *Cancer Res.* 2002;62:6764–6769.
25. Mellinghoff IK, Wang MY, Vivanco I, et al. Molecular determinants of the response of glioblastomas to EGFR kinase inhibitors. *N Engl J Med.* 2005;353:2012–2024.
26. Giacinti C, Giordano A. RB and cell cycle progression. *Oncogene.* 2006;25:5220–5227.
27. Ohgaki H, Dessen P, Jourde B, et al. Genetic pathways to glioblastoma: a population-based study. *Cancer Res.* 2004;64:6892–6899.
28. Weis SM, Cheresh DA. Pathophysiological consequences of VEGF-induced vascular permeability. *Nature.* 2005;437:497–504.
29. Rosenstein JM, Mani N, Silverman WF, Krum JM. Patterns of brain angiogenesis after vascular endothelial growth factor administration in vitro and in vivo. *Proc Natl Acad Sci USA.* 1998;95:7086–7091.
30. Jager PL, Vaalburg W, Pruim J, de Vries EG, Langen KJ, Piers DA. Radiolabeled amino acids: basic aspects and clinical applications in oncology. *J Nucl Med.* 2001;42:432–445.
31. Scott JN, Brasher PM, Sevick RJ, Rewcastle NB, Forsyth PA. How often are nonenhancing supratentorial gliomas malignant? A population study. *Neurology.* 2002;59:947–949.

10.   Erklärung

Ich versichere, dass ich die von mir vorgelegte Dissertation selbständig angefertigt, die benutzten Quellen und Hilfsmittel vollständig angegeben und die Stellen der Arbeit – einschließlich Tabellen, Karten und Abbildungen -, die anderen Werken im Wortlaut oder dem Sinn nach entnommen sind, in jedem Einzelfall als Entlehnung kenntlich gemacht habe; dass diese Dissertation noch keiner anderen Fakultät oder Universität zur Prüfung vorgelegen hat; dass sie – abgesehen von unten angegebenen Teilpublikationen – noch nicht veröffentlicht worden ist sowie, dass ich eine solche Veröffentlichung vor Abschluss des Promotionsverfahrens nicht vornehmen werde. Die Bestimmungen dieser Promotionsordnung sind mir bekannt. Die von mir vorgelegte Dissertation ist von Professor Dr. Andreas Jacobs betreut worden.

Curriculum vitae

Name   **Dr. med. Roland Tillmann Ullrich**

Address   Max-Planck Institut für Neurologische Forschung

              Molekulare Bildgebung

              Gleuelerstr. 50, 50931 Köln

              Tel.: 0221-4726-306

              Fax: 0221-4726-298

              E-mail: ullrich@nf.mpg.de

Date of birth 06.01.1978

Scientific Career

1999-2001   Medical School, Preclinical Studies: Philipps-Universität, Marburg

2001-2005   Medical School, Clinical Studies: Universität zu Köln, Université de Lyon, Université de Paris

2005   M.D., Medical School, Universität zu Köln

2006   Postdoctoral fellow at the Max-Planck Institute for Neurological Research

2008   Member of the European Society of Molecular Imaging